Electronic Journal of Qualitative Theory of Differential Equations
2026, No. **62**, 1–93; https://doi.org/10.14232/ejqtde.2026.1.62 www.math.u-szeged.hu/ejqtde/

Topological study of families with two infinite saddle-nodes of different types or with an infinite nilpotent singularity

Joan C. Artés[1], **Marcos C. Mota**[2] and **Alex C. Rezende**[✉3]

[1]Departament de Matemàtiques, Universitat Autònoma de Barcelona, 08193, Barcelona, Spain
[2]Instituto de Ciências Puras e Aplicadas, Universidade Federal de Itajubá, 35903-087, Itabira, Minas Gerais, Brazil
[3]Departamento de Matemática, Universidade Federal de São Carlos, 13565-905, São Carlos, São Paulo, Brazil

Received 6 April 2026, appeared 15 November 2026
Communicated by Gabriele Villari

Abstract. The classification modulo limit cycles of phase portraits in the Poincaré disc of quadratic differential systems, according to the structural stability, started in 1998 when Artés, Kooij and Llibre proved that there exist 44 structurally stable topologically distinct phase portraits modulo limit cycles. In 2018, Artés, Llibre and Rezende showed the existence of at least 202 (at most 209) structurally unstable topologically distinct codimension-one phase portraits, modulo limit cycles. Artés, Oliveira and Rezende (2020) started the study of the codimension-two systems, they described all the sets that must be studied in order to complete this classification, and they proved that the set (AA) has 34 topologically distinct phase portraits modulo limit cycles. In the sequence, Artés, Mota and Rezende (2021) studied the sets (AB) and (AC) and they proved that the set (AB) has 71 topologically distinct phase portraits modulo limit cycles and that the set (AC) has 40 ones. Recently, Artés (2024) proved that the set (AD) possesses at least 77 topologically different phase portraits, modulo limit cycles. Here we consider the set (BC), formed by all quadratic systems possessing either two infinite saddle-nodes of different types, or an infinite elliptic-saddle, or an infinite nilpotent saddle. We prove the existence of exactly 35 topologically different phase portraits modulo limit cycles. In this paper we also apply a notation for phase portraits of quadratic systems and assign definitive names to phase portraits given in previous papers using the same technique as here.

Keywords: quadratic differential system, structural stability, codimension two, phase portrait, infinite singularity.

2020 Mathematics Subject Classification: 34C23, 34A34, 37G10.

1 Introduction and statement of the main results

Mathematicians find immense satisfaction in resolving problems. The closure of a question, marked by a "q.e.d." or the simple act of solving an age-old inquiry, brings a joy that grows

✉Corresponding author. Email: alexcr@ufscar.br

with the passage of time between posing the question and arriving at the answer.

With the advent of differential calculus, a plethora of questions posed by medieval mathematicians found solutions. Simultaneously, this breakthrough sparked the emergence of numerous new inquiries. The quest for primitive functions, unattainable through algebraic or finite analytic expressions, complicated the trajectory of future research. Entire branches of mathematics arose to tackle these challenges. Moreover, when we extend the problem from finding primitives of differential equations in one dimension to multiple dimensions, the complexity increases exponentially.

Hence, nearly two centuries lapsed between the inception of the first linear system of differential equations and its full resolution by Laplace in 1812 [24]. Following the resolution of linear systems across all dimensions, attention naturally turned to classifying quadratic differential systems. Yet, it became apparent that this task would not yield to simple, swift solutions. Unlike their linear counterparts, quadratic systems (or those of higher degrees) generally defy analytical solutions, calculable within a finite set of terms.

Consequently, a different approach was adopted for solving nonlinear differential systems, leading to the birth of a new mathematical domain: the Qualitative Theory of Ordinary Differential Equations [27]. Unable to provide explicit mathematical expressions for the solutions of these systems, this theory aims to delineate, through comprehensive and precise graphical representations, the behavior of particles within vector fields governed by such equations, i.e. their phase portraits.

Despite the progress made in simplifying the problem, challenges persist. The main query among them is the presence of invariant sets such as limit cycles and graphics within phase portraits of differential systems. Unlike linear systems, which cannot engender limit cycles and, at most, exhibit wholly circular phase portraits with periodic orbits, differential systems in the plane – polynomial or otherwise, starting with quadratic ones – may feature numerous limit cycles. While it is natural to encounter an infinite number of these cycles in non-polynomial scenarios, intuition suggests that a polynomial system should not possess an infinite number of limit cycles, related to its impossibility to possess an infinite number of isolated singular points. Given the correlation between the number of singular points and the degree of the polynomial system, it seems reasonable to infer a similar relationship between the number of limit cycles and either the number of parameters or the degree of such systems, either directly or indirectly.

In 1900, David Hilbert [23] presented a compilation of 23 challenges intended to be tackled throughout the 20th century. Among them, the second part of his renowned 16th problem delves into determining the maximum number of limit cycles feasible for a polynomial differential system in the plane of degree n. Even after more than one hundred years, an upper bound for this general problem remains elusive, only discernible for specific subsets of such systems.

In 1966, Coppel [17] voiced the notion that the classification of phase portraits of quadratic systems could potentially be achieved through purely algebraic methods. This implies that, by employing algebraic equations and inequalities, one could theoretically discern the phase portrait of a quadratic system. This assertion posed a formidable challenge to refute at the time. This was partly due to the fact that the isolated finite singular points of a quadratic system could be found through a fourth-degree resultant, with their solutions calculable algebraically, similar to those at infinity. Furthermore, during that era, the means to induce limit cycles via a Hopf bifurcation were also known to be determined algebraically.

Conversely, in 1991, Dumortier and Fiddelears [19] demonstrated that, beginning with

quadratic systems (and extending to higher-degree systems), various geometric and topological phenomena arise in the phase portraits of such systems. These phenomena challenge precise determination through algebraic expressions. Specifically, the majority of connections between separatrices and the occurrence of double or semi-stable limit cycles escape algebraic resolution.

Consequently, the exhaustive classification of quadratic systems presents a formidable obstacle in the current landscape of research. Progress in this endeavor hinges on the approach, at least partially, the second part of Hilbert's 16th problem, even within the class of quadratic systems.

Nevertheless, despite these challenges, numerous inquiries pertaining to quadratic systems have emerged, many of which have found resolution. Indeed, over a thousand articles have been published directly addressing quadratic systems. Reyn compiled a bibliography on this topic, which saw multiple editions until his retirement (see [28–32]). It is noteworthy that in the past two decades, many more additional articles concerning quadratic systems have surfaced, potentially surpassing the initial count of one thousand publications on the subject.

Many of the inquiries posed and problems addressed have revolved around subclassifications of quadratic systems, involving systems sharing common characteristics. For instance, investigations have delved into systems exhibiting a center [26, 34, 35, 37], a weak third-order focus [4, 25], a nilpotent singularity [18], absence of real singular points [22], or possessing two invariant lines [28], among other variations, totaling over a thousand articles. While some studies have yielded comprehensive solutions, including the determination of limit cycles (their existence and number), others have focused on classifications modulo limit cycles. In such cases, all feasible phase portraits are considered irrespective of the presence or quantity of limit cycles. Given that in quadratic systems, a limit cycle can only encircle a single finite singular point, which must necessarily be a focus [17], identifying the outermost limit cycle within a cycle nesting suffices. Interpreting the stability of that point as the outer stability of this cycle, the analysis then extends to exploring all possible scenarios in the remaining space.

Among the various families of quadratic systems investigated throughout the 20th century, particular attention was drawn to the study of structurally stable quadratic systems modulo limit cycles. This entailed determining which phase portraits of a quadratic system remain unchanged under small perturbations in their coefficients. To establish a structurally stable system modulo limit cycles, certain conditions were imposed: exclusion of multiple singular points and connections of separatrices. Centers, weak foci, semi-stable limit cycles, and other unstable elements were considered within the quotient modulo limit cycles. A systematic examination (see [3]) revealed that structurally stable quadratic systems exhibit a total of 44 topologically distinct phase portraits.

Definition 1.1. A phase portrait of a quadratic vector field is *structurally stable* (it has topological codimension zero) if any sufficiently small perturbation in the parameter space leaves the phase portrait topologically equivalent to the previous one.

From this context, it becomes evident that any attempt to delve into the classification of phase portraits of quadratic systems prior to resolving the second part of Hilbert's 16th problem must be conducted modulo limit cycles.

Moreover, the entire spectrum of quadratic systems, by its definition, hinges on twelve parameters. However, owing to the influence of the real affine transformations group and time rescaling, this family ultimately reduces to depending on five parameters, although this still presents a considerable number.

Two systematic approaches exist for comprehensively studying all phase portraits of quadratic systems. One method, pioneered by Reyn, involves initially examining phase portraits of quadratic systems wherein all finite singular points have coalesced with infinite singular points [30]. Subsequently, he investigated cases where exactly three finite singular points have coalesced with points at infinity, leaving behind one real finite singularity. Finally, he concluded the study by analyzing instances where two finite singular points have coalesced with points at infinity, resulting in two real points, one double point, or two complex points. While his exploration of finite multiplicity three was incomplete, and his investigation into finite multiplicity four remained inaccessible.

Taking a different approach, rather than starting from the highest degrees of degeneracy and working downwards, the strategy reverses course. As previously mentioned, structurally stable quadratic systems yield 44 topologically distinct phase portraits. In [5], the authors undertook the classification of structurally unstable quadratic systems of codimension one modulo limit cycles, or simply, systems of *codimension one**.

For more details related to the following definition we recommend [9], in which the authors compiled the definitions that have been given so far of "codimension", which worked quite well for low codimensions, but did not fit as well when extended to higher codimensions.

Definition 1.2. A phase portrait of a quadratic vector field is considered *structurally unstable of codimension* $k \in \mathbb{N}$ if any sufficiently small perturbation in the parameter space either maintains the phase portrait's topological equivalence to the previous one, or transitions it to some lower codimension, with at least one perturbation capable of reducing it to codimension $k-1$, or there exists at least one couple of chained perturbations which perturbs the phase portrait into one of codimension $k-2$.

We remark that, if we consider cubic differential systems, this notion of codimension needs more precision due to new phenomena that may happen in their phase portraits and that do not happen for quadratic systems. More information can be found in [1, Remark 2] and the references therein.

The codimension-one systems exhibit one of the simplest structurally unstable elements: a saddle-node of multiplicity two (finite or infinite), a separatrix from one saddle point to another, or a separatrix forming a loop for a saddle point with nonzero divergence. All phase portraits of codimension one are divided into four sets based on the presence of a structurally unstable element: (A) possessing a finite semi-elemental saddle-node $\overline{sn}_{(2)}$ formed by the coalescence of a finite saddle and a finite node, (B) possessing an infinite semi-elemental saddle-node $\binom{\overline{0}}{2}SN$ formed by the coalescence of an infinite saddle and an infinite node, (C) possessing an infinite semi-elemental saddle-node $\binom{\overline{1}}{1}SN$, obtained by the coalescence of a finite saddle (respectively, finite node) with an infinite node (respectively, infinite saddle), and (D) possessing a separatrix connection. The latter set (D) is further subdivided into five subsets according to the type of connection: (a) finite-finite (heteroclinic orbit), (b) loop (homoclinic orbit), (c) finite-infinite, (d) infinite-infinite between symmetric points, and (e) infinite-infinite between adjacent points. The study of codimension-one systems spanned approximately 20 years, ultimately yielding at least 204 (and at most 211), which contains two errors and the definitive numbers are, respectively, 202 and 209, topologically distinct phase portraits of codimension one modulo limit cycles.

The methodology employed in these two studies (and subsequent ones) follows a similar pattern. Initially, it entails generating, through combinations of singularities and separatrices,

all *potential* (as per the definition provided below) phase portraits of a specified codimension and sharing some other property. Subsequently, the task involves either furnishing a concrete example of each phase portrait or demonstrating its impossibility through proof. We present here definitions and main results established in [1], which is the most recent work in the same direction as this present paper.

Definition 1.3. By a *potential phase portrait* we understand a phase portrait that is consistent with the number and types of singularities that may occur in a given class of systems.

Therefore, a potential phase portrait (i.e. phase portrait that can be drawn on paper) may remain unrealizable due to various underlying factors. In several prior publications, these phase portraits were simply referred to as "possible". However, the ambiguity inherent in this term might unsettle readers when something labeled as "possible" ultimately proves impossible or unattainable. Hence, we opted for a different terminology. The initial phase portraits obtained are regarded as potentially realizable, although their realization is not guaranteed in the end.

The methodologies employed to demonstrate the impossibility of certain phase portraits often revolve around analyzing the number of contact points between the flow and a straight line. More recent approaches delve into geometric principles such as the positioning and tangencies of orbits and characteristic directions. Furthermore, phase portraits that cannot be realized within a specific codimension become crucial evidence for demonstrating that related phase portraits in higher codimension are also impossible.

Examples of phase portraits are primarily derived from previously explored families of the same or higher codimensions. If they belong to the same codimension, they are directly identified within those investigations. Alternatively, if higher codimension examples are used, perturbations to one or more phase portraits are made to achieve the desired result.

The next step involves delving into codimension-two phase portraits, i.e. phase portraits with the presence of two unstable objects of codimension one or one object of codimension two (see Definition 1.2 for $k = 2$ and [1, Theorem 2]). The classification of phase portraits of quadratic systems of codimension two modulo limit cycles (or simply, systems of *codimension two**) is in progress and it counts with three published papers [1, 12, 14]. Artés, Oliveira and Rezende, in [14], introduced the framework for exploring codimension-two scenarios. Given the considerably larger number of cases in codimension two compared to codimension one, it was suggested to categorize them into several sets. They examined the first of these sets (namely, set (AA)), specifically focusing on phase portraits containing precisely two finite saddle-nodes or a cusp as the unique unstable elements. They obtained 34 topologically distinct phase portraits in the Poincaré disc, modulo limit cycles. Furthermore, this paper rectifies an error identified by the authors in the book by Artés, Llibre and Rezende [5], resulting in a reduction to 203 in the count of topologically distinct phase portraits of codimension one, modulo limit cycles.

In the sequence, in [12], the investigation continued, centering on phase portraits featuring exactly one finite and one infinite saddle-node (encompassing two distinct types) as the unique unstable elements (sets (AB) and (AC)). There, we found 71 (respectively, 40) topologically distinct phase portraits for the set (AB) (respectively, (AC)) modulo limit cycles.

More recently, in [1], the author topologically classified the families of quadratic vector fields possessing one finite saddle-node and a separatrix connection from set (AD), obtaining a minimum of 77 topologically different phase portraits modulo limit cycles. Moreover, an additional correction was made for the main result in [5], leading to a reduction to 202 in the

number of topologically distinct phase portraits of codimension one, modulo limit cycles.

We now present some definitions and notation used in these papers. We encourage the reader to go deep in these works to understand the background and to be aware of all definitions and results involved in the current classification.

The next two concepts define two objects that will appear in our classification: graphics and degenerate graphics. For more details, we refer the reader to [21].

Definition 1.4. A *(non-degenerate) graphic* is formed by a finite sequence of singular points r_1, r_2, ..., r_n (with possible repetitions) and non-trivial connecting orbits γ_i, for $i = 1, \dots, n$, such that γ_i has r_i as $\alpha-$limit set and r_{i+1} as $\omega-$limit set for $i < n$ and γ_n has r_n as $\alpha-$limit set and r_1 as $\omega-$limit set. Also normal orientations n_j of the non-trivial orbits must be coherent in the sense that, if γ_{j-1} has left-hand orientation, then so does γ_j. A polycycle is a graphic which has a Poincaré return map.

Definition 1.5. A *degenerate graphic* is formed by a finite sequence of singular points r_1, r_2, ..., r_n (with possible repetitions) and/or segments of curves of singular points γ_i, for $i = 1, \dots, n$, such that γ_i has r_i as $\alpha-$limit set and r_{i+1} as $\omega-$limit set for $i < n$ and γ_n has r_n as $\alpha-$limit set and r_1 as $\omega-$limit set. Also normal orientations n_j of the non-trivial orbits must be coherent in the sense that, if γ_{j-1} has left-hand orientation, then so does γ_j.

This paper aims to contribute to the classification of phase portraits of planar quadratic differential systems of codimension two, modulo limit cycles. As previously mentioned, in [14], due to the considerable number of codimension-two cases to be examined (more than 10), it is impractical to encompass all the results within a single paper. Therefore, following the approach outlined in [14], the authors have opted to divide this study into multiple papers, with the present article being the fourth in this series.

In this paper we often use the theory of invariants applied to quadratic differential systems. This theory is completely explained in the book [8] and relies on a set of polynomial invariants obtained from the coefficients of the system that completely rule the singularities of the systems. Also the notation for singularities introduced in [8] is used here. Since the description of these two elements takes a lot of pages, we suggest the reader to consult that book.

Consider the set $P_n(\mathbb{R}^2)$ comprising all polynomial vector fields on $\mathbb{R}^2$ represented as the generic form $X(x,y) = (P(x,y), Q(x,y))$, where P and Q are polynomials in the variables x and y of degree at most n (where $n \in \mathbb{N}$). Within this set, we adopt the coefficient topology, wherein each vector field $X \in P_n(\mathbb{R}^2)$ is associated with a point in $\mathbb{R}^{(n+1)(n+2)}$ (further information is presented in [5]).

Here, we present all the global phase portraits of the vector fields $X \in P_2(\mathbb{R}^2)$ belonging to set (BC) and we study their realizations. The set (BC) is formed by two disjoint subsets:

- (BC$_{SNSN}$) containing all quadratic systems possessing two infinite saddle-nodes of different types, i.e. the phase portrait of a system in this set possesses the infinite saddle-node $\overline{(^0_2)}SN$ plus the infinite saddle-node $\overline{(^1_1)}SN$ (remember page 4);
- (BC$_{ESNS}$) containing all the quadratic systems possessing either one infinite nilpotent elliptic-saddle (which can be of three types: $\widehat{(^1_2)}PHP - E$, $\widehat{(^1_2)}H - E$, or $\widehat{(^1_2)}PEP - H$), or one infinite nilpotent saddle $\widehat{(^1_2)}HHH - H$ (see [8] for details on this notation).

Let Σ_0^2 be the collection of all planar structurally stable vector fields, and $\Sigma_k^2(S)$ represent the set of structurally unstable vector fields $X \in P_2(\mathbb{R}^2)$ of codimension k, modulo limit cycles,

from the set S. Here, S denotes a set of vector fields exhibiting the same type of instability modulo orientation. For instance, in this paper, we focus on the set $\Sigma_2^2(BC)$ of structurally unstable vector fields $X \in P_2(\mathbb{R}^2)$ of codimension two, modulo limit cycles, from the set (BC).

The phase portraits in our classification are drawn in the Poincaré disc (see [20, Chapter 5]) and, in each picture representing such a phase portrait, we draw the *skeleton of separatrices*, as outlined in Definition 2 of [1], plus some additional curves (with thinner trace) to make the picture more comprehensive, as in the case we have an elliptic sector or a limit cycle.[1]

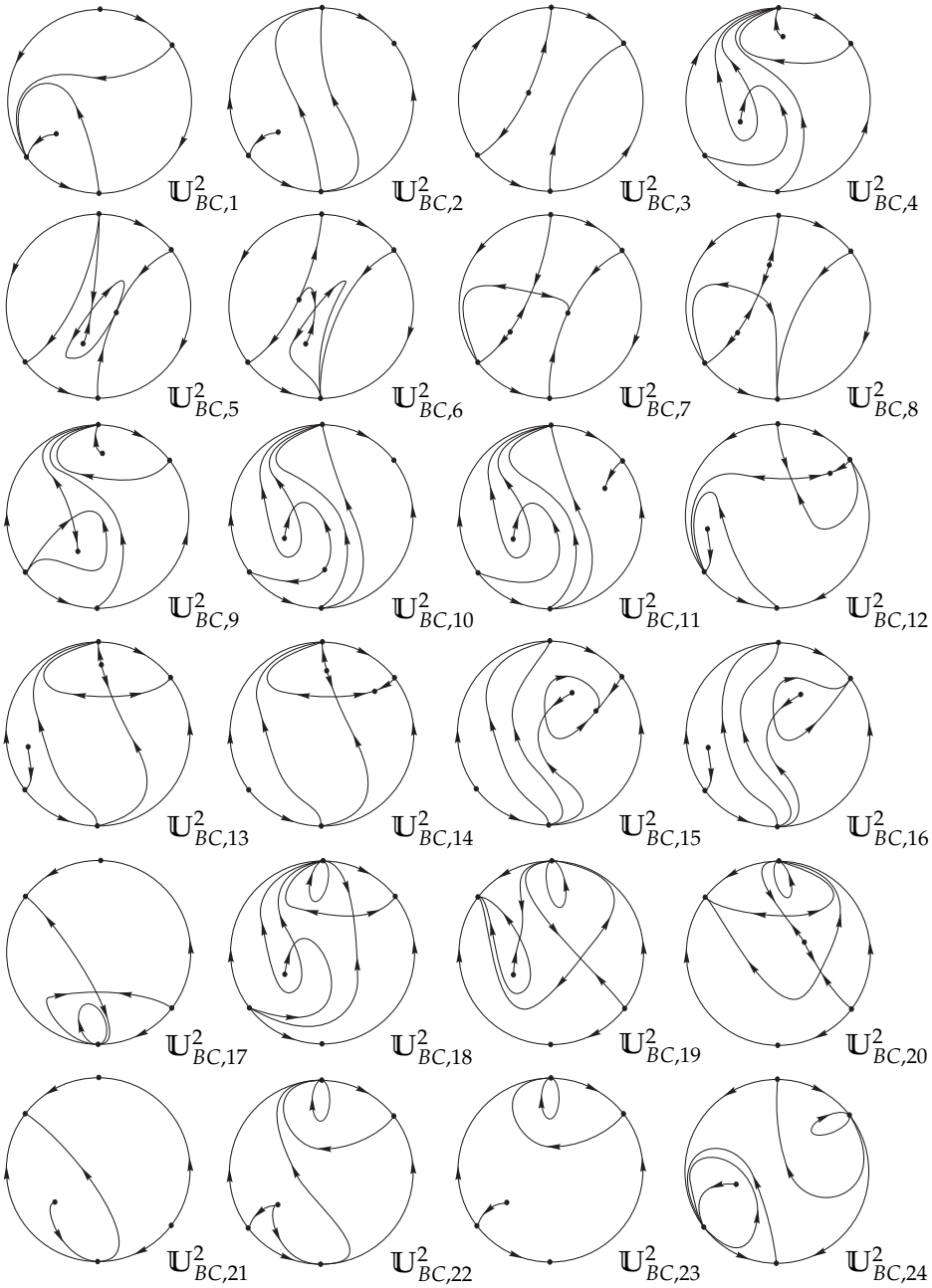


Figure 1.1: Structurally unstable quadratic phase portraits of *codimension two** of the set (BC).

[1]Even though we are interested in phase portraits without limit cycles, when studying their bifurcations we will find and draw some limit cycles that appear.

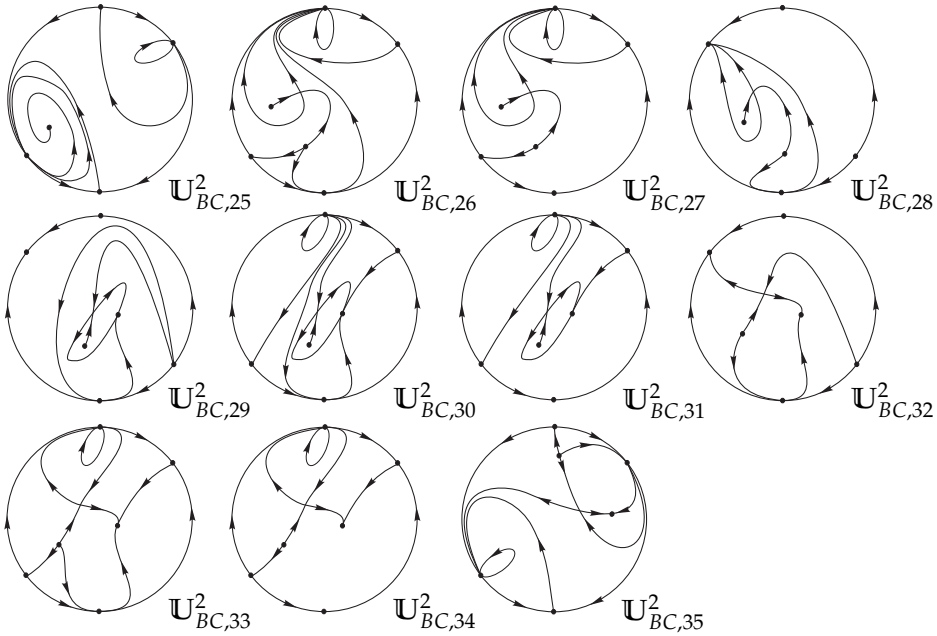


Figure 1.2: *(Cont. of Fig. 1.1)* Structurally unstable quadratic phase portraits of *codimension two** of the set (BC).

Notice that by considering modulo limit cycles, we merge all nests of limit cycles into a single singular point (a focus) within each nest. In other words, the phase portraits are *blind* to the presence of limit cycles. Moreover, the phase portraits do not differentiate between a singular point being a focus or a node, as these distinctions are not topological properties. However, while the phase portraits do not disregard other significant features, such as various types of curves, they do not distinguish between limit cycles and other types of graphics. In Section 5, we discuss the existence of both graphics and limit cycles within this study.

The main goal of this paper is to prove the following result.

Theorem 1.6. *If $X \in \Sigma_2^2(BC)$, then its phase portrait on the Poincaré disc is topologically equivalent, modulo orientation and modulo limit cycles, to one of the 35 phase portraits of Figures 1.1 and 1.2. In addition, among these phase portraits, 16 belong to the set (BC_{SNSN}), whereas the remaining 19 phase portraits belong to the set (BC_{ESNS}).*

This paper is structured as follows. Section 2 provides an overview of codimension-one phase portraits, which are essential for our analysis. Section 3 presents the specific results needed for the proof of Theorem 1.6. Section 4 is devoted to the proof of Theorem 1.6. To validate the realization of the corresponding phase portraits, each of them is computed using the numerical program P4 [2, 20]. Section 5 contains concluding remarks, and Section 6 introduces a definitive notation for all phase portraits of quadratic systems of codimension zero, one, and two obtained so far. In this section, we also assign definitive names to phase portraits presented in previous works using the same technique as in this paper.

2 Quadratic vector fields of codimension one

In this section we summarize the needed results from [5] (quadratic systems of *codimension one**) that are essential here. The following results are the restriction of Theorem 1.1 from

book [5] to the sets (B) and (C) (see page 4). We denote by $\sum_1^2(B)$ and $\sum_1^2(C)$ the set of all structurally unstable vector fields $X \in P_2(\mathbb{R}^2)$ of *codimension one** belonging to the sets (B) and (C), respectively.

Theorem 2.1. *If $X \in \sum_1^2(B)$, then its phase portrait on the Poincaré disc is topologically equivalent modulo orientation and modulo limit cycles to one of the* 40 *phase portraits of Figures 2.1 and 2.2, and all of them are realizable.*

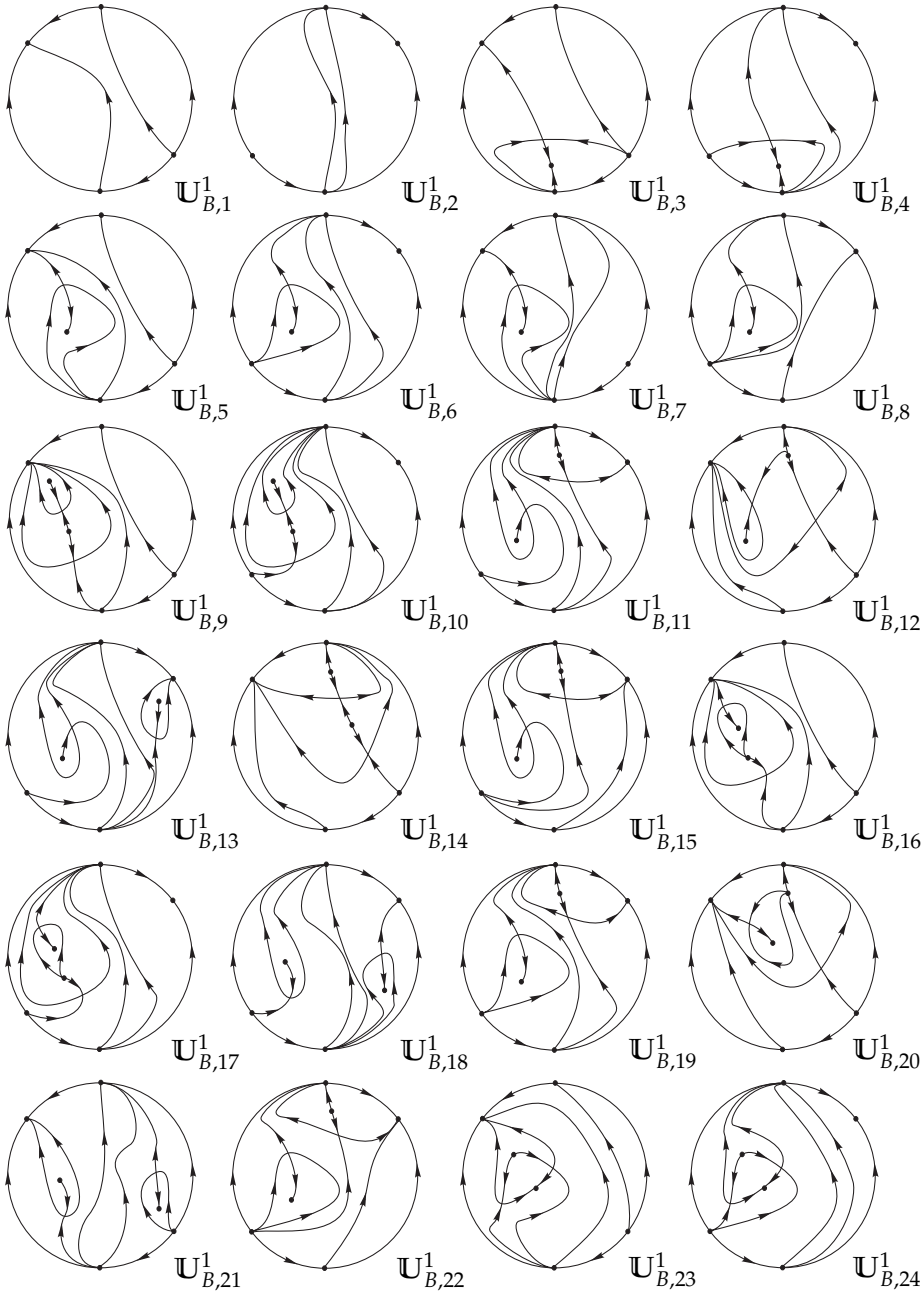


Figure 2.1: Unstable quadratic systems of *codimension one** of the set (B) (cases with an infinite saddle-node of type $\overline{\binom{0}{2}}SN$).

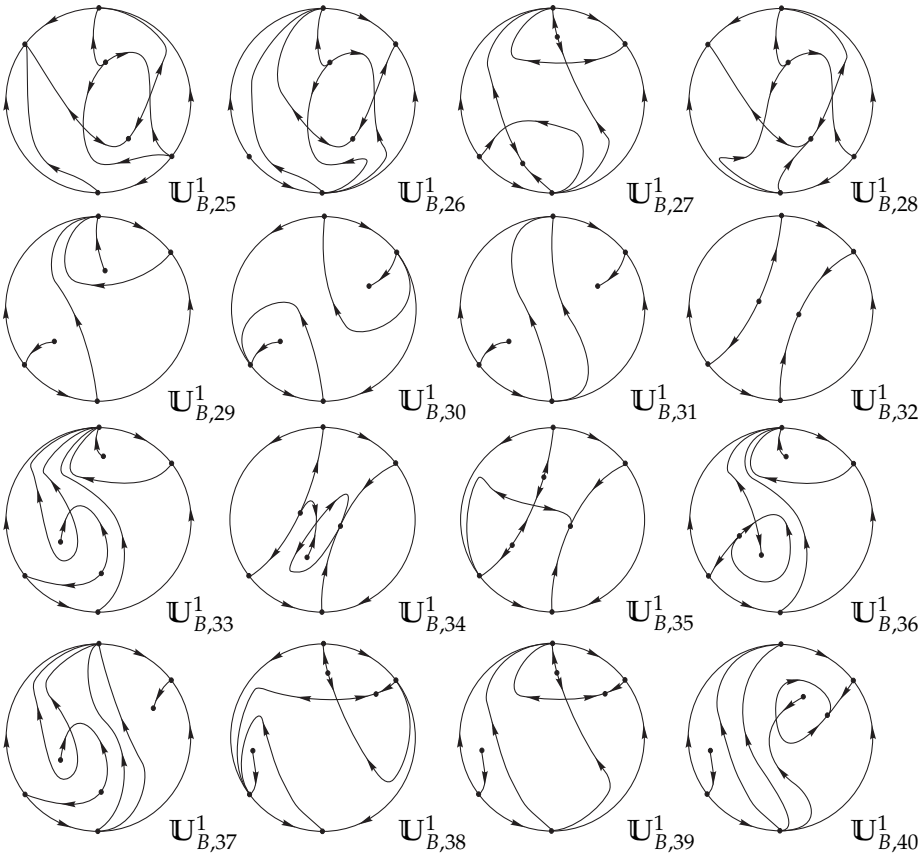


Figure 2.2: *(Cont. of Fig. 2.1)* Unstable quadratic systems of *codimension one** of the set (B) (cases with an infinite saddle-node of type $\overline{\binom{0}{2}}SN$).

Theorem 2.2. *If $X \in \sum_1^2(C)$, then its phase portrait on the Poincaré disc is topologically equivalent modulo orientation and modulo limit cycles to one of the* 32 *phase portraits of Figures 2.3 and 2.4, and all of them are realizable.*

Remark 2.3. It is important to mention that the two mistakes detected in the book [5] of codimension one affect sets (A) and (D), so cases (B) and (C) remain as they were stated on that book.

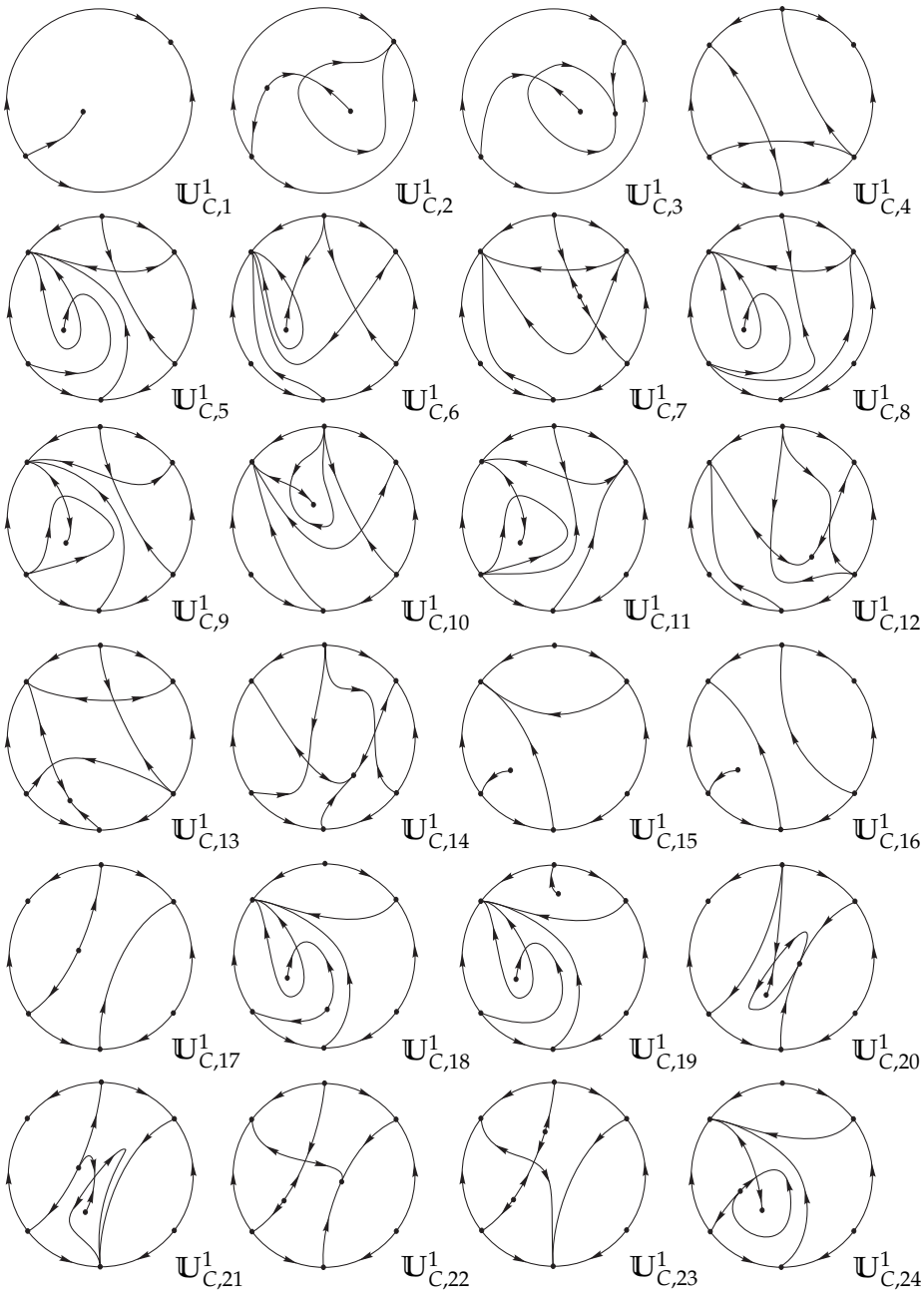


Figure 2.3: Unstable quadratic systems of *codimension one** of the set (C) (cases with an infinite saddle-node of type $\overline{\binom{1}{1}}SN$).

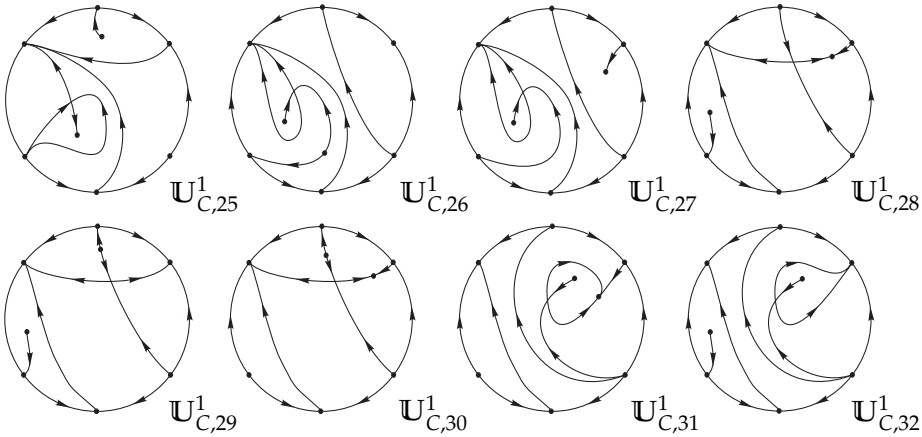


Figure 2.4: *(Cont. of Fig. 2.3)* Unstable quadratic systems of *codimension one** of the set (*C*) (cases with an infinite saddle-node of type $(\overline{1}_1)SN$).

3 Specific results for the proof of Theorem 1.6

In book [5] the authors obtained all the potential phase portraits of codimension one by coalescing a saddle with a node (finite or infinite) for every realizable phase portrait in [3] (plus those phase portraits with a separatrix connection). When one coalesces a saddle and a node, one obtains a semi-elemental saddle-node and this is the most trivial bifurcation by coalescence of singularities. In paper [12] we obtained all the potential phase portraits of classes (AB) and (AC) by coalescing a second couple saddle and node, so, essentially using the same bifurcation. In paper [14] there was a different type of coalescence because the authors considered the turning of a finite saddle-node into a cusp by folding two of its separatrices, which is another known type of bifurcation. In that paper they did not need to consider the cases of semi-elemental triple saddles or nodes because such cases are topologically equivalent to elemental saddles or nodes, respectively. Anyway, the triple semi-elemental saddles (respectively, nodes) are obtained when two saddles and one node (respectively, two nodes and one saddle) coalesce along the same direction of the singularity in the middle. This is another well-known bifurcation. All these mentioned bifurcations behave the same whether the resulting singularity is finite or infinite.

In this section we are going to explain how to produce phase portraits of codimension two from the sets (BC_{SNSN}) and (BC_{ESNS}). We shall see that the type of coalescences needed to produce the phase portraits from the set (BC_{SNSN}) are exactly the same as those explained for sets (B) and (C), but the type of coalescences to produce phase portraits in the set (BC_{ESNS}) are more complicated.

Notice that it is very important for these type of works that one must methodically produce all potential phase portraits, even though some of them cannot be realizable. The construction of all potential phase portraits must be complete and consistent so to be sure that no possibility escapes to this study. Otherwise, we could not claim later that we have all the phase portraits of a determined class. The papers done up to here hold this condition.

But now we are dealing with the coalescence of three elemental singularities to form a nilpotent singularity. Although this is a well-known bifurcation, it is better to describe in detail how an infinite nilpotent singularity is obtained. To do so, we should first consider a finite nilpotent singularity. The following argument applies to any planar differential system, not necessarily polynomial.

In Figure 3.1, we illustrate the formation of a finite nilpotent elliptic-saddle through the coalescence of two nodes and one saddle. As shown in picture (a), we start with one stable node, one unstable node, and a saddle (note that the semi-elemental triple node is formed by two nodes with the same stability). One stable separatrix from the saddle connects to the unstable node, and one unstable separatrix goes to the stable node. Assuming that neither node receives any other separatrix, all the orbits emanating from the unstable node are directed toward the stable one. In picture (b), the three points are shown closer together, and in picture (c), they have already coalesced. Two of the saddle's separatrices, which previously went to the nodes, have disappeared, while the other two persist, forming the hyperbolic sector. The orbits that previously went from one node to the other now form the elliptic sector. If either node had received one or more external separatrices, these would now originate or terminate at the nilpotent singularity, forming parabolic sectors between the hyperbolic and elliptic ones.

The reader might think that an invariant line passing through the nilpotent singularity is missing or find the presence of a non-convex elliptic orbit unusual. However, these features are only required in the case of nilpotent elliptic-saddles in quadratic systems. In higher-degree (or analytic) systems, such constraints do not necessarily apply.

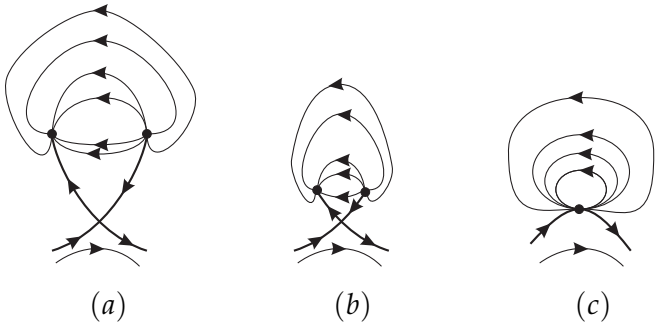


Figure 3.1: Coalescence to form an elliptic-saddle.

In Figure 3.2, we illustrate the formation of a finite nilpotent saddle through the coalescence of two saddles and one node. As shown in picture (a), we begin with one node and two saddles. One stable separatrix from each saddle originates at the unstable node. We emphasize that the separatrices of the saddles do not arrive along the same eigendirection of the node. If they did, the coalescence would cancel only one of the eigenvalues, resulting in a semi-elemental saddle that is tangentially equivalent to an elemental saddle. As the three singularities approach each other, the two eigenvectors of the node coalesce into a single one, and both eigenvalues tend to zero. In the limit, we obtain a sort of one-directional node where both eigenvalues are zero, yet the Jacobian matrix is not identically zero. In picture (b), the three points are depicted much closer together, and in picture (c), they have already coalesced. Of the eight separatrices from the original saddles, the two that previously emanated from the node vanish in the singularity. The two unstable separatrices of the left saddle merge with the two unstable separatrices of the right saddle, forming the two unstable separatrices of the nilpotent saddle. The other two stable separatrices remain unchanged.

Once again, the reader might be surprised not to see an invariant straight line, but this feature is only required in quadratic systems.

Notice that the coalescence of a saddle or a node with a saddle-node is just an intermediate case in each of the two examples previously explained.

Now that we understand how finite elemental singularities coalesce to form nilpotent



(a) (b) (c)

Figure 3.2: Coalescence to form a nilpotent saddle.

ones, we turn to the case of infinite singularities (in this case, the discussion is restricted to polynomial systems). The main difference is that the resulting nilpotent singularity at infinity always has exactly one invariant straight line.

In the case of the nilpotent elliptic-saddle, several configurations are possible: both separatrices may remain on the opposite side of infinity relative to the elliptic sector, or they may both locally align with the line at infinity near the singularity. It is also possible to have an infinite elliptic-saddle with only one affine separatrix.

As for a nilpotent saddle, two of its separatrices must lie along the segment of the line at infinity, while the other two must be affine separatrices. These affine separatrices may lie on the same side of infinity or on opposite sides; however, in the latter case, the singularity must be of higher multiplicity.

For example, the system $x' = y^2 - 5x^3/3$, $y' = -x^2y$ has a nilpotent singularity at $[0 : 1 : 0]$, whose geometric configuration is $H_\lambda H - H_\lambda H$. However, this singularity must have multiplicity at least 5, and its unfolding differs from what is shown in Figure 3.4. In fact, such a singularity results from the coalescence of an odd number (greater than 1) of infinite singularities together with an even number (greater than 0) of finite singularities.

Since we are dealing with quadratic systems, some of the aforementioned possibilities are restricted, as Lemma 3.1 will show.

Although we have already illustrated how three finite elemental singularities can coalesce to form a triple nilpotent singularity, it is also worth showing how an infinite singularity (either a saddle or a node) can coalesce with an infinite semi-elemental saddle-node $\overline{\binom{1}{1}}\,SN$ to form an elliptic-saddle or a nilpotent saddle. This is precisely the procedure we will use to generate all the potential phase portraits under consideration.

We begin with the production of an infinite elliptic-saddle. Consider a configuration consisting of a $\overline{\binom{1}{1}}\,SN$ and an infinite node. The saddle-node has only one affine separatrix, which we place at the "south pole" in Figure 3.3(a). Note that each infinite singularity possesses an eigenvector that is transverse to the line at infinity. In panel (b), the distance between the two singularities is reduced. The orbits in the upper region flow from the unstable node to the nodal part of the saddle-node, making the formation of the future elliptic sector already apparent.

It is important to highlight that the affine eigenvector of the infinite unstable node begins to rotate counterclockwise, while the affine eigenvector of the saddle-node rotates clockwise. This happens because, at the moment of coalescence in (c), there will be a single eigenvector tangent to the line at infinity. In the lower region, the singularities also approach one another, and, mirroring the behavior in the upper region, the eigenvector of the node rotates clockwise, while the eigenvector of the saddle-node (and its corresponding separatrix) rotates counterclockwise. Thus, at coalescence, the separatrix becomes tangent to the line at infinity.

Several configurations may result: if the affine separatrix does not coalesce with the line at

infinity, then a parabolic sector remains on the left, and simultaneously a new separatrix may emerge on the right. Alternatively, the affine separatrix may merge with the line at infinity on the left, with no new separatrix forming on the right (see Figure 3.3(d)). The mixed scenario, where one separatrix coalesces while another appears, is not realizable in quadratic systems, as Lemma 3.1 will demonstrate, though it may occur in higher-degree systems.

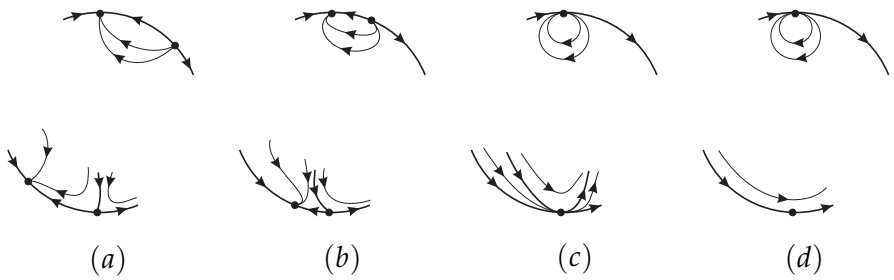


Figure 3.3: Coalescence to form an infinite elliptic-saddle.

We now carry out the analogous construction for the nilpotent infinite saddle. We start with a $\overline{\binom{1}{1}}\,SN$ and an infinite saddle. The saddle-node has only one affine separatrix, which we place at the "south pole" in Figure 3.4(a). As before, note that each infinite singularity has an eigenvector that is transversal to the line at infinity. In panel (b), the distance between the two singularities is reduced.

However, in this case, the affine eigenvector of the infinite saddle (located below) must rotate counterclockwise, while the affine eigenvector of the saddle-node (at the "south pole") must rotate clockwise. This is necessary because, at the moment of coalescence shown in (c), there will be a unique eigenvector tangent to the line at infinity. In the upper region, the singularities also approach each other, and, consistent with the behavior of the affine eigenvectors, the eigenvector of the saddle rotates clockwise, while that of the saddle-node rotates counterclockwise. Thus, at coalescence, the corresponding separatrix must be merged to the infinite line.

If, instead, the separatrix were to remain affine, a parabolic sector would persist at the "north pole", which is not possible in this configuration. Hence, the separatrix must coalesce with the line at infinity. Although this reasoning could already be seen as a proof of statement (3) of Lemma 3.1, we will also provide an algebraic proof for completeness.

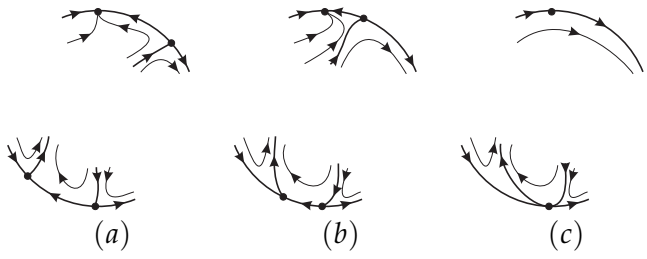


Figure 3.4: Coalescence to form an infinite nilpotent saddle.

Lemma 3.1. *Assume a quadratic system possesses a triple nilpotent singularity at infinity. Then the following statements hold:*

1. *In the case of a nilpotent saddle, both affine separatrices lie on the same side of the line at infinity;*

2. *In the case of an elliptic-saddle, either both affine separatrices lie on the same side of infinity or both are aligned with the line at infinity*[2].

3. *In the case of a nilpotent saddle, if we perturb the system so that the singularity splits into an infinite saddle-node (which must be a semi-elemental saddle-node* $\overline{(1_1)}$ *SN) and an infinite saddle, then the unique affine separatrix of the saddle-node will remain on the same side of infinity as the affine separatrices of the original nilpotent saddle.*

Proof. 1. This follows directly from [8, Diagram 6.7], where all the geometrically different classes of infinite singularities are described. The only occurrences of a nilpotent saddle appear on page 158 with the triple singularity $\widehat{(1_2)}\, H\!\curlywedge HH\!\curlywedge - H$, and on page 159 with the multiplicity five singularity $\widehat{(3_2)}\, H\!\curlywedge HH\!\curlywedge - H$. In both cases, there is another infinite singularity, which is a node. Therefore, the nilpotent saddle has three hyperbolic sectors on one side of infinity and just one on the other. Consequently, the two affine separatrices lie on the same side of infinity.

2. This also follows directly from [8, Diagram 6.7]. The only occurrences of a nilpotent elliptic-saddle appear on page 158 with the options $\widehat{(1_2)}\, \hat{P}\!\curlywedge E\hat{P}\!\curlywedge - H$, $\widehat{(1_2)}\, \hat{P}\!\curlywedge H\hat{P}\!\curlywedge - E$, and $\widehat{(1_2)}\, E - H$, and on page 159 with the multiplicity five case $\widehat{(3_2)}\, \hat{P}\!\curlywedge E\hat{P}\!\curlywedge - H$. These singularities appear in that diagram accompanied by another infinite elemental or semi-elemental singularity. Thus, from the geometric configuration of the singularities, we see that either both affine separatrices lie on the same side of infinity, or both must coincide with the infinite line.

3. Assume that the system has an infinite nilpotent saddle. By means of a rotation, this singularity may be moved to the point $[0 : 1 : 0]$, that is, the origin of the local chart U_2, or simply "the north pole". This is equivalent to considering the coefficient of y^2 in the first equation as zero. The system is then

$$\begin{aligned} \dot{x} &= a + cx + dy + gx^2 + 2hxy, \\ \dot{y} &= b + ex + fy + \ell x^2 + 2mxy + ny^2. \end{aligned} \tag{3.1}$$

Then the system at the local chart U_2 is:

$$\begin{aligned} \dot{w}_0 &= (2h - n)w_0 + dz_0 + (g - 2m)w_0^2 + (c - f)w_0z_0 + az_0^2 - \ell w_0^3 - ew_0^2z_0 - bw_0z_0^2, \\ \dot{z}_0 &= -nz_0 - 2mw_0z_0 - fz_0^2 - \ell w_0^2z_0 - ew_0z_0^2 - bz_0^3. \end{aligned} \tag{3.2}$$

The eigenvalues of the Jacobian matrix at the origin are clearly $2h - n$ and $-n$, while the Jacobian matrix is completed with d. Therefore, in order to have a nilpotent singularity, we need $n = h = 0$ and $d \neq 0$. At this point, the nilpotent singularity may still be any of the possibilities given by [20, Theorem 3.5] (except a cusp, focus, or center for obvious reasons), and one could follow its statements to find the conditions for a saddle. However, it is simpler to extract those conditions from [8, Diagram 6.7], which states that the triple infinite nilpotent saddle requires $\eta = \mu_0 = \kappa = 0$, μ_1, and $\widetilde{M}$ non-zero, with both $\widetilde{K}$ and $\widetilde{L}$ positive. Systems (3.1) with $n = h = 0$ and $d \neq 0$ already satisfy $\eta = \mu_0 = \kappa = 0$, and the rest of the conditions imply $\mu_1 = 4dgm^2x \neq 0$, $\widetilde{M} = -8(g - 2m)^2x^2 \neq 0$, $\widetilde{K} = 4gmx^2 > 0$, and $\widetilde{L} = 8g(g - 2m)x^2 > 0$.

[2]We attempted to construct a higher-degree system exhibiting the alternative possibility (i.e., with only one affine separatrix), but without success. Since this direction falls outside the main scope of the paper, we leave it as an open question.

Assume now that we already have $gm > 0$, $g(g-2m) > 0$, and $d \neq 0$, so we have a triple nilpotent saddle at infinity. Then, in order to determine whether the affine separatrices are at the north pole or at the south pole, one needs to perform the corresponding study using blow-ups, and we will follow the technique described in [8, Section 3.4]. We start from system (3.2).

For these systems, the origin $(0,0)$ is a nilpotent singular point, and $PCD(w_0, z_0) = -dz_0^2 \neq 0$. So, there is no need for a twist, and we can blow up directly with $j = 0$ (no change in time). After the blow-up, we obtain the systems:

$$\begin{aligned}\dot{w}_1 &= z_1^2\left(aw_1^2 - bw_1^3\right) + z_1\left(cw_1^2 + dw_1 - ew_1^3 - fw_1^2\right) - \ell w_1^3 + w_1^2(g-2m),\\ \dot{z}_1 &= -aw_1z_1^3 - z_1^2(cw_1+d) - gw_1z_1,\end{aligned}$$

for which $(0,0)$ is an intricate singular point. Now, $PCD(w_1, z_1) = -2w_1z_1(dz_1 + gw_1 - mw_1)$, and we need to make a k-twist. As explained in [8, Section 3.4 Example 3.1], we can assume $d \neq g - m$ and perform a 1-twist. Otherwise, we simply make a 2-twist for an equivalent result.

Thus, we get

$$\begin{aligned}\dot{w}_2 = {} & w_2\left(-3z_2^3(a+e) - 3bz_2^4 + z_2^2(-3c-3\ell+2f) + z_2(d-3g+4m)\right) +\\ & w_2^2\left(z_2^2(a+3e) + 3bz_2^3 + z_2(c+3\ell-f) + g - 2m\right) + z_2^4(2a+e) +\\ & w_2^3\left(-bz_2^2 - ez_2 - \ell\right) + bz_2^5 + z_2^3(2c+\ell-f) - 2z_2^2(d-g+m),\\ \dot{z}_2 = {} & w_2\left(-az_2^3 - cz_2^2 - gz_2\right) + az_2^4 + cz_2^3 + z_2^2(g-d).\end{aligned}$$

Now we perform a blow-up with $j = 1$ (time reduction of odd order) to obtain:

$$\begin{aligned}\dot{w}_3 = {} & w_3^3\left(z_3^4(2a+e) - 3z_3^3(a+e) + z_3^2(a+3e) - ez_3\right) + w_3^4\left(bz_3^5 - 3bz_3^4 + 3bz_3^3 - bz_3^2\right) +\\ & w_3^2\left(z_3^3(2c+\ell-f) + z_3^2(-3c-3\ell+2f) + z_3(c+3\ell-f) - \ell\right) +\\ & w_3\left(-2z_3^2(d-g+m) + z_3(d-3g+4m) + g - 2m\right),\\ \dot{z}_3 = {} & w_3^2\left(z_3^5(-2a-e) + z_3^4(4a+3e) + z_3^3(-2a-3e) + ez_3^2\right) +\\ & w_3^3\left(-bz_3^6 + 3bz_3^5 - 3bz_3^4 + bz_3^3\right) +\\ & w_3\left(z_3^4(-2c-\ell+f) + z_3^3(4c+3\ell-2f) + z_3^2(-2c-3\ell+f) + \ell z_3\right) +\\ & 2z_3^3(d-g+m) - 2z_3^2(d-2g+2m) - 2z_3(g-m).\end{aligned}$$

The singular points on the straight line $w_3 = 0$ are the solutions of the equation $2z_3^3(d-g+m) - 2z_3^2(d-2g+2m) - 2z_3(g-m) = 0$. So we have three singular points with Jacobian matrices:

Singular point	Corresponding Jacobian matrix
$(0,0)$	$\begin{pmatrix} g-2m & 0 \\ 0 & 2m-2g \end{pmatrix}$;
$(0,1)$	$\begin{pmatrix} -d & 0 \\ 0 & 2d \end{pmatrix}$;
$\left(0, \dfrac{g-m}{g-m-d}\right)$	$\begin{pmatrix} -\dfrac{dm}{d-g+m} & 0 \\ \star & \dfrac{2d(g-m)}{d-g+m} \end{pmatrix}$.

Then, since we have $gm > 0$, $g(g-2m) > 0$ and $d \neq 0$, independently of the sign of d, all three singularities are saddles. The only remaining question is whether the affine separatrices lie in the half-plane $z_0 > 0$ or $z_0 < 0$, which depends on whether $0 < (g-m)/(g-m-d) < 1$ or not. In Figure 3.5, the first row illustrates the case $(g-m)/(g-m-d) < 0$, and the second row shows the case $0 < (g-m)/(g-m-d) < 1$. The case $1 < (g-m)/(g-m-d)$ is equivalent to the first row.

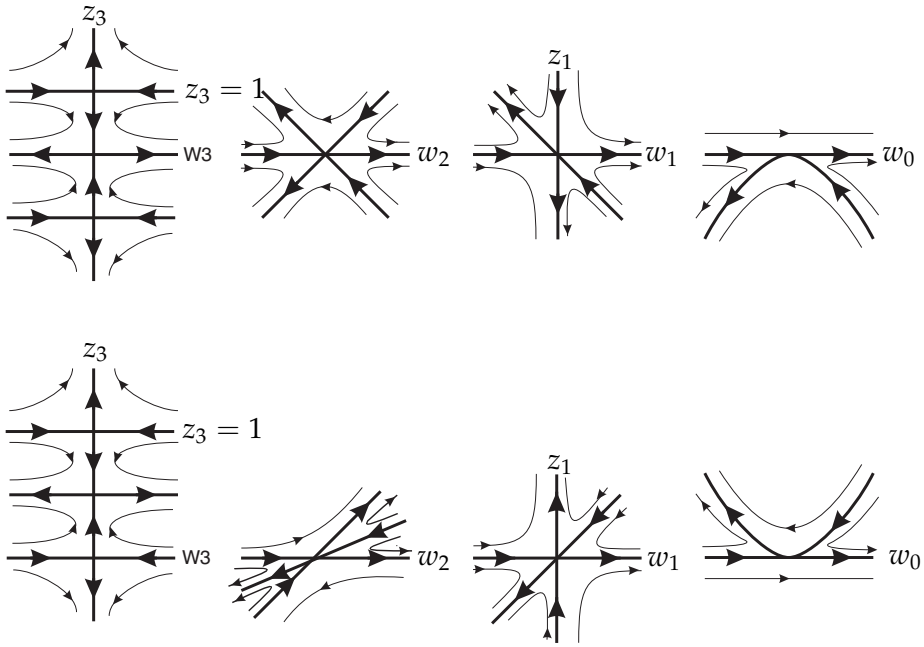


Figure 3.5: Position of separatrices of an infinite nilpotent saddle.

Now we must apply a small perturbation to system (3.1) with $h = n = 0$ and $(g-m)d < 0$, $gm > 0$, and $g(g-2m) > 0$, in order to split the nilpotent saddle at $[0:1:0]$ into a saddle-node that remains at the same location and another infinite singularity. The required perturbation must preserve the second eigenvalue of the infinite singularity as zero (so $n = 0$), but make the first non-zero (so $h = \varepsilon$). Note that it does not matter whether we take ε positive or negative: the new infinite singularity will appear either to the left or right of the original one and will always be a saddle, since the global index must be -1. As $d \neq 0$, we may, via a time rescaling, assume $d = 1$. Then the affine separatrices of the nilpotent saddle will lie at the "north pole" if $g < m < 0$. We start from the system

$$\begin{aligned} \dot{x} &= a + cx + y + gx^2 + 2\varepsilon xy, \\ \dot{y} &= b + ex + fy + \ell x^2 + 2mxy, \end{aligned} \tag{3.3}$$

and the system in the local chart U_2 is

$$\begin{aligned} \dot{w}_0 &= az_0^2 + w_0\left(-bz_0^2 + z_0(c-f) + 2\varepsilon\right) + dz_0 + w_0^2(-ez_0 + g - 2m) - \ell w_0^3, \\ \dot{z}_0 &= -bz_0^3 + w_0\left(-ez_0^2 - 2mz_0\right) - \ell w_0^2 z_0 - fz_0^2. \end{aligned} \tag{3.4}$$

Now we need to apply in full detail [20, Theorem 2.19] to system (3.4), not to establish that the origin is a saddle-node (we already know this) but to determine the exact position of the separatrix associated with the zero eigenvalue. To obtain the normal form given in [20, Theorem 2.19], we first perform the change $w_0 \leftrightarrow z_0$, along with a twist (this could be

done simultaneously, but presenting it this way is clearer), as illustrated in the first row of Figure 3.6. We already know that the direction $z_0 = 0$, corresponding to the infinite line, is invariant and composed of unstable separatrices, but there is another eigenvector whose role remains unclear: on which side its separatrix lies, its orbit orientation, and whether it even forms an invariant line. After making the two aforementioned changes and rewriting the system into the normal form of the theorem, we obtain the system:

$$\begin{aligned}
\dot{w}_2 = & -\frac{w_2^3\left(4b\varepsilon^2+d^2\ell-2de\varepsilon\right)}{8\varepsilon^3}+w_2^2\left(-\frac{z_2(e\varepsilon-d\ell)}{4\varepsilon^3}-\frac{f\varepsilon-dm}{2\varepsilon^2}\right)\\
& +w_2\left(-\frac{\ell z_2^2}{8\varepsilon^3}-\frac{mz_2}{2\varepsilon^2}\right),\\
\dot{z}_2 = & \, w_2^2\left(\frac{4a\varepsilon^2-2cd\varepsilon+d^2g}{4\varepsilon^2}-\frac{z_2\left(4b\varepsilon^2+d^2\ell-2de\varepsilon\right)}{8\varepsilon^3}\right)\\
& +w_2\left(\frac{z_2(c\varepsilon-dg+dm-f\varepsilon)}{2\varepsilon^2}-\frac{z_2^2(e\varepsilon-d\ell)}{4\varepsilon^3}\right)-\frac{\ell z_2^3}{8\varepsilon^3}+\frac{z_2^2(g-2m)}{4\varepsilon^2}+z_2.
\end{aligned} \tag{3.5}$$

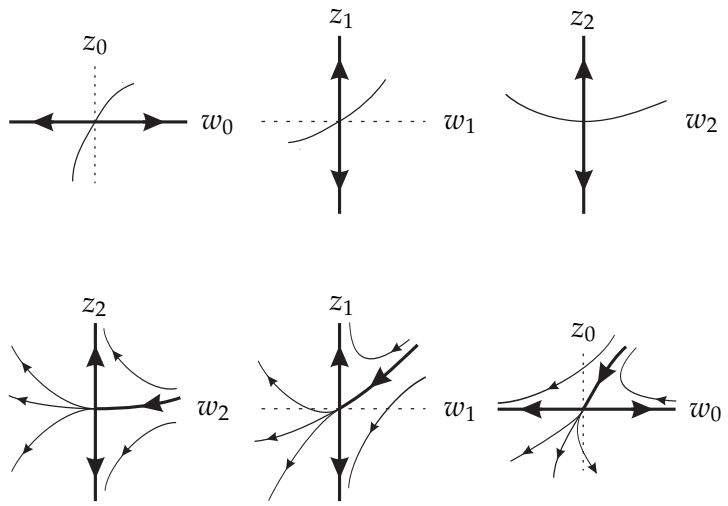


Figure 3.6: Study of the saddle-node.

Applying [20, Theorem 2.19], we observe that the coefficient determining on which side the flow along the center manifold is attractive or repelling is the coefficient of w_2^2 in the first equation, namely $(dm - f\varepsilon)/(2\varepsilon^2)$. For sufficiently small ε (regardless of its sign), this expression has the same sign as dm, which is negative. Therefore, the saddle-node is attractive on the right-hand side and repelling on the left-hand side. As a result, the hyperbolic sectors lie on the right, while the parabolic sectors lie on the left. Reversing the changes that led to this form, we conclude from the second row of Figure 3.6 that the separatrix not lying on the line at infinity must belong to the half-plane $z_0 > 0$, thereby completing the proof of the lemma.

□

Corollary 3.2. *If (in a quadratic system) an infinite node coalesces with an infinite* $\overline{\binom{1}{1}}$ *SN, one must consider two possibilities: either the resulting elliptic-saddle has two affine separatrices on the same side of infinity as the affine separatrix of the saddle-node, or there are no affine separatrices. If (in a quadratic system) an infinite saddle coalesces with an infinite* $\overline{\binom{1}{1}}$ *SN, there will always be two affine separatrices on the same side of infinity as the affine separatrix of the saddle-node.*

After producing the coalescence of the infinite singularity with the infinite saddle-node $\overline{\binom{1}{1}}\,SN$ (thus moving from a system of set (B) to one of set (BC)), we also want to unfold the system of set (BC) into systems of set (C). That is, we aim to eject one finite singularity from the nilpotent infinite singularity and leave at infinity another saddle-node, this time of type $\overline{\binom{0}{2}}\,SN$.

The next lemma describes how this may occur.

Lemma 3.3. *Assume a quadratic system with a triple nilpotent singularity at infinity. Consider a perturbation that changes the second eigenvalue to be nonzero. Then the following statements hold:*

1. *In the case of a nilpotent saddle, the finite singularity that appears is always located on the side where the affine separatrices were.*

2. *In the case of an elliptic-saddle, the finite singularity that appears is always located on the side where the elliptic sector was.*

3. *For a nilpotent saddle, the finite saddle that appears captures one of the affine separatrices of the original nilpotent saddle. Specifically, if this saddle is moved back to infinity (i.e., coalesces with the infinite singularity), one of its separatrices becomes an affine separatrix of the nilpotent saddle. The other three separatrices behave as follows: one terminates at the singularity, another escapes along the infinite line, and the third coalesces with the separatrix of the infinite saddle-node, forming the other affine separatrix of the nilpotent saddle (see Figure 3.7). Thus, one separatrix of the finite saddle originates from the parabolic sector of the infinite saddle-node. Its opposite separatrix heads toward the same singularity that the corresponding affine separatrix of the nilpotent saddle did. The remaining two separatrices are directed toward the same antisaddle that the infinite separatrix and the other affine separatrix of the nilpotent saddle previously went to (assuming there was no separatrix connection before unfolding). The second affine separatrix of the nilpotent saddle becomes the separatrix of the saddle-node, which is now transversal to infinity. On the opposite side of infinity, a new affine separatrix appears, whose stability depends on the unfolding. Consequently, there are two possible unfoldings of this type.*

4. *For an elliptic-saddle, the finite antisaddle that appears may be either an attractor or a repellor, depending on which side of the elliptic sector it unfolds. If any separatrix from another source was previously arriving at that side of the elliptic-saddle, it will now terminate at the new antisaddle, as will the separatrix of the infinite saddle-node that remains at infinity. Thus, whether the antisaddle acts as an attractor or a repellor determines the stability of the saddle-node separatrix and the nature of the parabolic sector (see Figure 3.8). If the elliptic-saddle originally had no affine separatrix, a new one appears on the opposite side of infinity with stability matching the unfolding. If the elliptic-saddle already had two separatrices on the other side of infinity, the one with the appropriate stability remains. Therefore, there are also two possible unfoldings of this type.*

Remark 3.4. The unfolding from set (BC) to (B) is slightly more complicated than the unfolding to (C). For this reason, we also attempted to coalesce finite singularities with the $\overline{\binom{1}{1}}\,SN$ in a consistent way, ensuring that all possible configurations were considered. Nevertheless, by performing the unfolding from set (BC) to (B), the reverse process also becomes clear. Throughout this study, we considered both possible directions of the unfolding and ultimately chose the one presented here for simplicity.

Remark 3.5. A focus may also emerge from an infinite nilpotent elliptic-saddle, potentially surrounded by one or more limit cycles. However, this situation, modulo limit cycles, is already covered by our lemma and does not require further analysis.

Proof of Lemma 3.3. 1. As shown in the proof of the previous lemma, a nilpotent saddle at infinity has its affine separatrices located at the "north pole" when the conditions $gm > 0$, $g(g-2m) < 0$, and $0 < (g-m)/(g-m-d) < 1$ hold. To perform a perturbation of system (3.2) such that the second eigenvalue becomes nonzero, we set $n = \varepsilon$. However, since this perturbation also affects the first eigenvalue, we must set $h = \varepsilon/2$ in order to compensate and keep the first eigenvalue equal to zero. For simplicity in the proof, and since $d \neq 0$, we perform a time rescaling and assume $d = 1$. This assumption leads directly to the condition $g - 2m < 0$.

Then the system in the local chart U_2 is

$$\begin{aligned} \dot{w}_0 &= z_0 + az_0^2 + w_0\left(z_0(c-f) - bz_0^2\right) + w_0^2(-ez_0 + g - 2m) - \ell w_0^3 := W(w_0, z_0), \\ \dot{z}_0 &= -z_0\varepsilon - bz_0^3 + w_0\left(-ez_0^2 - 2mz_0\right) - fz_0^2 - \ell w_0^2 z_0 := Z(w_0, z_0). \end{aligned} \tag{3.6}$$

To determine where the finite singularity moves, we solve the system $W(w_0, z_0) = Z(w_0, z_0) = 0$ in the form of power series. Specifically, we consider two power series

$$f_w(\varepsilon) = \sum_{i=1}^{\infty} a_i \varepsilon^i, \quad f_z(\varepsilon) = \sum_{i=1}^{\infty} b_i \varepsilon^i, \tag{3.7}$$

and substitute them into the system to obtain

$$W\big(f_w(\varepsilon), f_z(\varepsilon)\big) = \sum_{i=1}^{\infty} c_i \varepsilon^i, \quad Z\big(f_w(\varepsilon), f_z(\varepsilon)\big) = \sum_{i=1}^{\infty} d_i \varepsilon^i.$$

By expanding, we obtain the following relations: $d_1 = 0$, $c_1 = b_1$, and $d_2 = -b_1 - b_1^2 f$, which immediately implies $b_1 = 0$ and $d_2 = 0$. Proceeding, we compute

$$c_2 = b_2 + a_1^2(g - 2m), \quad d_3 = -b_2(1 + 2a_1 m).$$

Setting $c_2 = d_3 = 0$ yields two possible solutions: either $a_1 = b_2 = 0$, corresponding to the trivial singularity at $(w_0, z_0) = (0, 0)$, or

$$(a_1, b_2) = \left(-\frac{1}{2m}, \frac{2m - g}{4m^2}\right).$$

Thus, for $|\varepsilon| \ll 1$, the leading term of the ordinate of the singularity is

$$\frac{2m - g}{4m^2}\varepsilon^2,$$

which is positive. Therefore, the singularity lies in the half-plane $z_0 > 0$, precisely where the affine separatrices of the saddle were located.

2. The case of the nilpotent elliptic-saddle is almost identical to that of the nilpotent saddle, with a few exceptions. The invariant conditions for the existence of a nilpotent elliptic-saddle are

$$\eta = \mu_0 = \kappa = 0, \quad \mu_1 \neq 0, \quad \widetilde{M} \neq 0,$$

together with either $\widetilde{K} < 0$ or $\widetilde{K} > 0$ and $\widetilde{L} < 0$.

In order to determine whether the elliptic sector lies in the half-plane $z_0 > 0$ or $z_0 < 0$, we perform the same sequence of blow-ups as in Figure 3.5, with the difference that the singularity at $(0, (g-m)/(g-m-d))$ is now a node instead of a saddle. Nevertheless, the condition for the elliptic sector to be located in $z_0 > 0$ remains the same, namely

$$0 < \frac{g-m}{g-m-d} < 1.$$

Furthermore, this condition, combined with any of the requirements for the existence of an elliptic-saddle, also implies that $g - 2m < 0$.

Since the solution of the system $W(w_0, z_0) = Z(w_0, z_0) = 0$ in terms of power series is the same regardless of whether the original singularity is a nilpotent saddle or a nilpotent elliptic-saddle, the conclusion is that in this case, the finite singularity also appears on the same side where the elliptic sector was located.

3. Consider Figure 3.7(a). We aim to unfold a finite saddle from the nilpotent saddle. After the unfolding, a $\overline{\binom{1}{1}}\,SN$ remains at infinity. This type of saddle-node possesses separatrices on both sides of infinity. Consequently, the new finite saddle unfolds from the nilpotent saddle "along" one of its former affine separatrices. The orbit that connects the new saddle to the infinite saddle-node is no longer a separatrix of the infinite point, but rather of the finite saddle. The opposite separatrix of the finite saddle must go to the same singularity that the corresponding affine separatrix of the nilpotent saddle previously approached (assuming there was no separatrix connection that might break during the unfolding). The other affine separatrix of the nilpotent saddle now becomes the separatrix of the saddle-node at infinity. This separatrix is no longer tangent to the line at infinity, since the new infinite singularity has two distinct eigenvectors. Depending on which separatrix the new saddle chooses to unfold along, the resulting configuration corresponds either to Figure 3.7(b) or (c). In case (b), the saddle-node has an attractor parabolic sector, while in case (c) the parabolic sector is a repellor. The other two separatrices of the finite saddle unfold from the infinite line and from the separatrices of the nilpotent saddle. These orbits evolve following the limiting behavior defined by the separatrices from which they originate. On the opposite side of infinity, an additional separatrix unfolds from the infinite line, with stability matching the corresponding configuration.

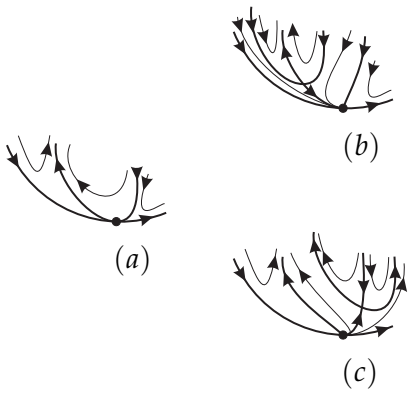


Figure 3.7: Unfolding of an infinite nilpotent saddle.

4. Consider Figure 3.8(a) and (b). We aim to unfold a finite antisaddle from the nilpotent elliptic-saddle. After the unfolding, a $\overline{\binom{1}{1}}\,SN$ remains at infinity. This type of saddle-node

possesses separatrices on both sides of infinity. The unfolding antisaddle may be either stable (an attractor) or unstable (a repellor). The saddle-node remaining at infinity must then have its parabolic sector with the opposite stability of the unfolding antisaddle, in order to preserve the structure of the set of orbits unfolding from the elliptic sector. Depending on the stability of the antisaddle, the separatrix from the infinite saddle-node must acquire the corresponding stability, which leads to the configurations shown in Figures 3.8(c) or (d). On the opposite side of infinity, the behavior depends on whether there were affine separatrices before the unfolding: if there were (case (a)), one separatrix disappears; if there were none (case (b)), a new separatrix appears. This separatrix must have the opposite stability to the one on the other side of infinity, as is characteristic of the $\overline{\binom{1}{1}}$ SN in polynomial systems of even degree.

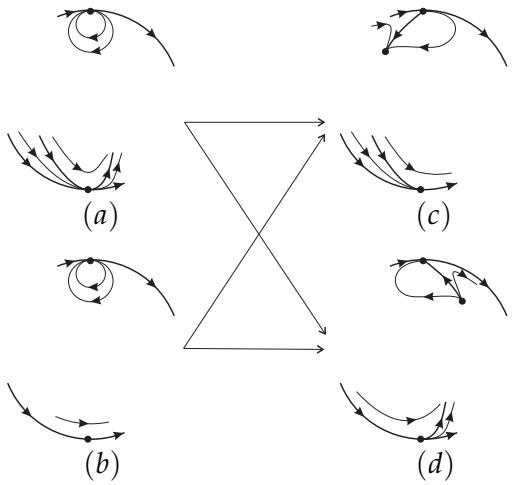


Figure 3.8: Unfolding of an infinite elliptic-saddle.

□

When studying the realization of phase portraits from the set (BC), the results presented below play a crucial role as analytical tools.

Lemma 3.6 ([5, Lemma 3.1])**.** *Any straight line has at most two contact points (counting multiplicities) with the orbits of a quadratic system, unless the straight line itself is a trajectory.*

In [5], the following classical result from Coppel [17] is mentioned:

Lemma 3.7 ([17, Theorem 6])**.** *If a quadratic vector field has a limit cycle, then in its interior there is exactly one singular point, which is a focus or a center.*

The next result is claimed to follow from it by a similar proof:

Lemma 3.8. *If a quadratic vector field has a loop or a cycle of separatrices, then in its interior there is exactly one singular point, which is a focus.*

This lemma was accepted in [5], where all singularities are at most semi-elemental. However, it is not valid in general. The correct generalization that can be derived from Lemma 3.7 is as follows:

Lemma 3.9. *If a quadratic vector field has a graphic, then in its interior there is at most one singular point, which is either a focus or a center. If there is no singularity in the interior, then exactly one of the singularities forming part of the graphic has a single elliptic sector.*

Proof. If there are singularities inside the graphic, the proof of Lemma 3.7 applies directly. If there are none, it is because a focus has collided with one of the singularities that make up the graphic, giving rise to an elliptic sector at that point. □

We also highlight the following result:

Corollary 3.10 ([5, Corollary 3.29])**.** *If one of the structurally stable vector fields that bifurcates from a potentially structurally unstable vector field of* codimension one* *is not realizable, then the unstable system itself is also not realizable.*

As an application of this result, we can easily prove the following lemma, which will be useful later.

Lemma 3.11. *The phase portraits* $\mathbb{U}^{1,I}_{B,a}$, $\mathbb{U}^{1,I}_{B,b}$, *and* $\mathbb{U}^{1,I}_{B,c}$, *shown in Figure 3.9, are impossible.*

Proof. The phase portraits $\mathbb{U}^{1,I}_{B,a}$, $\mathbb{U}^{1,I}_{B,b}$, and $\mathbb{U}^{1,I}_{B,c}$ feature an infinite saddle-node $\overline{\binom{0}{2}}$ *SN* (see page 4). In the second column of phase portraits in Figure 3.9, we observe the corresponding structurally stable bifurcations obtained by splitting the multiple infinite singularity.

These bifurcations are listed as impossible in [3, Figure 5.83]. Therefore, by Corollary 3.10, the impossibility of the original phase portraits follows. □

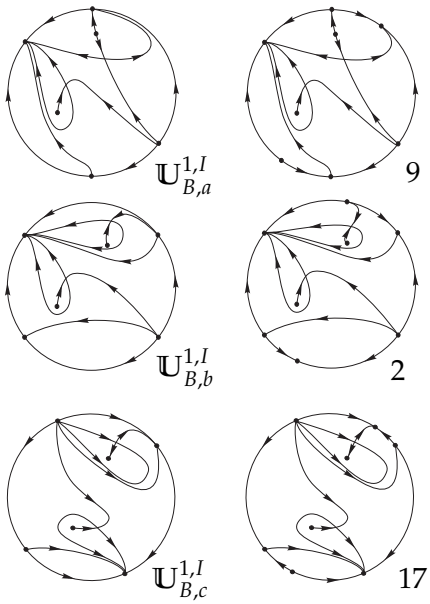


Figure 3.9: Impossibility of phase portraits $\mathbb{U}^{1,I}_{B,a}$, $\mathbb{U}^{1,I}_{B,b}$, and $\mathbb{U}^{1,I}_{B,c}$.

The following theorem is the analogue of Corollary 3.10 for the set (BC).

Theorem 3.12. *If a* codimension-one* *phase portrait that bifurcates from a potential* codimensiontwo* *phase portrait in the set (BC) is not realizable, then the* codimension-two* *phase portrait is also not realizable.*

Proof. We will prove the contrapositive statement: if a potential *codimension-two** phase portrait X from the set (BC) is realizable, then all *codimension-one** phase portraits that bifurcate from X are also realizable. Since the set (BC) is the disjoint union of the sets (BC_{SNSN}) and (BC_{ESNS}), we must prove this for each case. Both proofs will rely on Invariant Theory, as detailed in [8].

We begin with the set (BC_{SNSN}). Recall from page 4 that a realizable phase portrait belongs to this set if and only if it possesses the infinite saddle-nodes $\overline{\binom{1}{1}}SN$ and $\overline{\binom{0}{2}}SN$. We must show that any such phase portrait can be perturbed to yield a resulting phase portrait in either set (B) or set (C). This will be demonstrated using specific normal forms.

First, we demonstrate the existence of a perturbation that preserves the infinite saddle-node $\overline{\binom{1}{1}}SN$ while splitting the saddle-node $\overline{\binom{0}{2}}SN$ (or moving it to the complex plane). In [11], using Invariant Theory, the authors classified all real quadratic polynomial differential systems possessing a finite semi-elemental saddle-node $\overline{sn}_{(2)}$ at the origin and an infinite saddle-node $\overline{\binom{1}{1}}SN$ on the y-axis. This classification was performed with respect to the normal form

$$\begin{cases} \dot{x} = cx + cy - cx^2 + 2hxy, \\ \dot{y} = ex + ey - ex^2 + 2mxy, \end{cases} \tag{3.8}$$

where c, h, e, and m are real parameters satisfying the non-degeneracy condition $eh \neq cm$. The four-dimensional parameter space of this normal form can be projectivized; in that paper, the authors showed that all generic phenomena occur for $h = 1$. For normal form (3.8), the authors calculated

$$\mu_0 = 0, \quad \mu_1 = -4(eh - cm)^2 x \neq 0, \quad \mathbf{D} = 0, \quad \mathbf{P} \neq 0,$$

which, according to [8, Diagram 6.1], implies that these systems have one double and one simple real finite singular point. Furthermore, since the invariant polynomial

$$\eta = 4h^2[(c + 2m)^2 - 8eh]$$

is generically non-zero, it follows from [8, Diagram 6.2] that the systems have an infinite saddle-node $\overline{\binom{1}{1}}SN$ and two simple infinite singularities (real or complex). We now set $h = 1$. To ensure that the phase portraits of this family also possess an infinite saddle-node $\overline{\binom{0}{2}}SN$, we must impose the condition $\eta = 0$, which yields

$$e = \frac{(c + 2m)^2}{8}.$$

Our goal is to obtain phase portraits belonging to the set (BC_{SNSN}). To do this, we must split the finite saddle-node $\overline{sn}_{(2)}$ into a saddle and a node, or move it to the complex plane. Consider the normal form (3.8) with $h = 1$ and $e = (c + 2m)^2/8$. We introduce a perturbation by adding a parameter ε to the first equation, obtaining the system

$$\begin{cases} \dot{x} = \varepsilon + cx + cy - cx^2 + 2xy, \\ \dot{y} = \left((c + 2m)^2/8\right) x + \left((c + 2m)^2/8\right) y - \left((c + 2m)^2/8\right) x^2 + 2mxy. \end{cases} \tag{3.9}$$

For this system, if $\varepsilon > 0$, the finite saddle-node splits into a saddle and a node; if $\varepsilon < 0$, it moves to the complex plane. Indeed, a direct calculation for system (3.9) shows that

$$\mu_0 = 0, \quad \mu_1 \neq 0, \quad \mathbf{D} \neq 0, \quad \eta = 0, \quad \widetilde{M} \neq 0, \quad \kappa \neq 0.$$

According to [8, Diagrams 6.1 and 6.3], these conditions indicate that system (3.9) has simple finite singularities (real or complex) and, at infinity, the two saddle-nodes $\overline{\binom{1}{1}}SN$ and $\overline{\binom{0}{2}}SN$, as expected. To complete the proof of the contrapositive statement for the set (BC_{SNSN}), we must further perturb system (3.9) to obtain phase portraits belonging to the set (C).

We now apply a rotational perturbation, controlled by a small parameter α, to system (3.9):

$$\begin{cases} \dot{x} = \varepsilon + cx + cy - cx^2 + 2xy + \alpha\left[\dfrac{(c+2m)^2}{8}x + \dfrac{(c+2m)^2}{8}y - \dfrac{(c+2m)^2}{8}x^2 + 2mxy\right], \\ \dot{y} = \dfrac{(c+2m)^2}{8}x + \dfrac{(c+2m)^2}{8}y - \dfrac{(c+2m)^2}{8}x^2 + 2mxy. \end{cases}$$

For a sufficiently small α, computations show that

$$\mu_0 = 0, \quad \mu_1 \neq 0, \quad \mathbf{D} \neq 0, \quad \eta \neq 0.$$

These invariants imply that the perturbation preserves the finite singularities and the infinite saddle-node $\overline{\binom{1}{1}}SN$, but eliminates the infinite saddle-node $\overline{\binom{0}{2}}SN$.

More precisely, the outcome depends on the sign of $\alpha(c-2m)$. If $\alpha(c-2m) > 0$, the saddle-node $\overline{\binom{0}{2}}SN$ splits into an infinite saddle and an infinite node. Conversely, if $\alpha(c-2m) < 0$, it is replaced by two complex infinite singular points. And once known the sign of $c - 2m \neq 0$, α may be elected with one or another sign so to obtain the desired bifurcation. Notice also that, if $c = 2m$, then

$$\mu_0 = \mu_1 = \mu_2 = \mu_3 = 0,$$
$$\mu_4 = 4m^2\varepsilon^2x^2(y - mx)^2.$$

So, for $\varepsilon = 0$ we have a degenerate system and we are not in the set (BC).

Next, we prove the existence of a perturbation that splits the infinite saddle-node $\overline{\binom{1}{1}}SN$ while preserving $\overline{\binom{0}{2}}SN$. In [15], the authors used Invariant Theory to show that any system with a finite semi-elemental saddle-node $\overline{sn}_{(2)}$ (with eigenvectors on the coordinate axes and with the eigenvector associated with the zero eigenvalue on the horizontal axis) and an infinite saddle-node $\overline{\binom{0}{2}}SN$ located in the endpoints of the bisector of the first and third quadrants can be transformed, via affine transformations and time rescaling, into the normal form

$$\begin{cases} \dot{x} = gx^2 + 2hxy + (n - g - 2h)y^2, \\ \dot{y} = y + \ell x^2 + (2g + 2h - 2\ell - n)xy + (2h + \ell + 2(n - g - 2h))y^2, \end{cases} \tag{3.10}$$

where g, h, ℓ, and n are real parameters with $g \neq 0$. The four-dimensional parameter space of this normal form can be projectivized, and the authors proved that all generic phenomena occur for $g = 1$. For this normal form, the authors calculated

$$\mu_0 = n^2(-(g-\ell)(g+2h+\ell) + gn), \quad \mathbf{D} = 0, \quad \mathbf{T} \neq 0,$$

which implies, by [8, Diagram 6.1], that these systems have one double and two simple finite singular points (real or complex). Since $\eta = 0$ and $\widetilde{M} \neq 0$, the systems also have an infinite saddle-node $\overline{\binom{0}{2}}SN$ and one real simple infinite singularity. To ensure the phase portraits also have an infinite saddle-node $\overline{\binom{1}{1}}SN$, we must impose the condition $\mu_0 = 0$, which yields

$$h = \frac{g(n-g) + \ell^2}{2(g-\ell)}.$$

Our goal is to obtain phase portraits in the set (BC$_{SNSN}$). First, we must split the finite saddle-node $\overline{sn}_{(2)}$. Considering normal form (3.10) with $g = 1$ and $h = (n-1+\ell^2)/(2(1-\ell))$, we introduce a perturbation ε in the second equation:

$$\begin{cases} \dot{x} = x^2 + 2hxy + (n-1-2h)y^2, \\ \dot{y} = \varepsilon + y + \ell x^2 + (2+2h-2\ell-n)xy + (2h+\ell+2(n-1-2h))y^2. \end{cases} \tag{3.11}$$

If $\varepsilon < 0$, the finite saddle-node splits into a saddle and a node; if $\varepsilon > 0$, it moves to the complex plane. A calculation for system (3.11) shows that

$$\mu_0 = 0, \quad \mu_1 \neq 0, \quad \mathbf{D} \neq 0, \quad \eta = 0, \quad \widetilde{M} \neq 0, \quad \kappa \neq 0.$$

As expected, these results from [8, Diagrams 6.1 and 6.3] confirm that the system possesses simple finite singularities and, at infinity, both saddle-nodes $\overline{\binom{1}{1}}SN$ and $\overline{\binom{0}{2}}SN$.

To complete the proof, we must perturb system (3.11) to obtain phase portraits belonging to the set (B). This can be achieved by perturbing the parameter h so that $\mu_0 \neq 0$. We replace $h = (n-1+\ell^2)/(2(1-\ell))$ with

$$h = \frac{n-1+\ell^2}{2(1-\ell)} + \beta,$$

where β is a sufficiently small parameter. This yields the perturbed system

$$\begin{cases} \dot{x} = x^2 + 2hxy + (n-1-2h)y^2, \\ \dot{y} = \varepsilon + y + \ell x^2 + (2+2h-2\ell-n)xy + (2h+\ell+2(n-1-2h))y^2. \end{cases} \tag{3.12}$$

For this system, a computation shows that

$$\mu_0 \neq 0, \quad \mathbf{D} \neq 0, \quad \eta = 0, \quad \widetilde{M} \neq 0.$$

These invariants imply that the perturbation preserves the infinite saddle-node $\overline{\binom{0}{2}}SN$ but eliminates $\overline{\binom{1}{1}}SN$. Specifically, if $\beta > 0$, the saddle-node $\overline{\binom{1}{1}}SN$ releases a saddle into the finite part of the plane. If $\beta < 0$, it releases a node. In either case, the resulting phase portrait belongs to the set (B).

There are two more nongeneric cases for this case whose proof is a simple reduction of what we have done.

This completes the proof of the contrapositive statement for the set (BC$_{SNSN}$).

Finally, we address the set (BC$_{ESNS}$). In [13], the authors showed that this set consists of phase portraits possessing either three distinct real finite singular points or one real and two complex finite singular points. They used the notation $\mathbf{Q\widehat{ES}}(\mathbf{A})$ to denote the former class and $\mathbf{Q\widehat{ES}}(\mathbf{B})$ for the latter. To prove the contrapositive statement for the set (BC$_{ESNS}$), we must demonstrate its validity for both of these subclasses.

We begin with the class $\mathbf{Q\widehat{ES}}(\mathbf{A})$. In [13], the authors proved that any nondegenerate quadratic system possessing three real finite singular points, in addition to either an infinite nilpotent elliptic-saddle or an infinite nilpotent saddle, can be transformed via affine transformations and time rescaling into the normal form

$$\begin{cases} x' = cx + y - cx^2, \\ y' = ex + \left(\dfrac{e+f}{c} - 1\right) y - ex^2 + 2xy, \end{cases} \tag{3.13}$$

where the parameters $c \in \mathbb{R} \setminus \{0\}$, $f \in \mathbb{R}^+ \cup \{0\}$, and $e \in \mathbb{R}$ describe the class $\mathbf{Q\widehat{ES}}(\mathbf{A})$. For these systems, a calculation shows that

$$\mu_0 = 0, \quad \mu_1 \neq 0, \quad \mathbf{D} \neq 0, \quad \eta = 0, \quad \widetilde{M} \neq 0, \quad \kappa = 0.$$

These results confirm that the phase portraits of system (3.13) have three distinct real finite singular points. At infinity, they exhibit a singular point formed by the coalescence of one finite singular point with two infinite ones.

We now apply the following perturbation, controlled by a small parameter γ, to system (3.13):

$$\begin{cases} x' = cx + y - cx^2 + 2\gamma xy, \\ y' = ex + \left(\dfrac{e+f}{c} - 1\right) y - ex^2 + 2xy + 2\gamma y^2. \end{cases}$$

For a sufficiently small γ, a calculation shows that

$$\mu_0 \neq 0, \quad \mathbf{D} \neq 0, \quad \eta = 0, \quad \widetilde{M} \neq 0.$$

These invariants imply that, at infinity, the perturbed system has a saddle-node $\overline{\binom{0}{2}}SN$ and another simple singular point. Therefore, the resulting phase portrait belongs to the set (B).

Alternatively, we can apply the following rotational perturbation to system (3.13), controlled by a small parameter λ:

$$\begin{cases} x' = cx + y - cx^2 + \lambda \left[ex + \left(\dfrac{e+f}{c} - 1\right) y - ex^2 + 2xy\right], \\ y' = ex + \left(\dfrac{e+f}{c} - 1\right) y - ex^2 + 2xy, \end{cases}$$

where the parameters c, f, and e are as defined previously. For a sufficiently small λ, a calculation shows that

$$\mu_0 = 0, \quad \mu_1 \neq 0, \quad \mathbf{D} \neq 0, \quad \eta \neq 0.$$

These invariants imply that, at infinity, the perturbed system now possesses a saddle-node $\overline{\binom{1}{1}}SN$ along with two other simple singular points. Consequently, the resulting phase portrait belongs to the set (C).

Finally, we consider the class $\mathbf{Q\widehat{ES}}(\mathbf{B})$. In [13], the authors proved that any nondegenerate quadratic system with one real and two complex finite singular points, in addition to either an infinite nilpotent elliptic-saddle or an infinite nilpotent saddle, can be transformed via affine transformations and time rescaling into the normal form

$$\begin{cases} x' = -2gux + g(1+u^2)y + gx^2, \\ y' = -2(\ell u - 1)x + \ell(1+u^2)y + \ell x^2 - 2xy, \end{cases} \tag{3.14}$$

where the parameters $g \in \mathbb{R} \setminus \{0\}$, $u \in \mathbb{R}^+ \cup \{0\}$, and $\ell \in \mathbb{R}$ describe the class $\mathbf{Q\widehat{ES}}(\mathbf{B})$. For these systems, a calculation shows that

$$\mu_0 = 0, \quad \mu_1 \neq 0, \quad \mathbf{D} > 0, \quad \eta = 0, \quad \widetilde{M} \neq 0, \quad \kappa = 0.$$

As confirmed by $\mathbf{D} > 0$, these results show that the phase portraits of system (3.14) possess one real and two complex finite singular points. At infinity, they exhibit a singular point formed by the coalescence of one finite singular point with two infinite ones.

We now introduce a perturbation controlled by a small parameter δ:

$$\begin{cases} x' = -2gux + g(1+u^2)y + gx^2 + \delta xy, \\ y' = -2(\ell u - 1)x + \ell(1+u^2)y + \ell x^2 - 2xy + \delta y^2, \end{cases}$$

where g, u, and ℓ are as previously defined. For a sufficiently small δ, a calculation shows that

$$\mu_0 \neq 0, \quad \mathbf{D} \neq 0, \quad \eta = 0, \quad \widetilde{M} \neq 0.$$

These invariants imply that, at infinity, the perturbed system has a saddle-node $(\overline{\begin{smallmatrix}0\\2\end{smallmatrix}})SN$ and a simple singular point. Therefore, the resulting phase portrait belongs to the set (B).

Alternatively, we can apply a rotational perturbation to system (3.14), controlled by a small parameter ψ:

$$\begin{cases} x' = -2gux + g(1+u^2)y + gx^2 + \psi\left[-2(\ell u - 1)x + \ell(1+u^2)y + \ell x^2 - 2xy\right], \\ y' = -2(\ell u - 1)x + \ell(1+u^2)y + \ell x^2 - 2xy, \end{cases}$$

where the parameters g, u, and ℓ are as previously defined. For a sufficiently small ψ, a calculation shows that

$$\mu_0 = 0, \quad \mu_1 \neq 0, \quad \mathbf{D} > 0, \quad \eta \neq 0.$$

These invariants imply that, at infinity, the system possesses a saddle-node $(\overline{\begin{smallmatrix}1\\1\end{smallmatrix}})SN$ along with two other simple singular points. Consequently, the resulting phase portrait belongs to the set (C).

This shows that the contrapositive statement also holds for the set (BC_{ESNS}), which completes the proof of the theorem. □

The following remark introduces a key notion for our study.

Remark 3.13. When a *codimension-two** phase portrait is obtained from a *codimension-one** phase portrait, we say that the former is an "evolution" of the latter (see [12, Remark 2.13]).

Therefore, to prove Theorem 1.6, we must first find all phase portraits in the set (BC) that are evolutions of the *codimension-one** phase portraits from sets (B) and (C). As explained on page 5, such phase portraits are potentially realizable in the set (BC), but their realizability must be verified independently.

Following this strategy in our study led to an interesting situation, which we describe next.

3.1 A tricky limit cycle

Among the various types of singularity coalescence, we encountered a complex case that requires a detailed explanation. Our analysis begins with the phase portrait V_{16} from [13]. This phase portrait is shown in Figure 3.10, alongside five of its neighbors within the family of quadratic differential systems that have an infinite elliptic-saddle. The figure is an expanded version of [13, Fig. 15], supplemented with two additional phase portraits. All of these phase portraits are generated by the normal form:

$$\begin{cases} \dot{x} = -2gux + g(1+u^2)y + gx^2, \\ \dot{y} = -2(\ell u - 1)x + \ell(1+u^2)y + \ell x^2 - 2xy. \end{cases} \tag{3.15}$$

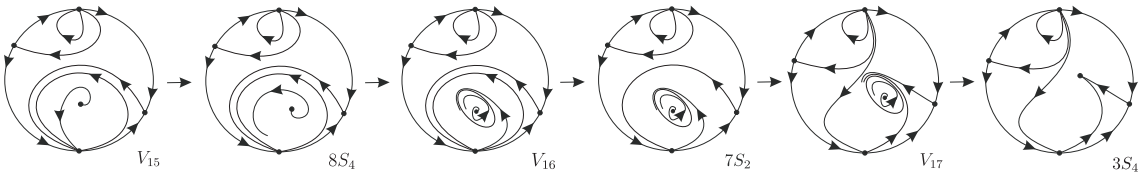


Figure 3.10: Some neighbors of V_{16} inside the family with an infinite elliptic-saddle, see [13].

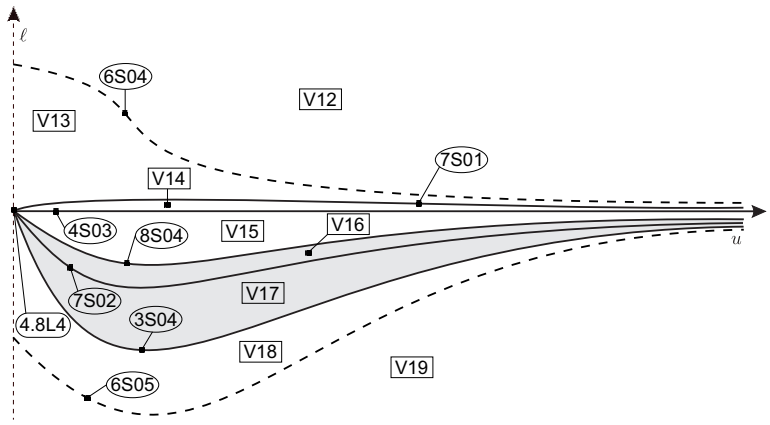


Figure 3.11: Bifurcation diagram for $g = -3/2$ of systems (3.15) (the gray region indicates that the phase portraits have a limit cycle, see the original colored picture in [13, Figure 16]).

Figure 3.11, taken from [13, Figure 16], shows the bifurcation diagram for systems (3.15) with $g = -3/2$. This value represents a generic slice of the 3-dimensional bifurcation diagram; any value of $g \in (-2, -1)$ yields a topologically equivalent diagram. Our analysis focuses on the half-plane where $\ell < 0$.

The bifurcations labeled $8S_4$, $3S_4$, and $6S_5$ are defined by algebraic curves. More precisely:

- The curve $8S_4$ is part of the surface $S_8 : \ell - 2u - 2gu + \ell u^2 = 0$. It corresponds to the existence of an invariant parabola formed by the two affine separatrices of the elliptic-saddle;
- The curve $3S_4$ is part of the surface $S_3 : 2g^2(1+u^2)(-\ell + 2gu - \ell u^2)(4 - 8g + 4g^2 + \ell^2 - 4\ell u + 4u^2 + 2\ell^2 u^2 - 4\ell u^3 + \ell^2 u^4) = 0$. This bifurcation occurs when the finite focus becomes weak of the first order;
- The curve $6S_5$ is part of the surface S_6, which governs the conversion of the finite anti-saddle from a focus to a node. As this curve is not relevant to the present argument, we omit its lengthy polynomial expression.

In contrast, the curve $7S_2$ is not algebraic. It corresponds to a separatrix connection between the stable affine separatrix of the elliptic-saddle and the unstable separatrix of the infinite elemental saddle. It is known from [13] that this curve lies between $8S_4$ and $3S_4$. Numerical checks confirm that it is significantly closer to $8S_4$ than the figure might suggest. While such diagrams are topologically accurate, they are not always drawn to scale, in order to improve visual clarity.

To generate a sequence of phase portraits similar to those in Figure 3.10, one can fix a value for u and vary ℓ in the interval between the bifurcation curves $8S_4$ and $3S_4$. Intuitively,

the most logical approach would be to select a value of $u \in (\sqrt{3}/2, 1)$ near the minima of both curves, where the distance between them is maximal.

However, this reasoning is flawed because the crucial distance is between the curves $8S_4$ and $7S_2$. For instance, when $u = 1$, the bifurcation $8S_4$ occurs at $\ell = -1/2$, while the $7S_2$ bifurcation occurs at $\ell \approx -0.50003$. While this narrow interval is sufficient to corroborate the phase portraits in Figure 3.10, it is too small to permit a numerical analysis of the system's unfolding using the P4 software.

If we select a smaller value, such as $u = 1/2$, the parameter range corresponding to the V_{16} region becomes $\ell \in (-0.40033\ldots, -0.4)$. This larger interval makes it feasible to analyze the unfolding of system (3.15) into the perturbed system (3.16):

$$\begin{cases} \dot{x} = -2gux + g(1+u^2)y + gx^2 + \varepsilon xy, \\ \dot{y} = -2(\ell u - 1)x + \ell(1+u^2)y + \ell x^2 - 2xy. \end{cases} \tag{3.16}$$

The addition of the term εxy to the first equation of system (3.16) perturbs the infinite elliptic-saddle at $[0:1:0]$. The first eigenvalue of this singularity becomes non-zero, while the second remains null. This means an infinite node bifurcates from the elliptic-saddle, while the south pole persists as a saddle-node of the type $\overline{\binom{1}{1}}\,SN$. Specifically, if $\varepsilon < 0$, a stable node bifurcates to the left of the south pole, and the saddle-node has a stable separatrix; if $\varepsilon > 0$, an unstable node bifurcates to the right, and the saddle-node has an unstable separatrix; in both cases, the limit cycle clearly persists. We focus on the case $\varepsilon < 0$, where a numerical puzzle arose: simulations with the P4 software initially suggested that the original hyperbolic limit cycle vanished during the unfolding. This result was confounding, as it would contradict the well-established principle that hyperbolic limit cycles persist under small perturbations [36, Theorem 4.5]. Clearly, a different explanation was required.

This prompted us to select a different parameter value, $u = 1/8$. Although the distance between the bifurcation curves $8S_4$ and $3S_4$ is smaller for this value, the crucial distance between $8S_4$ and $7S_2$ is larger. For $u = 1/8$, the parameter range for the V_{16} region is $\ell \in (-8/65 - 0.064\ldots, -8/65)$, and the limit cycle is significantly smaller than it was for $u = 1/2$. With this setup, applying a relatively large perturbation, such as $\varepsilon = -0.04$, reveals a crucial phenomenon (using P4): the original, small limit cycle coexists with a new, much larger limit cycle located near the stable separatrix of the infinite saddle-node. This large limit cycle is generated from the graphic formed by the stable separatrix of the original elliptic-saddle and it exists for any $-1 \ll \varepsilon < 0$. As $|\varepsilon|$ increases, the small limit cycle grows and the large limit cycle shrinks, until they merge and annihilate in a double limit cycle bifurcation. Numerical checks confirm that for $\varepsilon = -0.1$, both limit cycles have vanished.

The appearance of this large limit cycle can be explained by analogy. In the unperturbed phase portrait V_{16}, the graphic formed by the stable separatrix is obstructed by an internal unstable separatrix, which prevents the formation of a Poincaré return map. This mechanism is not unprecedented; a similar situation occurs with the homoclinic loop of a finite saddle-node (denoted as graphic F_2^1 in [21]), which is formed when the center manifold of the saddle-node connects to its own parabolic sector. There, the bifurcation that eliminates the saddle-node also removes the internal separatrix, forcing a limit cycle to emerge from the former loop (see Figure 3.12). In the present case, the singularity does not disappear but instead splits into a saddle and a node. This splitting similarly eliminates the internal unstable separatrix of the original elliptic-saddle, freeing the graphic to form a limit cycle.

This phenomenon can also be viewed from the reverse direction. Consider the coalescence of an infinite node with a saddle-node of the type $\overline{\binom{1}{1}}\,SN$ to form an elliptic-saddle with a local

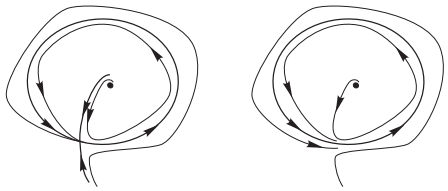


Figure 3.12: Bifurcation of a saddle-node with a graphic F_2^1.

structure similar to that in V_{16}. For this to occur, the system must already possess two limit cycles prior to the coalescence, often created through a double limit cycle bifurcation. During the coalescence, one of these limit cycles is destroyed in the formation of the elliptic-saddle's graphic, while the other survives. A system that cannot generate these two limit cycles before the coalescence will not exhibit this behavior.

To illustrate, if we had chosen $\ell = -0.1$ (corresponding to phase portrait V_{15}, which has no limit cycles) instead of a value in the V_{16} range, the perturbation in (3.16) for $-1 \ll \varepsilon < 0$ would not necessarily create any limit cycles. However, starting exactly on the bifurcation boundary at $\ell = -8/65$ (the $8S_4$ portrait), a suitable simultaneous perturbation of the form $-1 \ll \varepsilon < 0$ and $\ell = -8/65 + f(\varepsilon)$ can generate the required two cycles.

Thus, when considering an evolution from class (C) to class (BC) where infinite singularities coalesce to form a graphic around a focus, it is crucial to verify that the system can support two pre-existing limit cycles.

Remark 3.14. The P4 software is sufficiently reliable to prove the existence of these two limit cycles. The large size of the limit cycles does not pose a computational issue, as the program integrates the vector field using an appropriate local chart that minimizes the magnitude of the coordinates. Alternatively, one could compute the vector field in the local chart U_2 and repeat the analysis on a system where the limit cycles are contained within a small, bounded region. This highlights that the phenomenon is not exclusively related to infinite singularities, as it can also occur in the affine plane, for instance, in cubic systems.

4 Proof of Theorem 1.6

In this section, we prove Theorem 1.6. We begin by deriving all topologically potential phase portraits for the set (BC_{SNSN}) in Subsection 4.1, and for the set (BC_{ESNS}) in Subsection 4.2. During this analysis, we prove that several potential portraits are non-realizable. Finally, in Subsection 4.3, we provide the explicit realizations for the 35 remaining phase portraits that constitute the theorem's classification.

4.1 The topologically potential phase portraits from the set (BC_{SNSN})

The main goal of this subsection is to obtain all topologically potential phase portraits from the set (BC_{SNSN}).

Recall that phase portraits in the set (BC_{SNSN}) are of *codimension two** and are characterized by the presence of two infinite saddle-nodes: $\binom{\overline{0}}{2}SN$ and $\binom{\overline{1}}{1}SN$. A phase portrait in this set can be considered an evolution from a *codimension-one** portrait in either set (B) or set (C). However, since the order of evolution does not matter (i.e., the set of evolutions from (B) and then (C) is the same as from (C) and then (B)), the analysis can be simplified. It is sufficient to

consider only one evolutionary path: starting from phase portraits in set (C), which already contain a $\overline{\binom{1}{1}}SN$, and inducing a bifurcation to create the $\overline{\binom{0}{2}}SN$.

We therefore begin with the 32 realizable, structurally unstable quadratic vector fields of *codimension one** from the set (C). To obtain a phase portrait in (BC$_{SNSN}$), we induce a bifurcation that creates a $\overline{\binom{0}{2}}SN$ by coalescing an infinite saddle with an infinite node, while the existing $\overline{\binom{1}{1}}SN$ is preserved. Conversely, this process can be reversed: a phase portrait in (BC$_{SNSN}$) can be perturbed, causing the $\overline{\binom{0}{2}}SN$ to split into an infinite saddle and an infinite node (or into complex singularities), thereby returning the system to a *codimension-one** state in the set (C).

We introduce the following notation. A topologically potential phase portrait of *codimension two** from the set (BC) will be denoted by $\mathbb{U}^2_{BC,k}$, for $k \in \{1,\dots,16\}$. Phase portraits that are determined to be impossible will be denoted by $\mathbb{U}^{2,I}_{BC,j}$, for $j \in \mathbb{N}$.

We begin by eliminating phase portraits from set (C) that cannot evolve into a phase portrait in (BC$_{SNSN}$). Phase portraits $\mathbb{U}^1_{C,1}$ to $\mathbb{U}^1_{C,3}$ are excluded because they have only one infinite singularity, which is insufficient to form a second saddle-node. Similarly, phase portraits $\mathbb{U}^1_{C,4}$ to $\mathbb{U}^1_{C,14}$ are excluded; although they possess two infinite singularities in addition to the existing $\overline{\binom{1}{1}}SN$, both are nodes. Since the formation of a $\overline{\binom{0}{2}}SN$ requires the coalescence of a saddle and a node, these portraits cannot produce the desired evolution.

The remaining 18 phase portraits, $\mathbb{U}^1_{C,15}$ to $\mathbb{U}^1_{C,32}$, each possess one infinite saddle and one infinite node, in addition to the $\overline{\binom{1}{1}}SN$. Therefore, a coalescence of this saddle and node can produce exactly one evolution into the set (BC$_{SNSN}$) for each candidate. This gives a total of 18 topologically potential phase portraits, which we now analyze individually.

As a first example, the phase portrait $\mathbb{U}^1_{C,15}$ has $\mathbb{U}^2_{BC,1}$ as its evolution. Perturbing the resulting $\mathbb{U}^2_{BC,1}$ by causing the $\overline{\binom{0}{2}}SN$ to split into two complex singularities yields the phase portrait $\mathbb{U}^1_{C,1}$ (modulo limit cycles). Figure 4.1 illustrates this relationship, showing $\mathbb{U}^1_{C,15}$, $\mathbb{U}^2_{BC,1}$, and $\mathbb{U}^1_{C,1}$, respectively. This presentation format will be used for all subsequent figures in this subsection.

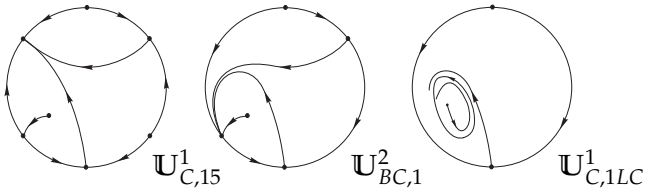


Figure 4.1: Unstable system $\mathbb{U}^2_{BC,1}$.

Remark 4.1. Whenever a phase portrait has a limit cycle, we will place the corresponding label in the figure followed by the letters LC to emphasize the presence of the limit cycle, as in the drawing $\mathbb{U}^1_{C,1LC}$. However, in the text, we will simply write $\mathbb{U}^1_{C,1}$.

The phase portrait $\mathbb{U}^1_{C,16}$ evolves into $\mathbb{U}^2_{BC,2}$ (see Figure 4.2). Subsequently, perturbing $\mathbb{U}^2_{BC,2}$ by causing the infinite saddle-node $\overline{\binom{0}{2}}SN$ to split into complex singularities yields the phase portrait $\mathbb{U}^1_{C,1}$.

The phase portrait $\mathbb{U}^1_{C,17}$ evolves into $\mathbb{U}^2_{BC,3}$ (see Figure 4.3). Subsequently, perturbing $\mathbb{U}^2_{BC,3}$ by causing the infinite saddle-node $\overline{\binom{0}{2}}SN$ to split into complex singularities yields the phase portrait $\mathbb{U}^1_{C,1}$.

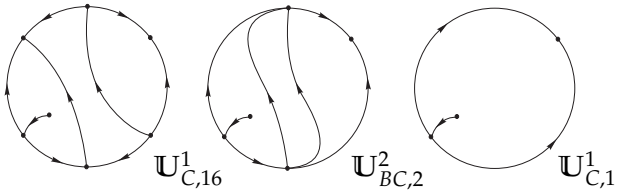


Figure 4.2: Unstable system $\mathbb{U}^2_{BC,2}$.

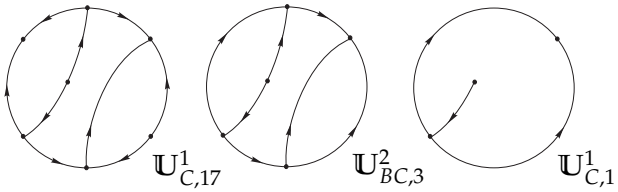


Figure 4.3: Unstable system $\mathbb{U}^2_{BC,3}$.

The evolution of phase portrait $\mathbb{U}^1_{C,18}$ results in $\mathbb{U}^{2,I}_{BC,1}$. This potential portrait is impossible due to the presence of a graphic that violates Lemma 3.9.

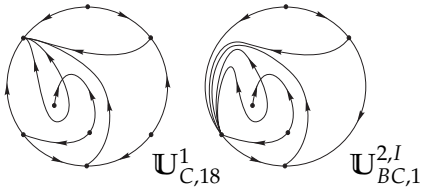


Figure 4.4: Impossible unstable phase portrait $\mathbb{U}^{2,I}_{BC,1}$.

Table 4.1 summarizes the evolutions of phase portraits $\mathbb{U}^1_{C,19}$ through $\mathbb{U}^1_{C,23}$. The first column lists the initial phase portrait from set (C). The second column shows its evolution into a portrait in set (BC) after the formation of a $\binom{\overline{0}}{2}SN$. The third column displays the resulting phase portrait (modulo limit cycles) after this saddle-node is removed by a subsequent perturbation. The final column provides a reference to the figure illustrating this sequence.

Table 4.1: Phase portraits from the set (BC) obtained by evolution of phase portraits $\mathbb{U}^1_{C,19}$ to $\mathbb{U}^1_{C,23}$ from the set (C).

Phase portrait from the set (C)	**Phase portrait from the set (BC)**	**Phase portrait from the set (C)**	**Figure**
$\mathbb{U}^1_{C,19}$	$\mathbb{U}^2_{BC,4}$	$\mathbb{U}^1_{C,3}$	Figure 4.5
$\mathbb{U}^1_{C,20}$	$\mathbb{U}^2_{BC,5}$	$\mathbb{U}^1_{C,3}$	Figure 4.6
$\mathbb{U}^1_{C,21}$	$\mathbb{U}^2_{BC,6}$	$\mathbb{U}^1_{C,2}$	Figure 4.7
$\mathbb{U}^1_{C,22}$	$\mathbb{U}^2_{BC,7}$	$\mathbb{U}^1_{C,3}$	Figure 4.8
$\mathbb{U}^1_{C,23}$	$\mathbb{U}^2_{BC,8}$	$\mathbb{U}^1_{C,2}$	Figure 4.9

The evolution of phase portrait $\mathbb{U}^1_{C,24}$ results in $\mathbb{U}^{2,I}_{BC,2}$ (see Figure 4.10). This potential portrait is impossible due to the presence of a graphic that violates Lemma 3.9.

Table 4.2 summarizes the analysis for the remaining phase portraits, $\mathbb{U}^1_{C,25}$ through $\mathbb{U}^1_{C,32}$, following the same format as Table 4.1. This concludes the topological classification of the set (BC_{SNSN}).

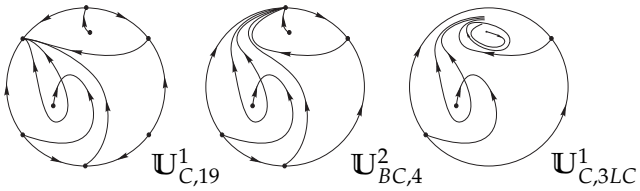


Figure 4.5: Unstable system $\mathbb{U}^2_{BC,4}$.

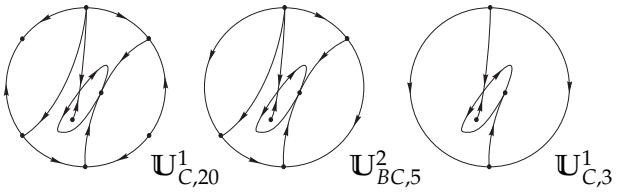


Figure 4.6: Unstable system $\mathbb{U}^2_{BC,5}$.

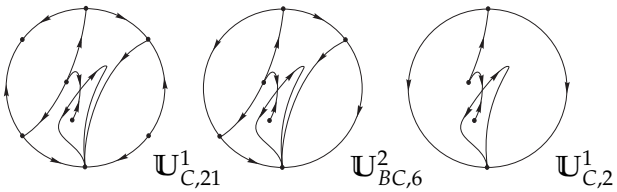


Figure 4.7: Unstable system $\mathbb{U}^2_{BC,6}$.

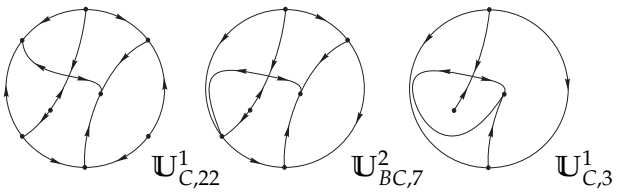


Figure 4.8: Unstable system $\mathbb{U}^2_{BC,7}$.

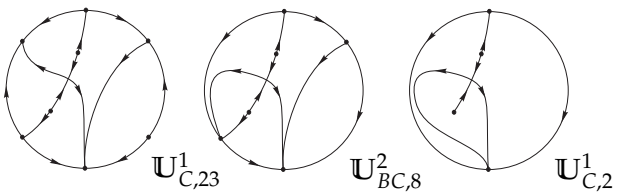


Figure 4.9: Unstable system $\mathbb{U}^2_{BC,8}$.

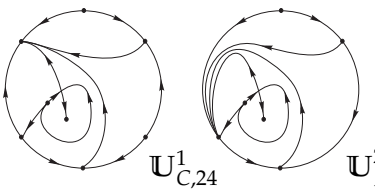


Figure 4.10: Impossible unstable phase portrait $\mathbb{U}^{2,I}_{BC,2}$.

4.2 The topologically potential phase portraits from the set (BC_{ESNS})

The main goal of this subsection is to derive all topologically potential phase portraits for the set (BC_{ESNS}). Recall that the *codimension-two** unstable structures in this set are an infinite nilpotent elliptic-saddle or an infinite nilpotent saddle.

Table 4.2: Phase portraits from the set (BC) obtained by evolution of phase portraits $\mathbb{U}^1_{C,25}$ to $\mathbb{U}^1_{C,32}$ from the set (C).

Phase portrait from the set (C)	**Phase portrait from the set (BC)**	**Phase portrait from the set (C)**	**Figure**
$\mathbb{U}^1_{C,25}$	$\mathbb{U}^2_{BC,9}$	$\mathbb{U}^1_{C,2}$	Figure 4.11
$\mathbb{U}^1_{C,26}$	$\mathbb{U}^2_{BC,10}$	$\mathbb{U}^1_{C,2}$	Figure 4.12
$\mathbb{U}^1_{C,27}$	$\mathbb{U}^2_{BC,11}$	$\mathbb{U}^1_{C,3}$	Figure 4.13
$\mathbb{U}^1_{C,28}$	$\mathbb{U}^2_{BC,12}$	$\mathbb{U}^1_{C,2}$	Figure 4.14
$\mathbb{U}^1_{C,29}$	$\mathbb{U}^2_{BC,13}$	$\mathbb{U}^1_{C,2}$	Figure 4.15
$\mathbb{U}^1_{C,30}$	$\mathbb{U}^2_{BC,14}$	$\mathbb{U}^1_{C,3}$	Figure 4.16
$\mathbb{U}^1_{C,31}$	$\mathbb{U}^2_{BC,15}$	$\mathbb{U}^1_{C,3}$	Figure 4.17
$\mathbb{U}^1_{C,32}$	$\mathbb{U}^2_{BC,16}$	$\mathbb{U}^1_{C,2}$	Figure 4.18

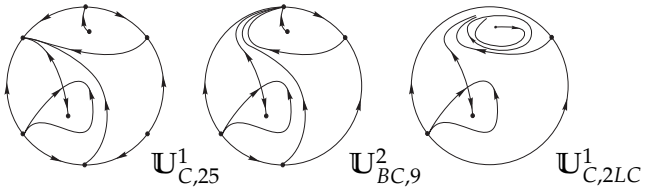


Figure 4.11: Unstable system $\mathbb{U}^2_{BC,9}$.

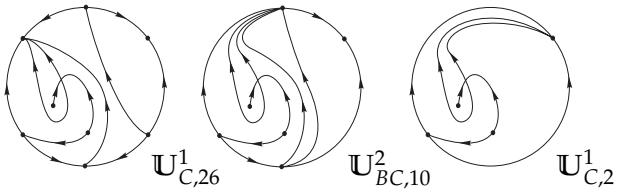


Figure 4.12: Unstable system $\mathbb{U}^2_{BC,10}$.

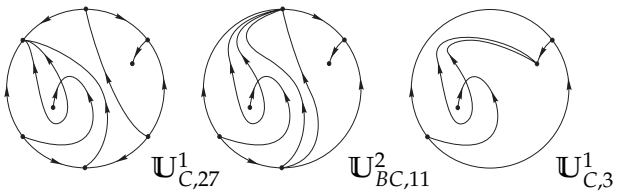


Figure 4.13: Unstable system $\mathbb{U}^2_{BC,11}$.

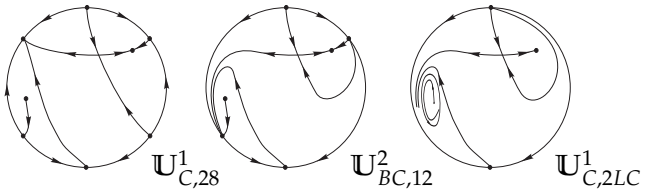


Figure 4.14: Unstable system $\mathbb{U}^2_{BC,12}$.

It is known from [6, Diagram 3], via Invariant Theory, that the formation of either of these structures requires the following conditions on the invariant polynomials:

$$\eta = 0, \quad \widetilde{M} \neq 0, \quad \mu_0 = 0, \quad \mu_1 \neq 0, \quad \kappa = 0.$$

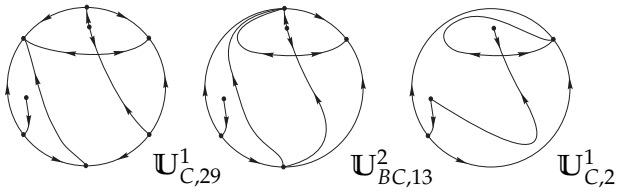


Figure 4.15: Unstable system $\mathbb{U}^2_{BC,13}$.

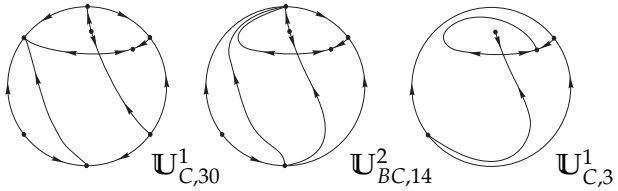


Figure 4.16: Unstable system $\mathbb{U}^2_{BC,14}$.

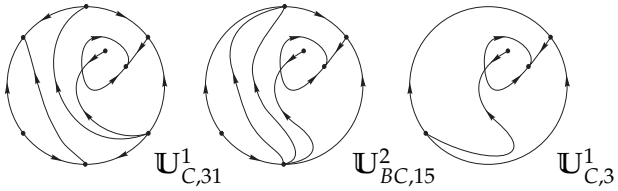


Figure 4.17: Unstable system $\mathbb{U}^2_{BC,15}$.

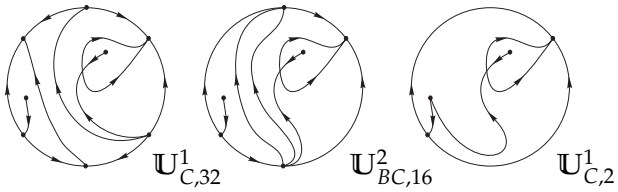


Figure 4.18: Unstable system $\mathbb{U}^2_{BC,16}$.

Geometrically, these conditions imply that these specific infinite singularities are formed by the coalescence of three singular points: one finite and two infinite. In the same reference, the authors also used the polynomial invariants $\widetilde{K}$, $\widetilde{L}$, and $\widetilde{N}$ to classify all possible configurations of infinite singular points that can arise. Their main result in this regard is summarized in Table 4.3 and Figure 4.19.

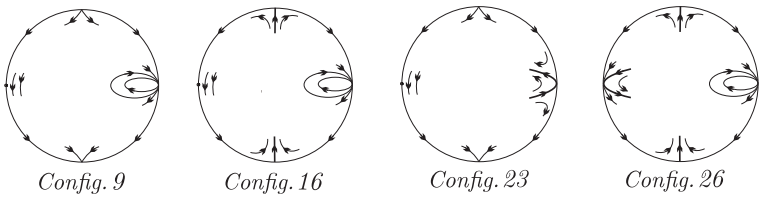


Figure 4.19: Configurations of infinite singularities (see also [6, Figure 6]).

Remark 4.2. For the *codimension-two** systems considered here, the only possible configurations of infinite singular points are those presented in Table 4.3 and Figure 4.19. These are Config. 9, 16, and 26, which feature an infinite nilpotent elliptic-saddle, and Config. 23, which features an infinite nilpotent saddle.

Conditions			Infinite singularities	Configuration
$\widetilde{K} < 0$			$(\widehat{1}_2)PEP - H,\ N$	*Config.9*
$\widetilde{K} > 0$	$\widetilde{L} < 0$	$\widetilde{N} < 0$	$(\widehat{1}_2)PEP - H,\ S$	*Config.16*
		$\widetilde{N} > 0$	$(\widehat{1}_2)PHP - E,\ S$	*Config.26*
		$\widetilde{N} = 0$	$(\widehat{1}_2)H - E,\ S$	*Config.16*
	$\widetilde{L} > 0$		$(\widehat{1}_2)HHH - H,\ N$	*Config.23*

Table 4.3: Conditions for the existence of an infinite nilpotent elliptic-saddle or an infinite nilpotent saddle (see also [6, Diagram 3 and Figure 6]). In the first column we present the conditions in terms of the polynomial invariants, in the second column we list the corresponding types of finite singularities a quadratic system can have, and in the third column we indicate the corresponding configurations of infinite singular points (presented in Figure 4.19).

To obtain the *codimension-two** phase portraits in the set (BC$_{ESNS}$), one must consider evolutions from portraits in both sets (B) and (C). However, the analysis can be simplified. Since the final set of phase portraits is independent of the order of bifurcations (i.e., the set (BC$_{ESNS}$) is identical to (CB$_{ESNS}$)), it is sufficient to study only one evolutionary path. We will therefore derive the desired phase portraits by starting exclusively with phase portraits from set (C).

Recall that the target structures, namely the infinite nilpotent elliptic-saddle and the infinite nilpotent saddle, are formed by the coalescence of three singular points: one finite and two infinite. Our procedure is therefore to begin with a phase portrait from set (C), which by definition possesses an infinite saddle-node $(\overline{1}_1)SN$, and then induce a coalescence between an existing infinite singular point (either a saddle or a node) and this $(\overline{1}_1)SN$. This process is guided by Corollary 3.2, which provides the geometric conditions for this type of coalescence and requires careful consideration of which available infinite singular point participates in the bifurcation.

As in Subsection 4.1, we consider the 32 realizable structurally unstable quadratic vector fields of *codimension one** from set (C). According to Corollary 3.2, to obtain a phase portrait of *codimension two** belonging to set (BC$_{ESNS}$) from a phase portrait in set (C), it suffices to coalesce an infinite singular point (node or saddle) with the saddle-node $(\overline{1}_1)SN$.

Conversely, from the phase portraits of *codimension two** in set (BC$_{ESNS}$), one can obtain phase portraits of *codimension one** belonging to either set (B) or set (C). Transitioning to set (C) involves splitting the triple point into one infinite singularity (located on the side opposite its initial position) plus $(\overline{1}_1)SN$. Transitioning to set (B) involves splitting the triple point into one finite singularity plus $(\overline{0}_2)SN$. However, in this study, we shall consider only the bifurcation inside set (B).

In what follows, we continue using the notation $\mathbb{U}^2_{BC,k}$ established in the previous subsection, where $\mathbb{U}^2_{BC}$ denotes a structurally unstable quadratic vector field of *codimension two** from set (BC) and $k \in \{17, \ldots, 35\}$. We also maintain the notation $\mathbb{U}^{2,I}_{BC,j}$ for the *Impossible* codimension two* *from the set (BC)*, with $j \geq 3$.

Note that phase portraits $\mathbb{U}^1_{C,1}$ through $\mathbb{U}^1_{C,3}$ cannot evolve into phase portraits belonging to set (BC_{ESNS}), as each possesses only one infinite singularity.

We now study the evolution of phase portrait $\mathbb{U}^1_{C,4}$ inside set (BC_{ESNS}). We detail the study of this first case fully; for subsequent cases, we present only the essential information. Following the approach established in Corollary 3.2, we begin by identifying the infinite saddle-node $\overline{\binom{1}{1}}SN$ and the other infinite singular points. Since phase portrait $\mathbb{U}^1_{C,4}$ has two infinite nodes (in addition to the saddle-node $\overline{\binom{1}{1}}SN$ located on the y-axis), there are two distinct ways to perform a coalescence of an infinite node with the saddle-node $\overline{\binom{1}{1}}SN$. These are indicated as C1 and C2 (coalescence 1 and coalescence 2, respectively) in Figure 4.20. Recall that infinite singular points appear in pairs.

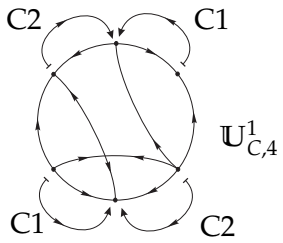


Figure 4.20: Analysis of phase portrait $\mathbb{U}^1_{C,4}$: Two possible coalescence of infinite nodes with the saddle-node $\overline{\binom{1}{1}}SN$ located at the end of the y-axis.

Therefore, one might expect the existence of at least two potential evolutions for phase portrait $\mathbb{U}^1_{C,4}$. However, Corollary 3.2 indicates a greater number of possibilities. It states that the coalescence of an infinite node with an infinite saddle-node $\overline{\binom{1}{1}}\,SN$ yields two distinct cases: the resulting elliptic-saddle either possesses two affine separatrices on the same side of infinity as the original saddle-node's separatrix, or it possesses no affine separatrices.

Remark 4.3. It is crucial to note that this study seeks evolutions of phase portraits from set (C) that belong specifically to set (BC_{ESNS}). Consequently, any resulting phase portrait must possess a singularity configuration listed in Table 4.3. As we proceed, we will encounter phase portraits generated via Corollary 3.2 that do not match any configuration in Table 4.3; these will be discarded as they are inadmissible within set (BC_{ESNS}).

We begin by considering coalescence C1 (see Figure 4.20). We coalesce the infinite repelling node in the third quadrant with the saddle-node located at the south pole, thereby generating an elliptical sector. Note that the separatrix of the finite saddle, which previously reached the infinite saddle-node at the south pole transversally, must become tangent to infinity at the moment of coalescence. Moreover:

- According to the first possibility in Corollary 3.2, the separatrix reaching the saddle-node at the north pole may persist and become tangent to infinity during coalescence. However, since a point with a sectorial decomposition PHP requires two separatrices on the same side of infinity, a second separatrix must emerge, as seen in the impossible phase portrait $\mathbb{U}^{2,I}_{BC,3}$ in Figure 4.21 (first arrow). Consequently, $\mathbb{U}^1_{C,4}$ evolves into $\mathbb{U}^{2,I}_{BC,3}$, which is impossible because its configuration of infinite singular points does not correspond to any listed in Table 4.3.

- Alternatively, according to the second possibility in Corollary 3.2, the separatrix of the saddle-node at the north pole may simply vanish during coalescence, resulting in a

$\widehat{\binom{1}{2}}\,PEP-H$ singularity. In this case, phase portrait $\mathbb{U}^1_{C,4}$ evolves into $\mathbb{U}^2_{BC,17}$ (see Figure 4.21, second arrow). Proceeding as described in item 4 of Lemma 3.3, the infinite elliptic-saddle releases a node into the finite plane, yielding two phase portraits topologically equivalent to $\mathbb{U}^1_{B,3}$ after bifurcation.

We now turn to coalescence C2 (see Figure 4.20). Analogous to the study of coalescence C1, we coalesce the infinite repelling node in the fourth quadrant with the saddle-node located at the south pole, thereby generating an elliptical sector. Observe that the separatrix of the finite saddle, which previously reached the infinite saddle-node at the south pole transversally, must become tangent to infinity at the moment of coalescence. In addition:

- Following the first possibility outlined in Corollary 3.2, the separatrix arriving at the saddle-node at the north pole may persist and become tangent to infinity during coalescence. This forces the appearance of a second separatrix, as seen in the impossible phase portrait $\mathbb{U}^{2,I}_{BC,4}$ in Figure 4.21 (third arrow). Consequently, $\mathbb{U}^1_{C,4}$ evolves into $\mathbb{U}^{2,I}_{BC,4}$. This case is impossible because the resulting configuration of infinite singular points does not correspond to any configuration listed in Table 4.3.

- Alternatively, under the second possibility in Corollary 3.2, the separatrix of the saddle-node at the north pole may vanish during coalescence. This causes the separatrix of the finite saddle to connect directly to the infinite stable node in the first quadrant, resulting in a $\widehat{\binom{1}{2}}\,PEP-H$ singularity. In this instance, phase portrait $\mathbb{U}^1_{C,4}$ evolves into $\mathbb{U}^2_{BC,17}$ (see Figure 4.21, fourth arrow). Proceeding as described in item 4 of Lemma 3.3, the infinite elliptic-saddle releases a node into the finite plane, yielding two phase portraits topologically equivalent to $\mathbb{U}^1_{B,3}$ after bifurcation.

Remark 4.4. We outline four key points regarding the continuation of this study:

- Beginning with the analysis of phase portrait $\mathbb{U}^1_{C,5}$, we will provide only essential explanations, omitting arguments that are identical to those established for phase portrait $\mathbb{U}^1_{C,4}$.

- To derive evolutions of phase portraits from set (C), we rely on the possibilities outlined in Corollary 3.2. Cases yielding singularity configurations inconsistent with those expected for set (BC_{ESNS}) (see Table 4.3) will be designated as impossible. For completeness, these phase portraits will be labeled $\mathbb{U}^{2,I}_{BC,j}$ with $j > 4$.

- For evolutions considered impossible for reasons unrelated to singularity configurations, we will provide the corresponding proof of impossibility.

- Subsequent figures will follow the structure of Figure 4.21, where arrows indicate the transition from unstable *codimension-one** phase portraits in set (C) to their respective *codimension-two** evolutions. Additionally, where relevant, we will display the corresponding unfolding to the right of the *codimension-two** phase portraits, in accordance with Lemma 3.3.

We proceed with the analysis of phase portrait $\mathbb{U}^1_{C,5}$. This phase portrait possesses an infinite saddle-node $\overline{\binom{1}{1}}\,SN$ and two infinite nodes. Applying Corollary 3.2 yields the four evolutions depicted in Figure 4.22: the impossible phase portraits $\mathbb{U}^{2,I}_{BC,5}$, $\mathbb{U}^{2,I}_{BC,6}$, and $\mathbb{U}^{2,I}_{BC,7}$, as well as the phase portrait $\mathbb{U}^2_{BC,18}$.

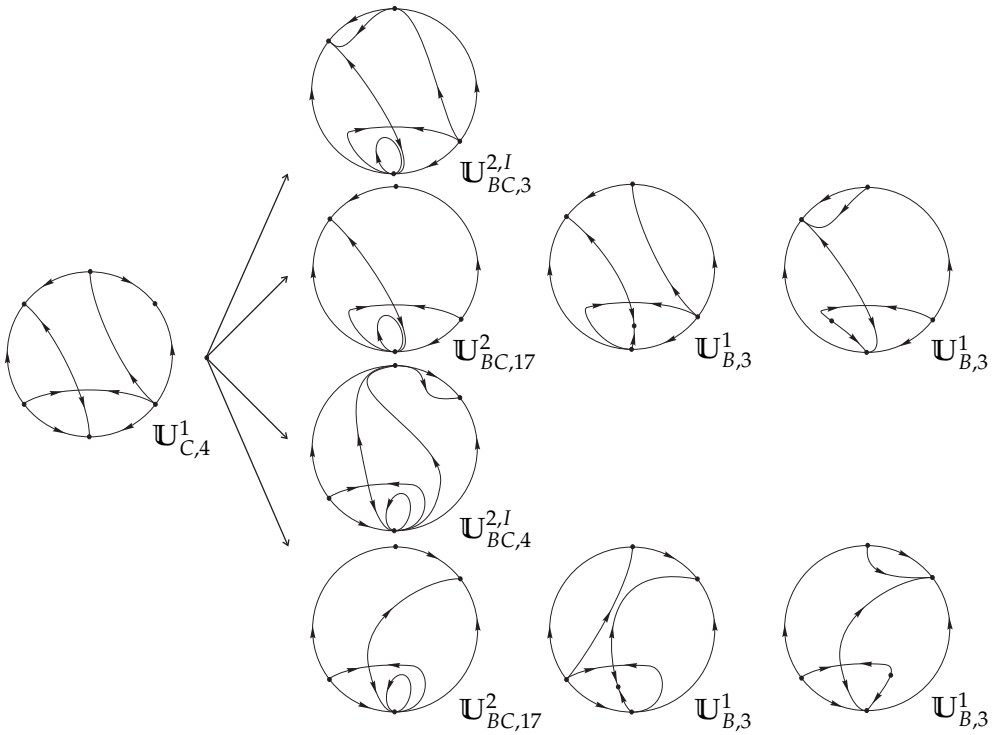


Figure 4.21: Unstable system $\mathbb{U}^{2}_{BC,17}$ and impossible unstable phase portraits $\mathbb{U}^{2,I}_{BC,3}$, $\mathbb{U}^{2,I}_{BC,4}$.

- Phase portraits $\mathbb{U}^{2,I}_{BC,5}$ and $\mathbb{U}^{2,I}_{BC,7}$ are impossible due to their configuration of infinite singularities.

- Regarding $\mathbb{U}^{2,I}_{BC,6}$, the bifurcation described in item 4 of Lemma 3.3 results in phase portrait $\mathbb{U}^{1,I}_{B,a}$. Since $\mathbb{U}^{1,I}_{B,a}$ is proven impossible in Lemma 3.11, it follows from Theorem 3.12 that $\mathbb{U}^{2,I}_{BC,6}$ is also impossible.

- Regarding $\mathbb{U}^{2}_{BC,18}$, proceeding as described in item 4 of Lemma 3.3, where the infinite elliptic-saddle releases a node into the finite plane, yields phase portraits $\mathbb{U}^{1}_{B,15}$ and $\mathbb{U}^{1}_{B,20}$.

Phase portrait $\mathbb{U}^{1}_{C,6}$ possesses an infinite saddle-node $\overline{\binom{1}{1}}\,SN$ along with two infinite nodes. Applying Corollary 3.2 yields the four evolutions depicted in Figure 4.23: the impossible phase portraits $\mathbb{U}^{2,I}_{BC,8}$, $\mathbb{U}^{2,I}_{BC,9}$, and $\mathbb{U}^{2,I}_{BC,10}$, as well as the phase portrait $\mathbb{U}^{2}_{BC,19}$.

- Phase portraits $\mathbb{U}^{2,I}_{BC,8}$ and $\mathbb{U}^{2,I}_{BC,9}$ are impossible due to their configuration of infinite singularities.

- Phase portrait $\mathbb{U}^{2,I}_{BC,10}$ is impossible due to the presence of a graphic that violates Lemma 3.9.

- Regarding $\mathbb{U}^{2}_{BC,19}$, proceeding according to item 4 of Lemma 3.3, where the infinite elliptic-saddle releases a node into the finite plane, yields phase portraits $\mathbb{U}^{1}_{B,12}$ and $\mathbb{U}^{1}_{B,22}$.

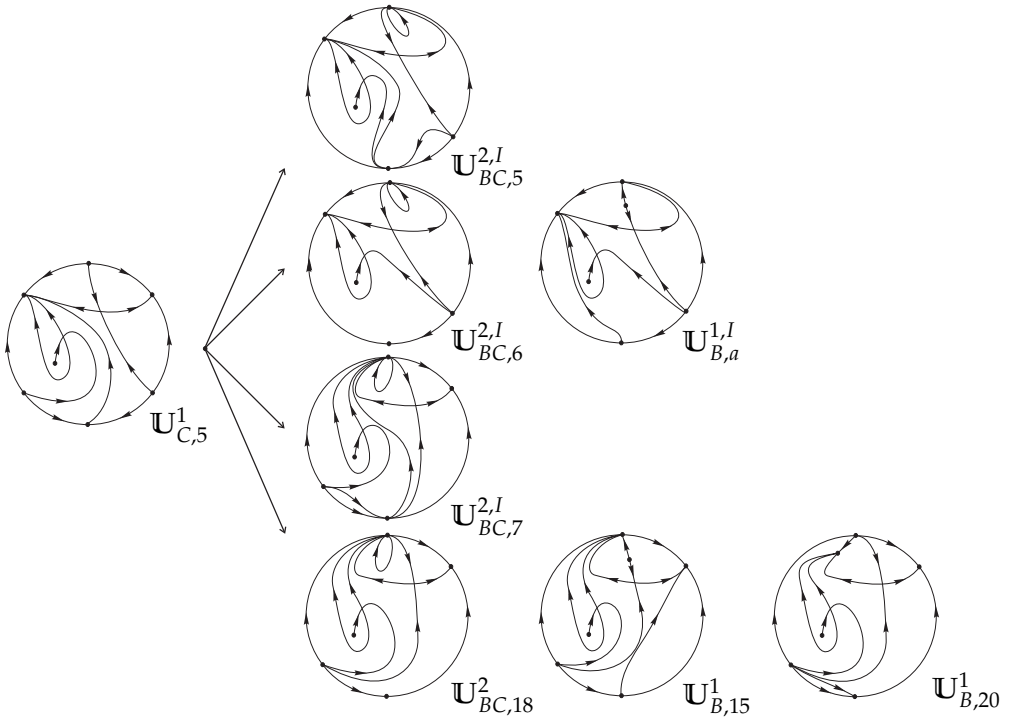


Figure 4.22: Unstable system $\mathbb{U}^{2}_{BC,18}$ and impossible unstable phase portraits $\mathbb{U}^{2,I}_{BC,5}$, $\mathbb{U}^{2,I}_{BC,6}$, $\mathbb{U}^{2,I}_{BC,7}$.

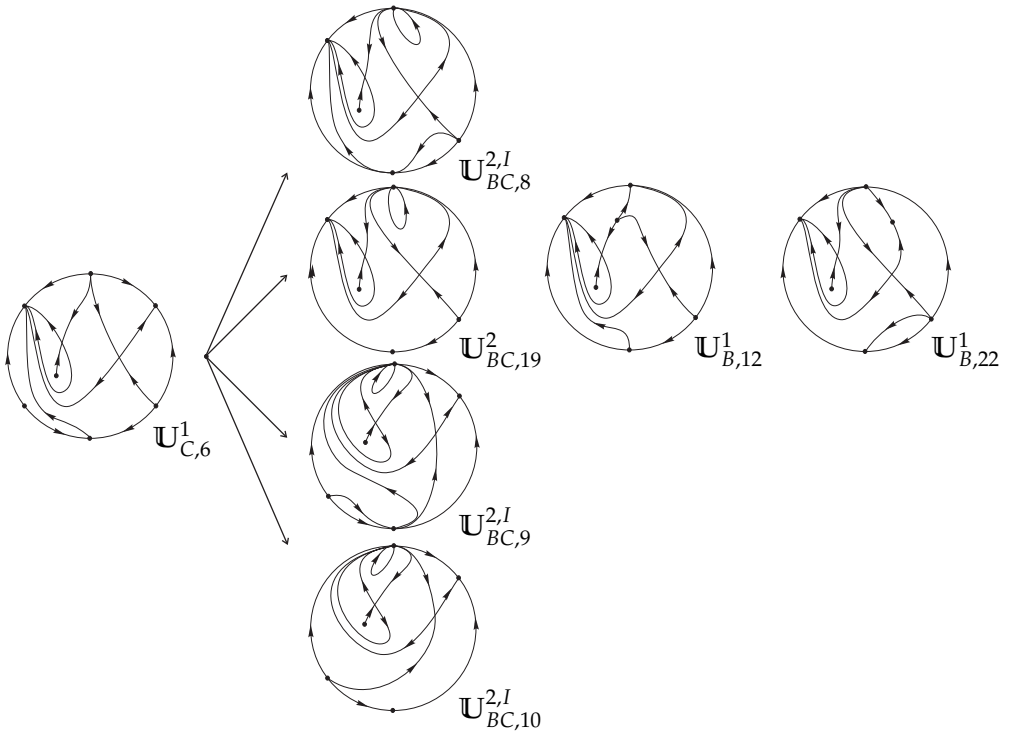


Figure 4.23: Unstable system $\mathbb{U}^{2}_{BC,19}$ and impossible unstable phase portraits $\mathbb{U}^{2,I}_{BC,8}$, $\mathbb{U}^{2,I}_{BC,9}$, $\mathbb{U}^{2,I}_{BC,10}$.

Phase portrait $\mathbb{U}^{1}_{C,7}$ possesses an infinite saddle-node $\overline{\binom{1}{1}}\,SN$ as well as two infinite nodes. Applying Corollary 3.2 yields the four evolutions depicted in Figure 4.24: the impossible

phase portraits $\mathbb{U}^{2,I}_{BC,11}$ and $\mathbb{U}^{2,I}_{BC,12}$, and phase portrait $\mathbb{U}^{2}_{BC,20}$ (obtained twice).

- Phase portraits $\mathbb{U}^{2,I}_{BC,11}$ and $\mathbb{U}^{2,I}_{BC,12}$ are impossible due to their configuration of infinite singularities.
- Regarding $\mathbb{U}^{2}_{BC,20}$, proceeding according to item 4 of Lemma 3.3, where the infinite elliptic-saddle releases a node into the finite plane, yields phase portraits $\mathbb{U}^{1}_{B,14}$ and $\mathbb{U}^{1}_{B,25}$.

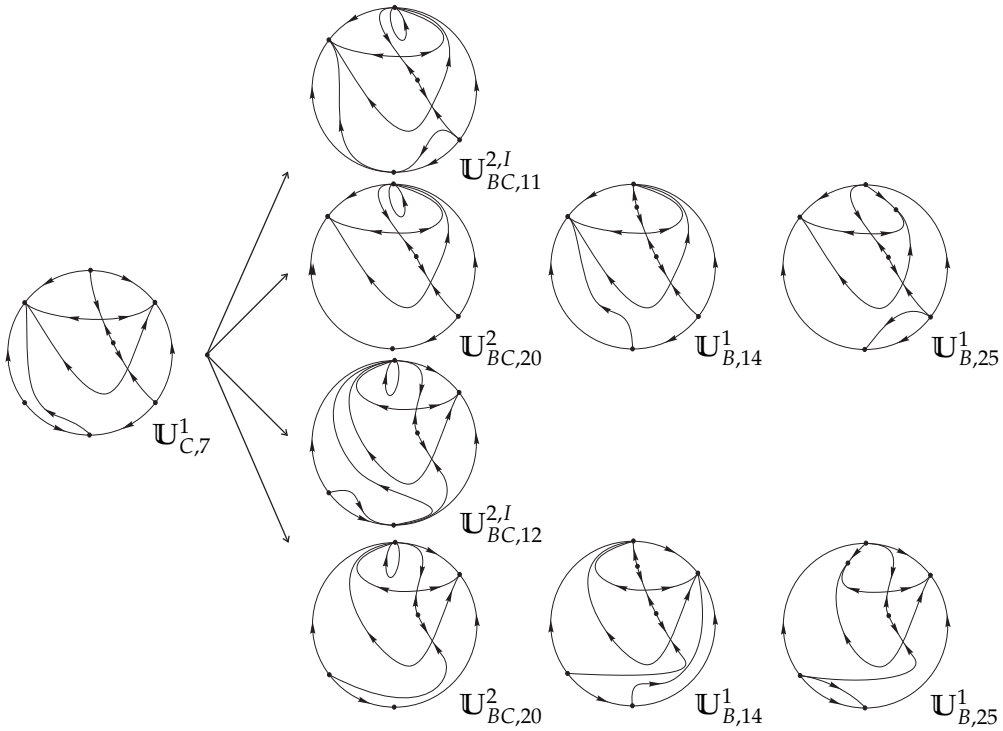


Figure 4.24: Unstable system $\mathbb{U}^{2}_{BC,20}$ and impossible unstable phase portraits $\mathbb{U}^{2,I}_{BC,11}$, $\mathbb{U}^{2,I}_{BC,12}$.

Phase portrait $\mathbb{U}^{1}_{C,8}$ possesses an infinite saddle-node $\overline{\binom{1}{1}}\,SN$ and two infinite nodes. Applying Corollary 3.2 yields the four evolutions depicted in Figure 4.25: the impossible phase portraits $\mathbb{U}^{2,I}_{BC,13}$, $\mathbb{U}^{2,I}_{BC,6}$, and $\mathbb{U}^{2,I}_{BC,14}$, as well as phase portrait $\mathbb{U}^{2}_{BC,18}$.

- Phase portraits $\mathbb{U}^{2,I}_{BC,13}$ and $\mathbb{U}^{2,I}_{BC,14}$ are impossible due to their configuration of infinite singularities.
- Phase portrait $\mathbb{U}^{2,I}_{BC,6}$ has previously been shown to be impossible.
- Regarding $\mathbb{U}^{2}_{BC,18}$, proceeding according to item 4 of Lemma 3.3, where the infinite elliptic-saddle releases a node into the finite plane, yields phase portraits $\mathbb{U}^{1}_{B,15}$ and $\mathbb{U}^{1}_{B,20}$.

Phase portrait $\mathbb{U}^{1}_{C,9}$ possesses an infinite saddle-node $\overline{\binom{1}{1}}\,SN$ and two infinite nodes. Applying Corollary 3.2 yields the four evolutions depicted in Figure 4.26: the impossible phase portraits $\mathbb{U}^{2,I}_{BC,15}$, $\mathbb{U}^{2,I}_{BC,6}$, and $\mathbb{U}^{2,I}_{BC,16}$, as well as phase portrait $\mathbb{U}^{2}_{BC,19}$.

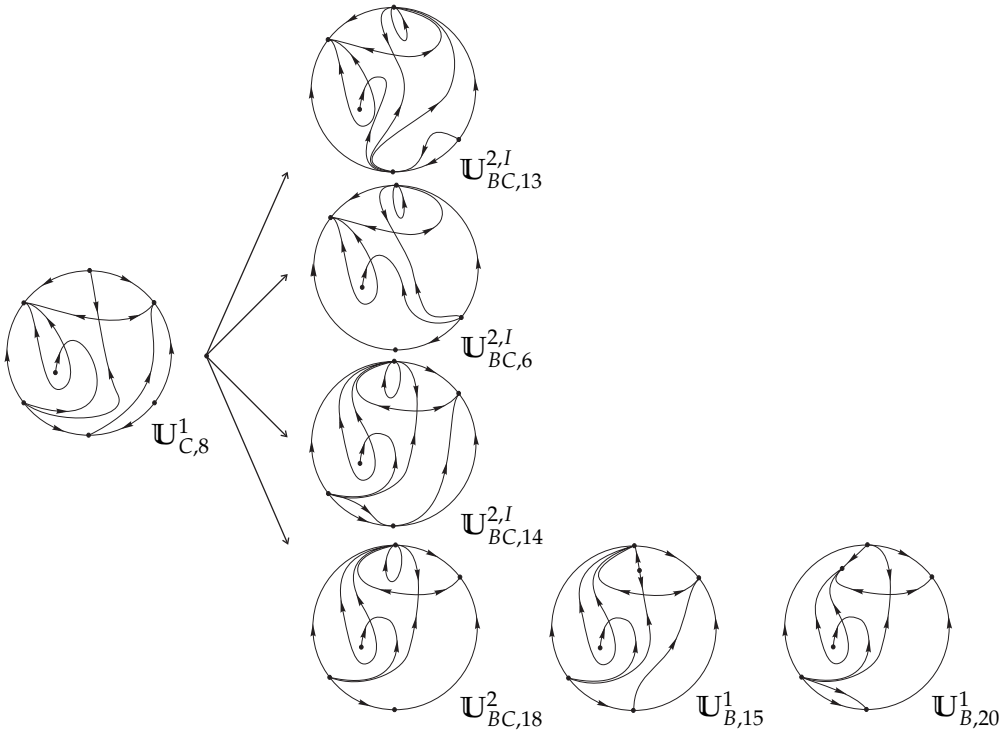


Figure 4.25: Unstable system $\mathbb{U}^{2}_{BC,18}$ and impossible unstable phase portraits $\mathbb{U}^{2,I}_{BC,13}$, $\mathbb{U}^{2,I}_{BC,6}$, $\mathbb{U}^{2,I}_{BC,14}$.

- Phase portraits $\mathbb{U}^{2,I}_{BC,15}$ and $\mathbb{U}^{2,I}_{BC,16}$ are impossible due to their configuration of infinite singularities.
- Phase portrait $\mathbb{U}^{2,I}_{BC,6}$ has previously been shown to be impossible.
- Regarding $\mathbb{U}^{2}_{BC,19}$, proceeding according to item 4 of Lemma 3.3, where the infinite elliptic-saddle releases a node into the finite plane, yields phase portraits $\mathbb{U}^{1}_{B,22}$ and $\mathbb{U}^{1}_{B,12}$.

Phase portrait $\mathbb{U}^{1}_{C,10}$ possesses an infinite saddle-node $\overline{\binom{1}{1}}\,SN$ and two infinite nodes. Applying Corollary 3.2 yields the four evolutions depicted in Figure 4.27: the impossible phase portraits $\mathbb{U}^{2,I}_{BC,17}$, $\mathbb{U}^{2,I}_{BC,18}$, and $\mathbb{U}^{2,I}_{BC,19}$, as well as phase portrait $\mathbb{U}^{2}_{BC,18}$.

- Phase portraits $\mathbb{U}^{2,I}_{BC,17}$ and $\mathbb{U}^{2,I}_{BC,18}$ are impossible due to their configuration of infinite singularities.
- Phase portrait $\mathbb{U}^{2,I}_{BC,19}$ is impossible due to the presence of a graphic that violates Lemma 3.9.
- Regarding $\mathbb{U}^{2}_{BC,18}$, proceeding according to item 4 of Lemma 3.3, where the infinite elliptic-saddle releases a node into the finite plane, yields phase portraits $\mathbb{U}^{1}_{B,20}$ and $\mathbb{U}^{1}_{B,15}$.

Phase portrait $\mathbb{U}^{1}_{C,11}$ possesses an infinite saddle-node $\overline{\binom{1}{1}}\,SN$ and two infinite nodes. Applying Corollary 3.2 yields the four evolutions depicted in Figure 4.28: the impossible phase portraits $\mathbb{U}^{2,I}_{BC,20}$, $\mathbb{U}^{2,I}_{BC,6}$, and $\mathbb{U}^{2,I}_{BC,21}$, as well as phase portrait $\mathbb{U}^{2}_{BC,19}$.

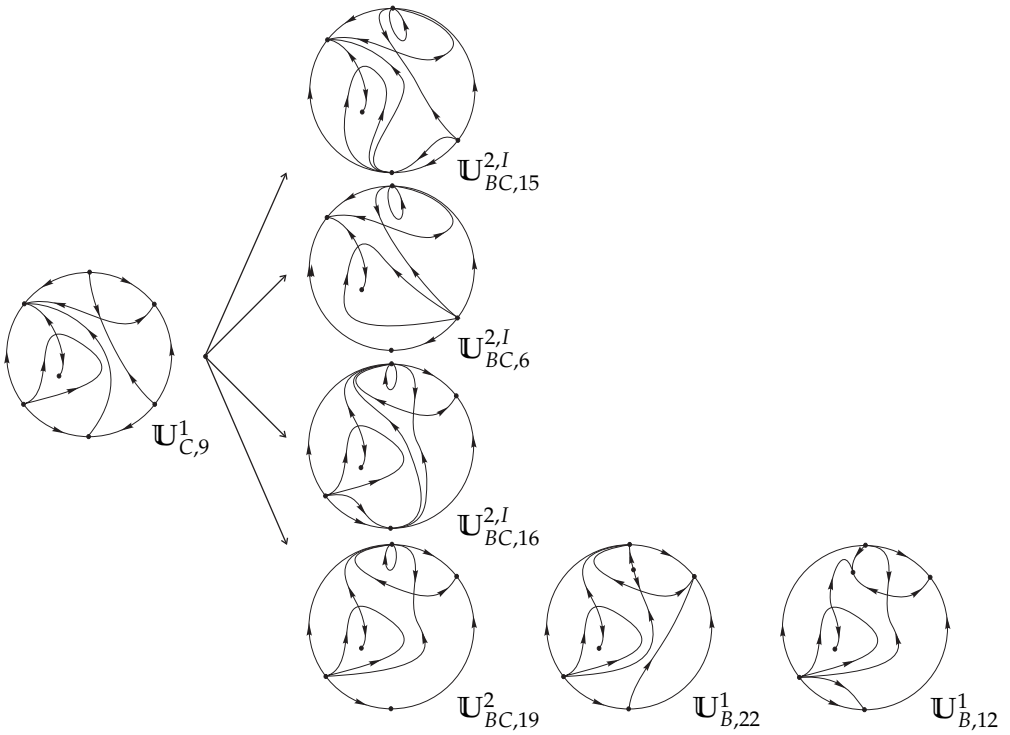


Figure 4.26: Unstable system $\mathbb{U}^{2}_{BC,19}$ and impossible unstable phase portraits $\mathbb{U}^{2,I}_{BC,15}$, $\mathbb{U}^{2,I}_{BC,6}$, $\mathbb{U}^{2,I}_{BC,16}$.

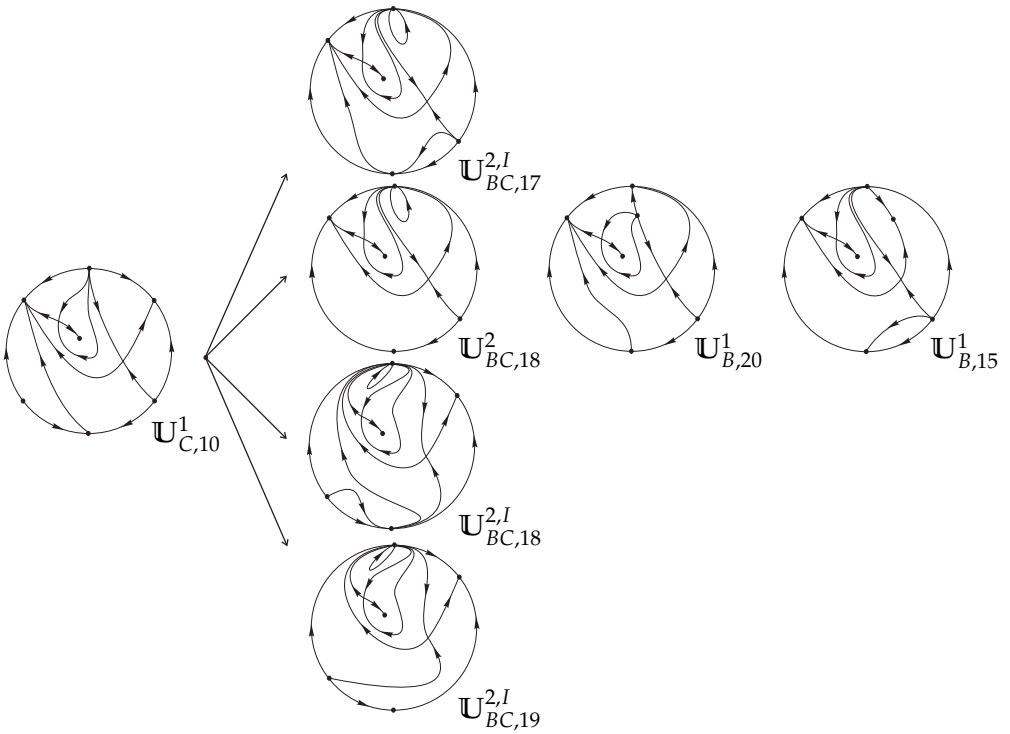


Figure 4.27: Unstable system $\mathbb{U}^{2}_{BC,18}$ and impossible unstable phase portraits $\mathbb{U}^{2,I}_{BC,17}$, $\mathbb{U}^{2,I}_{BC,18}$, $\mathbb{U}^{2,I}_{BC,19}$.

- Phase portraits $\mathbb{U}^{2,I}_{BC,20}$ and $\mathbb{U}^{2,I}_{BC,21}$ are impossible due to their configuration of infinite

singularities.

- Phase portrait $\mathbb{U}^{2,I}_{BC,6}$ has previously been shown to be impossible.
- Regarding $\mathbb{U}^{2}_{BC,19}$, proceeding according to item 4 of Lemma 3.3, where the infinite elliptic-saddle releases a node into the finite plane, yields phase portraits $\mathbb{U}^{1}_{B,22}$ and $\mathbb{U}^{1}_{B,12}$.

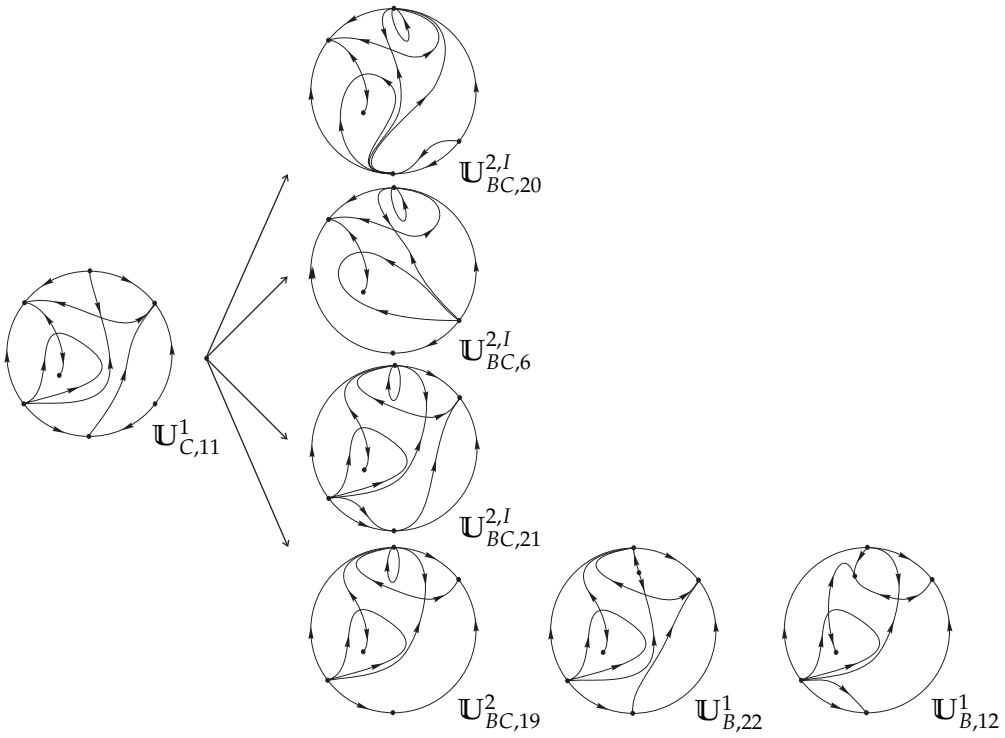


Figure 4.28: Unstable system $\mathbb{U}^{2}_{BC,19}$ and impossible unstable phase portraits $\mathbb{U}^{2,I}_{BC,20}$, $\mathbb{U}^{2,I}_{BC,6}$, $\mathbb{U}^{2,I}_{BC,21}$.

Phase portrait $\mathbb{U}^{1}_{C,12}$ possesses an infinite saddle-node $\overline{\binom{1}{1}}\,SN$ and two infinite nodes. Applying Corollary 3.2 yields the four evolutions depicted in Figure 4.29: the impossible phase portraits $\mathbb{U}^{2,I}_{BC,11}$ and $\mathbb{U}^{2,I}_{BC,22}$, as well as phase portrait $\mathbb{U}^{2}_{BC,20}$ (obtained twice).

- Phase portrait $\mathbb{U}^{2,I}_{BC,11}$ has previously been shown to be impossible.
- Phase portrait $\mathbb{U}^{2,I}_{BC,22}$ is impossible due to its configuration of infinite singularities.
- Regarding $\mathbb{U}^{2}_{BC,20}$, proceeding according to item 4 of Lemma 3.3, where the infinite elliptic-saddle releases a node into the finite plane, yields phase portraits $\mathbb{U}^{1}_{B,25}$ and $\mathbb{U}^{1}_{B,14}$.

Phase portrait $\mathbb{U}^{1}_{C,13}$ possesses an infinite saddle-node $\overline{\binom{1}{1}}\,SN$ and two infinite nodes. Applying Corollary 3.2 yields the four evolutions depicted in Figure 4.30: the impossible phase portraits $\mathbb{U}^{2,I}_{BC,23}$, $\mathbb{U}^{2,I}_{BC,6}$, and $\mathbb{U}^{2,I}_{BC,24}$, as well as phase portrait $\mathbb{U}^{2}_{BC,19}$.

- Phase portraits $\mathbb{U}^{2,I}_{BC,23}$ and $\mathbb{U}^{2,I}_{BC,24}$ are impossible due to their configuration of infinite singularities.

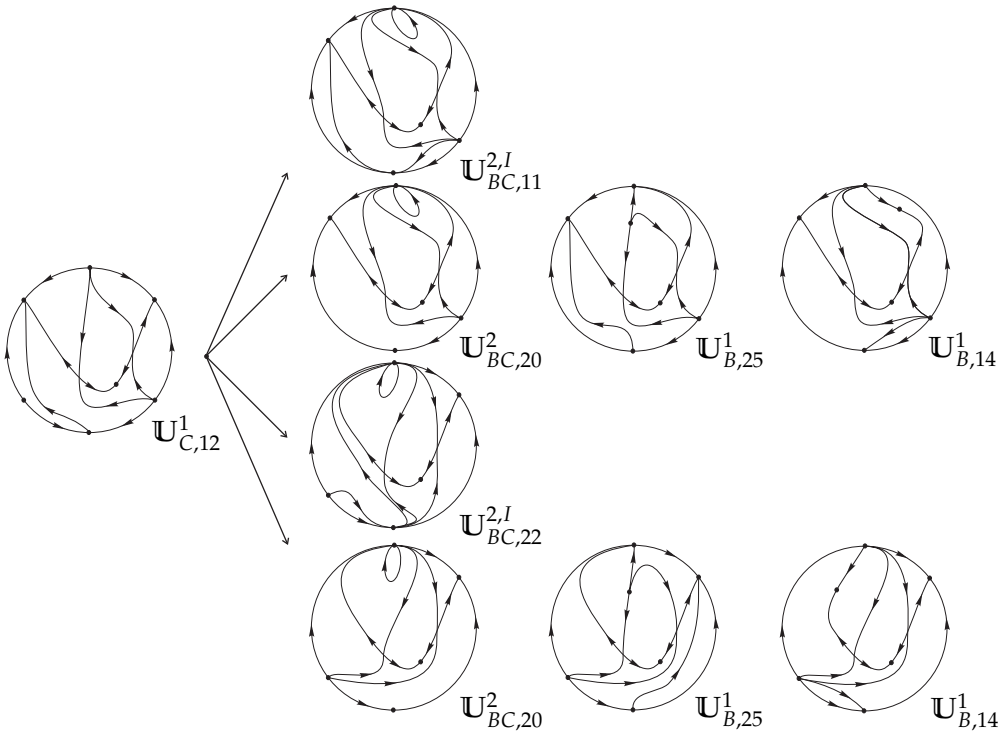


Figure 4.29: Unstable system $\mathbb{U}^{2}_{BC,20}$ and impossible unstable phase portraits $\mathbb{U}^{2,I}_{BC,11}$, $\mathbb{U}^{2,I}_{BC,22}$.

- Phase portrait $\mathbb{U}^{2,I}_{BC,6}$ has previously been shown to be impossible.
- Regarding $\mathbb{U}^{2}_{BC,19}$, proceeding according to item 4 of Lemma 3.3, where the infinite elliptic-saddle releases a node into the finite plane, yields phase portraits $\mathbb{U}^{1}_{B,22}$ and $\mathbb{U}^{1}_{B,12}$.

Phase portrait $\mathbb{U}^{1}_{C,14}$ possesses an infinite saddle-node $\overline{\binom{1}{1}}\,SN$ and two infinite nodes. Given the symmetry with respect to the y-axis and applying Corollary 3.2, we obtain the two evolutions depicted in Figure 4.31: the impossible phase portrait $\mathbb{U}^{2,I}_{BC,25}$ and phase portrait $\mathbb{U}^{2}_{BC,20}$.

- Phase portrait $\mathbb{U}^{2,I}_{BC,25}$ is impossible due to its configuration of infinite singularities.
- Regarding $\mathbb{U}^{2}_{BC,20}$, proceeding according to item 4 of Lemma 3.3, where the infinite elliptic-saddle releases a node into the finite plane, yields phase portraits $\mathbb{U}^{1}_{B,25}$ and $\mathbb{U}^{1}_{B,14}$.

Phase portrait $\mathbb{U}^{1}_{C,15}$ possesses an infinite saddle-node $\overline{\binom{1}{1}}\,SN$, an infinite node, and an infinite saddle. Applying Corollary 3.2 yields the three evolutions depicted in Figure 4.32. Specifically, evolution $\mathbb{U}^{2}_{BC,21}$ results from the coalescence of the infinite saddle with the infinite saddle-node $\overline{\binom{1}{1}}\,SN$, while evolutions $\mathbb{U}^{2}_{BC,22}$ and $\mathbb{U}^{2}_{BC,23}$ result from the coalescence of the infinite node with the infinite saddle-node $\overline{\binom{1}{1}}\,SN$.

- Regarding $\mathbb{U}^{2}_{BC,21}$, proceeding according to item 3 of Lemma 3.3, where the infinite elliptic-saddle releases a saddle into the finite plane, yields phase portraits $\mathbb{U}^{1}_{B,3}$ and $\mathbb{U}^{1}_{B,5}$.

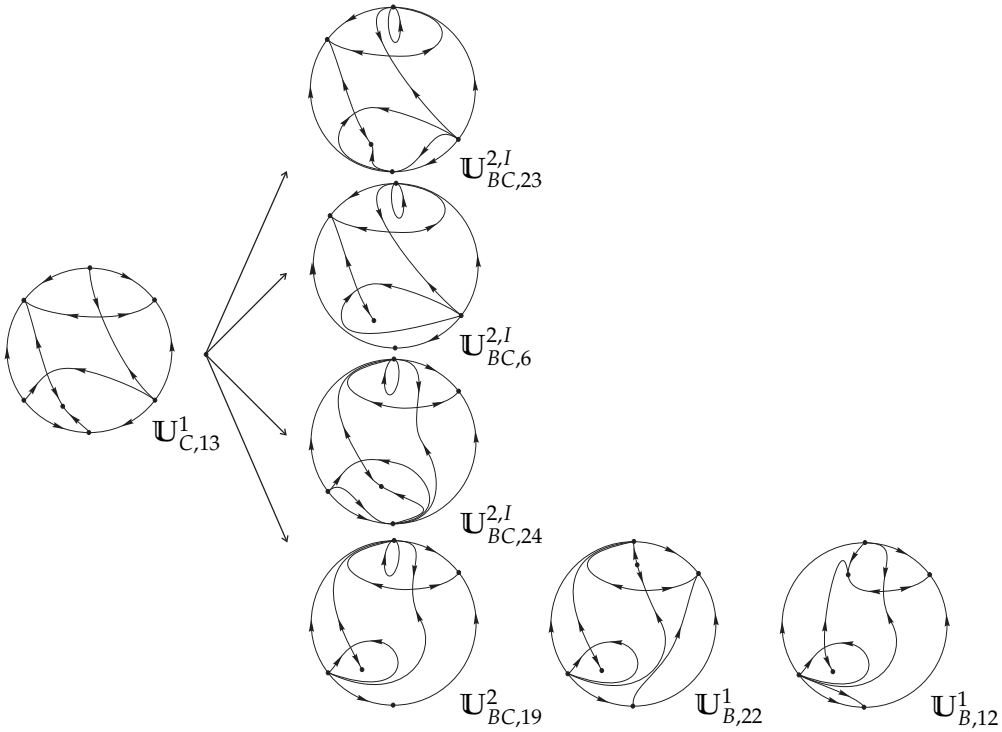


Figure 4.30: Unstable system $\mathbb{U}^2_{BC,19}$ and impossible unstable phase portraits $\mathbb{U}^{2,I}_{BC,23}$, $\mathbb{U}^{2,I}_{BC,6}$, $\mathbb{U}^{2,I}_{BC,24}$.

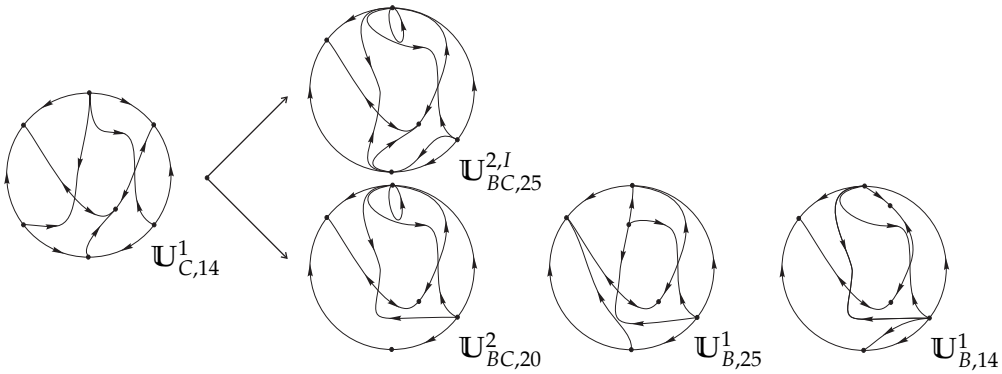


Figure 4.31: Unstable system $\mathbb{U}^2_{BC,20}$ and impossible unstable phase portrait $\mathbb{U}^{2,I}_{BC,25}$.

- Regarding both $\mathbb{U}^2_{BC,22}$ and $\mathbb{U}^2_{BC,23}$, proceeding according to item 4 of Lemma 3.3, where the infinite elliptic-saddle releases a node into the finite plane, yields phase portraits $\mathbb{U}^1_{B,32}$ and $\mathbb{U}^1_{B,29}$.

Phase portrait $\mathbb{U}^1_{C,16}$ possesses an infinite saddle-node $\overline{\binom{1}{1}}\,SN$, an infinite node, and an infinite saddle. While Corollary 3.2 initially suggests three possible evolutions, we must also account for the scenario involving two limit cycles surrounding a focus, as detailed in Section 3.1. Consequently, we identify the four evolutions depicted in Figure 4.33. Specifically, evolution $\mathbb{U}^2_{BC,21}$ results from the coalescence of the infinite saddle with the infinite saddle-node $\overline{\binom{1}{1}}\,SN$. In contrast, evolutions $\mathbb{U}^2_{BC,24}$, $\mathbb{U}^2_{BC,23}$, and $\mathbb{U}^2_{BC,25}$ arise from the coalescence of the infinite node with the infinite saddle-node $\overline{\binom{1}{1}}\,SN$, with the latter case ($\mathbb{U}^2_{BC,25}$) corresponding to the potential existence of two limit cycles in $\mathbb{U}^1_{C,16}$.

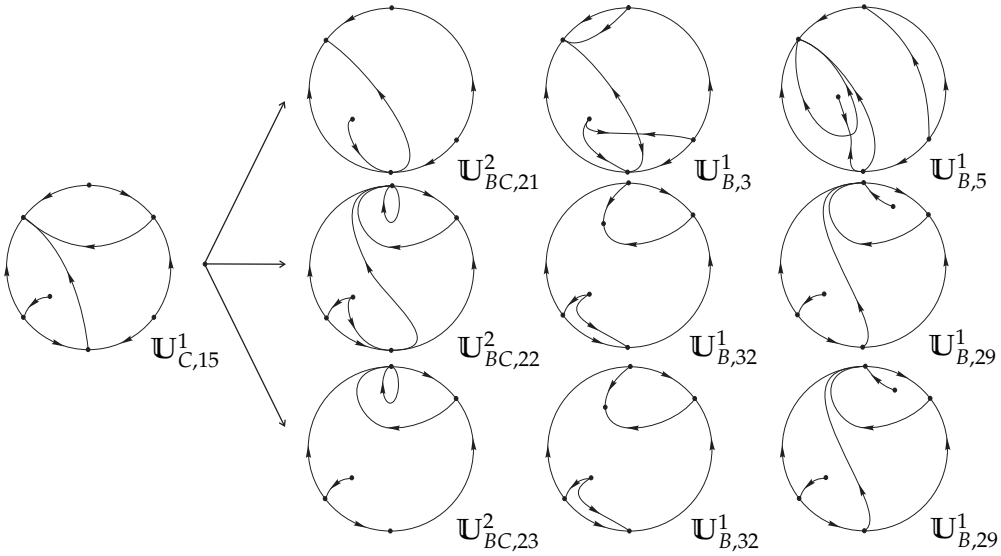


Figure 4.32: Unstable systems $\mathbb{U}^2_{BC,21}$, $\mathbb{U}^2_{BC,22}$, $\mathbb{U}^2_{BC,23}$.

- Regarding $\mathbb{U}^2_{BC,21}$, proceeding according to item 3 of Lemma 3.3, where the infinite elliptic-saddle releases a saddle into the finite plane, yields phase portraits $\mathbb{U}^1_{B,3}$ and $\mathbb{U}^1_{B,5}$.
- Regarding $\mathbb{U}^2_{BC,24}$ and $\mathbb{U}^2_{BC,25}$, proceeding according to item 4 of Lemma 3.3, where the infinite elliptic-saddle releases a node into the finite plane, yields phase portraits $\mathbb{U}^1_{B,30}$ and $\mathbb{U}^1_{B,32}$ (modulo limit cycles). Similarly, the bifurcation of evolution $\mathbb{U}^2_{BC,23}$ yields phase portraits $\mathbb{U}^1_{B,29}$ and $\mathbb{U}^1_{B,32}$ (modulo limit cycles).

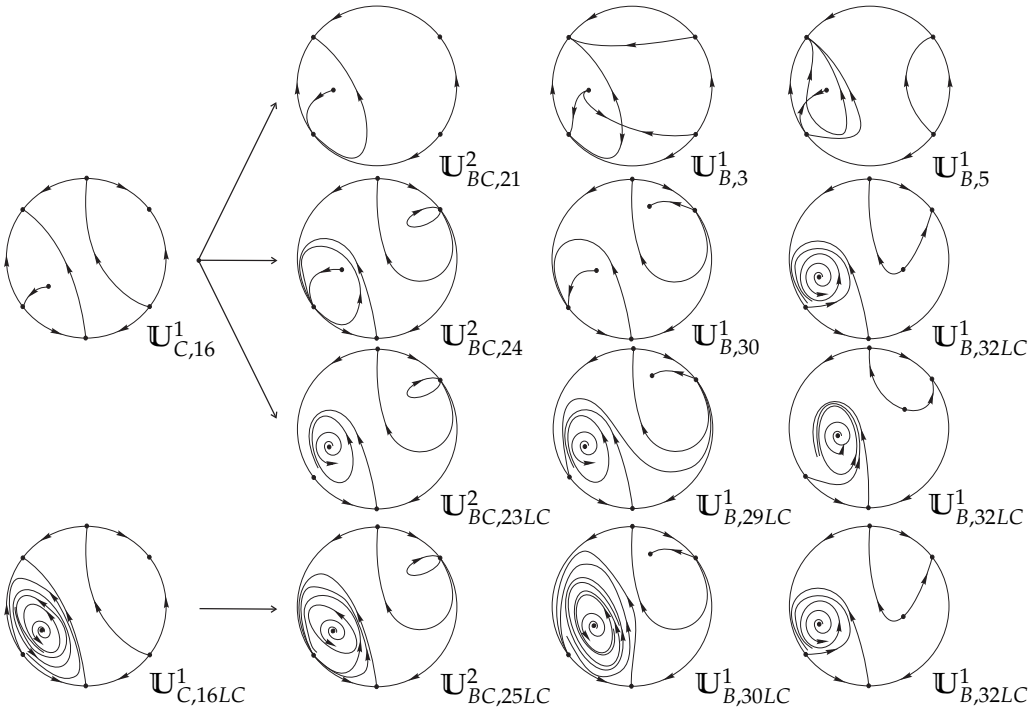


Figure 4.33: Unstable systems $\mathbb{U}^2_{BC,21}$, $\mathbb{U}^2_{BC,24}$, $\mathbb{U}^2_{BC,23}$, $\mathbb{U}^2_{BC,25}$.

Remark 4.5. Since our classification is modulo limit cycles, we represent phase portrait $\mathbb{U}^2_{BC,25}$ as shown in Figure 4.34.

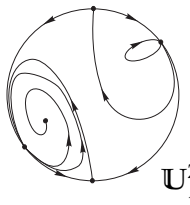


Figure 4.34: Unstable system $\mathbb{U}^2_{BC,25}$.

Phase portrait $\mathbb{U}^1_{C,17}$ possesses an infinite saddle-node $\overline{\binom{1}{1}}\,SN$, an infinite node, and an infinite saddle. Applying Corollary 3.2 yields the three evolutions depicted in Figure 4.35. Specifically, evolutions $\mathbb{U}^2_{BC,22}$ and $\mathbb{U}^2_{BC,23}$ result from the coalescence of the infinite node with the infinite saddle-node $\overline{\binom{1}{1}}\,SN$, while evolution $\mathbb{U}^2_{BC,21}$ results from the coalescence of the infinite saddle with the infinite saddle-node $\overline{\binom{1}{1}}\,SN$.

- Regarding $\mathbb{U}^2_{BC,21}$, proceeding according to item 3 of Lemma 3.3, where the infinite elliptic-saddle releases a saddle into the finite plane, yields phase portraits $\mathbb{U}^1_{B,3}$ and $\mathbb{U}^1_{B,5}$.
- Regarding both $\mathbb{U}^2_{BC,22}$ and $\mathbb{U}^2_{BC,23}$, proceeding according to item 4 of Lemma 3.3, where the infinite elliptic-saddle releases a node into the finite plane, yields phase portraits $\mathbb{U}^1_{B,29}$ and $\mathbb{U}^1_{B,32}$.

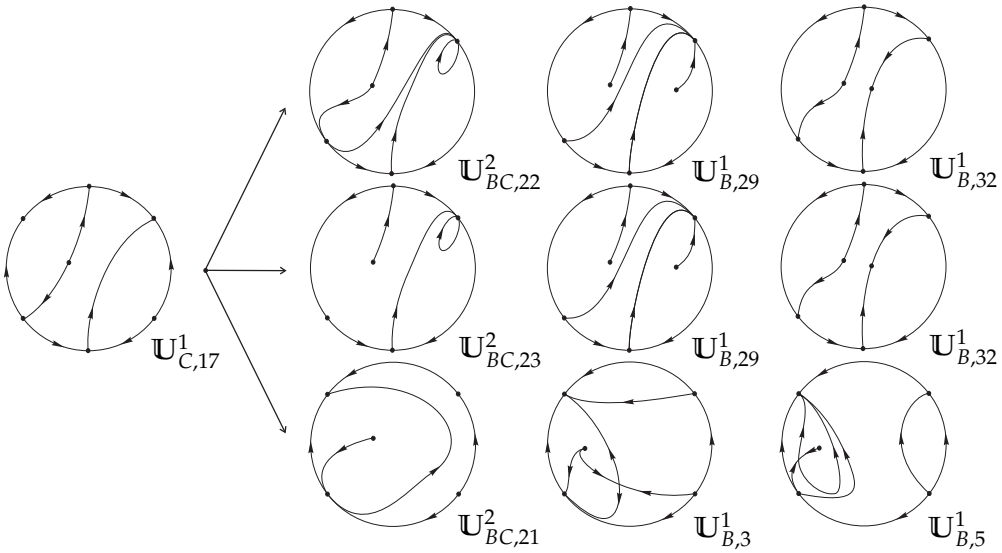


Figure 4.35: Unstable systems $\mathbb{U}^2_{BC,22}$, $\mathbb{U}^2_{BC,23}$, $\mathbb{U}^2_{BC,21}$.

Phase portrait $\mathbb{U}^1_{C,18}$ possesses an infinite saddle-node $\overline{\binom{1}{1}}\,SN$, an infinite node, and an infinite saddle. Applying Corollary 3.2 yields the three evolutions depicted in Figure 4.36. Specifically, evolutions $\mathbb{U}^2_{BC,26}$ and $\mathbb{U}^2_{BC,27}$ result from the coalescence of the infinite node with the infinite saddle-node $\overline{\binom{1}{1}}\,SN$, whereas evolution $\mathbb{U}^2_{BC,28}$ results from the coalescence of the infinite saddle with the infinite saddle-node $\overline{\binom{1}{1}}\,SN$.

- Regarding $\mathbb{U}^2_{BC,28}$, proceeding according to item 3 of Lemma 3.3, where the infinite elliptic-saddle releases a saddle into the finite plane, yields phase portraits $\mathbb{U}^1_{B,9}$ and $\mathbb{U}^1_{B,12}$.
- Regarding both $\mathbb{U}^2_{BC,26}$ and $\mathbb{U}^2_{BC,27}$, proceeding according to item 4 of Lemma 3.3, where the infinite elliptic-saddle releases a node into the finite plane, yields phase portraits $\mathbb{U}^1_{B,33}$ and $\mathbb{U}^1_{B,34}$.

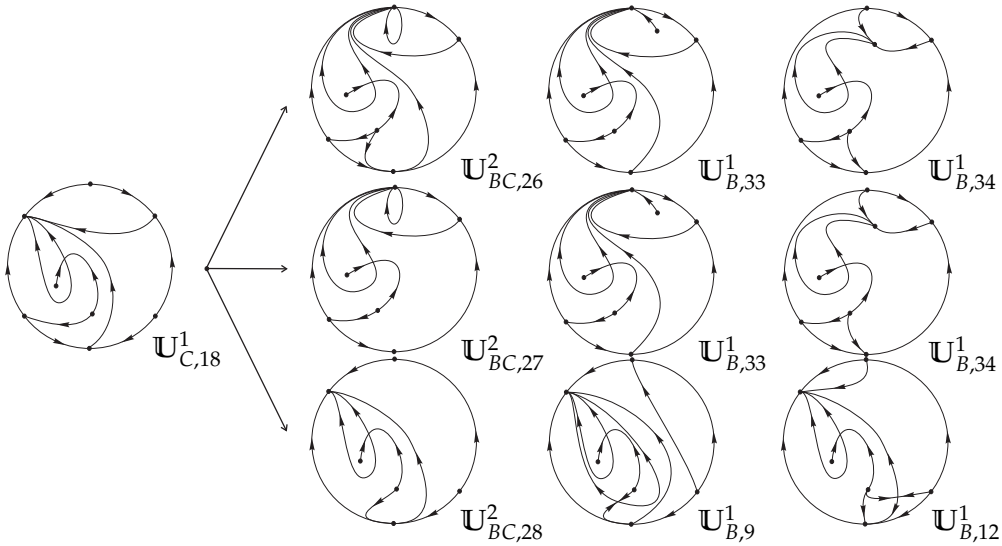


Figure 4.36: Unstable systems $\mathbb{U}^2_{BC,26}$, $\mathbb{U}^2_{BC,27}$, $\mathbb{U}^2_{BC,28}$.

Phase portrait $\mathbb{U}^1_{C,19}$ possesses an infinite saddle-node $\overline{\binom{1}{1}}\,SN$, an infinite node, and an infinite saddle. Applying Corollary 3.2 yields the three evolutions depicted in Figure 4.37. Specifically, we obtain the impossible phase portraits $\mathbb{U}^{2,I}_{BC,26}$, $\mathbb{U}^{2,I}_{BC,27}$, and $\mathbb{U}^{2,I}_{BC,28}$.

- Phase portraits $\mathbb{U}^{2,I}_{BC,26}$ and $\mathbb{U}^{2,I}_{BC,27}$ are impossible due to the presence of graphics that violate Lemma 3.9.
- Regarding $\mathbb{U}^{2,I}_{BC,28}$, proceeding according to item 3 of Lemma 3.3 yields phase portrait $\mathbb{U}^{1,I}_{B,b}$. Since $\mathbb{U}^{1,I}_{B,b}$ is proven impossible in Lemma 3.11, it follows from Theorem 3.12 that $\mathbb{U}^{2,I}_{BC,28}$ is also impossible.

Phase portrait $\mathbb{U}^1_{C,20}$ possesses an infinite saddle-node $\overline{\binom{1}{1}}\,SN$, an infinite node, and an infinite saddle. Applying Corollary 3.2 yields the three evolutions depicted in Figure 4.38. Specifically, evolution $\mathbb{U}^2_{BC,29}$ results from the coalescence of the infinite saddle with the infinite saddle-node $\overline{\binom{1}{1}}\,SN$, while evolutions $\mathbb{U}^2_{BC,30}$ and $\mathbb{U}^2_{BC,31}$ result from the coalescence of the infinite node with the infinite saddle-node $\overline{\binom{1}{1}}\,SN$.

- Regarding $\mathbb{U}^2_{BC,29}$, proceeding according to item 3 of Lemma 3.3, where the infinite elliptic-saddle releases a saddle into the finite plane, yields phase portraits $\mathbb{U}^1_{B,16}$ and $\mathbb{U}^1_{B,20}$.
- Regarding both $\mathbb{U}^2_{BC,30}$ and $\mathbb{U}^2_{BC,31}$, proceeding according to item 4 of Lemma 3.3, where the infinite elliptic-saddle releases a node into the finite plane, yields phase portraits $\mathbb{U}^1_{B,34}$ and $\mathbb{U}^1_{B,36}$.

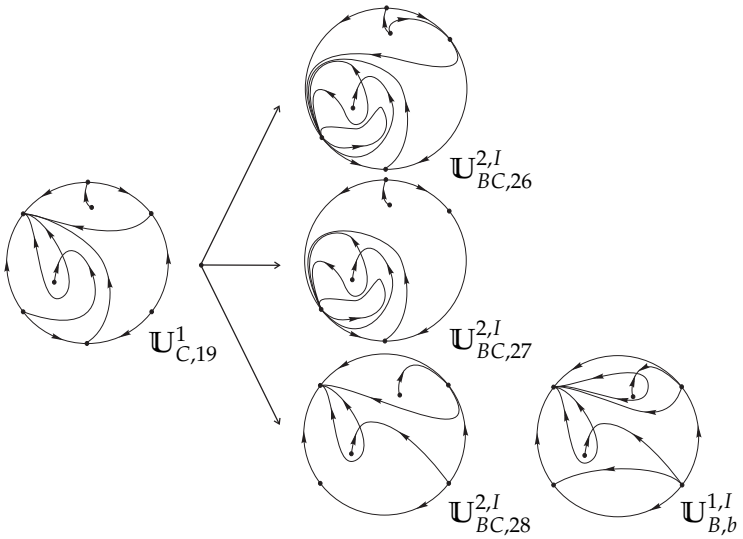


Figure 4.37: Impossible unstable phase portraits $\mathbb{U}^{2,I}_{BC,26}$, $\mathbb{U}^{2,I}_{BC,27}$, $\mathbb{U}^{2,I}_{BC,28}$.

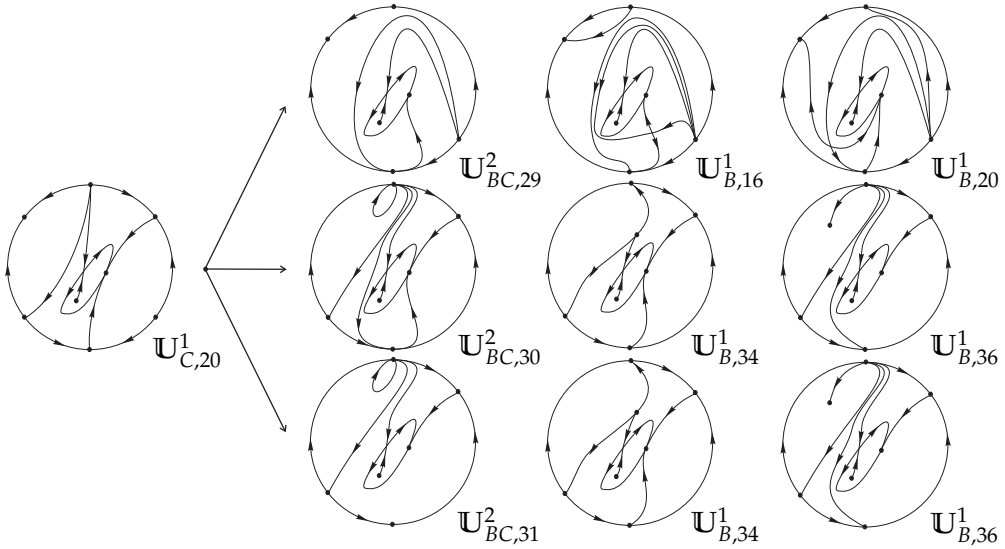


Figure 4.38: Unstable systems $\mathbb{U}^{2}_{BC,29}$, $\mathbb{U}^{2}_{BC,30}$, $\mathbb{U}^{2}_{BC,31}$.

Phase portrait $\mathbb{U}^{1}_{C,21}$ possesses an infinite saddle-node $\overline{\binom{1}{1}}\,SN$, an infinite node, and an infinite saddle. Applying Corollary 3.2 yields the three evolutions depicted in Figure 4.39. Specifically, evolution $\mathbb{U}^{2}_{BC,28}$ results from the coalescence of the infinite saddle with the infinite saddle-node $\overline{\binom{1}{1}}\,SN$, while evolutions $\mathbb{U}^{2}_{BC,26}$ and $\mathbb{U}^{2}_{BC,27}$ result from the coalescence of the infinite node with the infinite saddle-node $\overline{\binom{1}{1}}\,SN$.

- Regarding $\mathbb{U}^{2}_{BC,28}$, proceeding according to item 3 of Lemma 3.3, where the infinite elliptic-saddle releases a saddle into the finite plane, yields phase portraits $\mathbb{U}^{1}_{B,9}$ and $\mathbb{U}^{1}_{B,12}$.

- Regarding both $\mathbb{U}^{2}_{BC,26}$ and $\mathbb{U}^{2}_{BC,27}$, proceeding according to item 4 of Lemma 3.3, where the infinite elliptic-saddle releases a node into the finite plane, yields phase portraits $\mathbb{U}^{1}_{B,33}$ and $\mathbb{U}^{1}_{B,34}$.

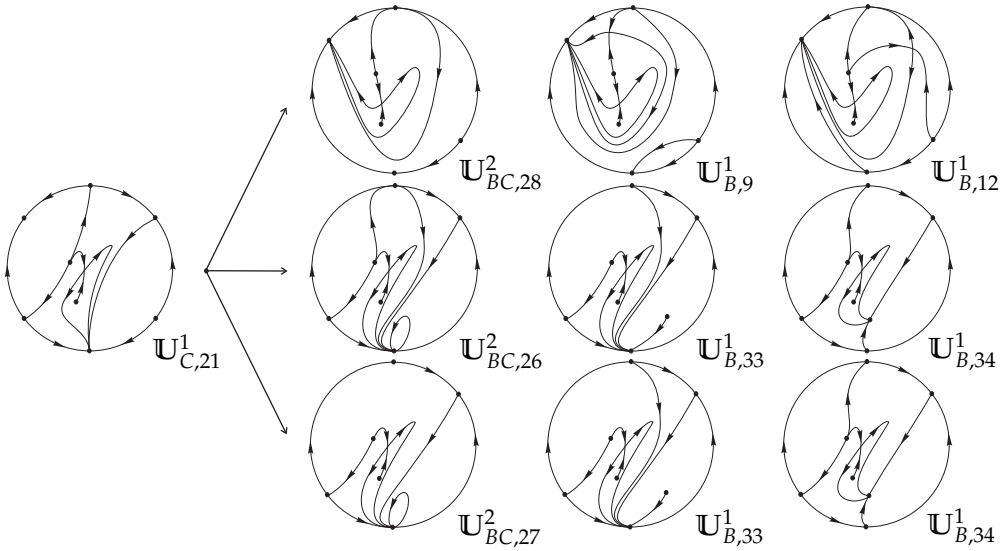


Figure 4.39: Unstable systems $\mathbb{U}^2_{BC,28}$, $\mathbb{U}^2_{BC,26}$, $\mathbb{U}^2_{BC,27}$.

Phase portrait $\mathbb{U}^1_{C,22}$ possesses an infinite saddle-node $\overline{\binom{1}{1}}\,SN$, an infinite node, and an infinite saddle. Applying Corollary 3.2 yields the three evolutions depicted in Figure 4.40. Specifically, evolution $\mathbb{U}^2_{BC,32}$ results from the coalescence of the infinite saddle with the infinite saddle-node $\overline{\binom{1}{1}}\,SN$, while evolutions $\mathbb{U}^2_{BC,33}$ and $\mathbb{U}^2_{BC,34}$ result from the coalescence of the infinite node with the infinite saddle-node $\overline{\binom{1}{1}}\,SN$.

- Regarding $\mathbb{U}^2_{BC,32}$, proceeding according to item 3 of Lemma 3.3, where the infinite elliptic-saddle releases a saddle into the finite plane, yields two phase portraits topologically equivalent to $\mathbb{U}^1_{B,25}$.
- Regarding both $\mathbb{U}^2_{BC,33}$ and $\mathbb{U}^2_{BC,34}$, proceeding according to item 4 of Lemma 3.3, where the infinite elliptic-saddle releases a node into the finite plane, yields phase portraits topologically equivalent to $\mathbb{U}^1_{B,35}$.

Phase portrait $\mathbb{U}^1_{C,23}$ possesses an infinite saddle-node $\overline{\binom{1}{1}}\,SN$, an infinite node, and an infinite saddle. Applying Corollary 3.2 yields the three evolutions depicted in Figure 4.41. Specifically, evolution $\mathbb{U}^2_{BC,28}$ results from the coalescence of the infinite saddle with the infinite saddle-node $\overline{\binom{1}{1}}\,SN$, while evolutions $\mathbb{U}^2_{BC,27}$ and $\mathbb{U}^{2,I}_{BC,29}$ result from the coalescence of the infinite node with the infinite saddle-node $\overline{\binom{1}{1}}\,SN$.

- Regarding $\mathbb{U}^2_{BC,28}$, proceeding according to item 3 of Lemma 3.3, where the infinite elliptic-saddle releases a saddle into the finite plane, yields phase portraits $\mathbb{U}^1_{B,9}$ and $\mathbb{U}^1_{B,12}$.
- Regarding $\mathbb{U}^2_{BC,27}$, proceeding according to item 4 of Lemma 3.3, where the infinite elliptic-saddle releases a node into the finite plane, yields phase portraits $\mathbb{U}^1_{B,33}$ and $\mathbb{U}^1_{B,34}$.
- Regarding $\mathbb{U}^{2,I}_{BC,29}$, applying item 4 of Lemma 3.3 yields phase portraits $\mathbb{U}^1_{B,33}$ and $\mathbb{U}^1_{B,35}$. However, evolution $\mathbb{U}^{2,I}_{BC,29}$ is impossible, as demonstrated later in Proposition 4.6.

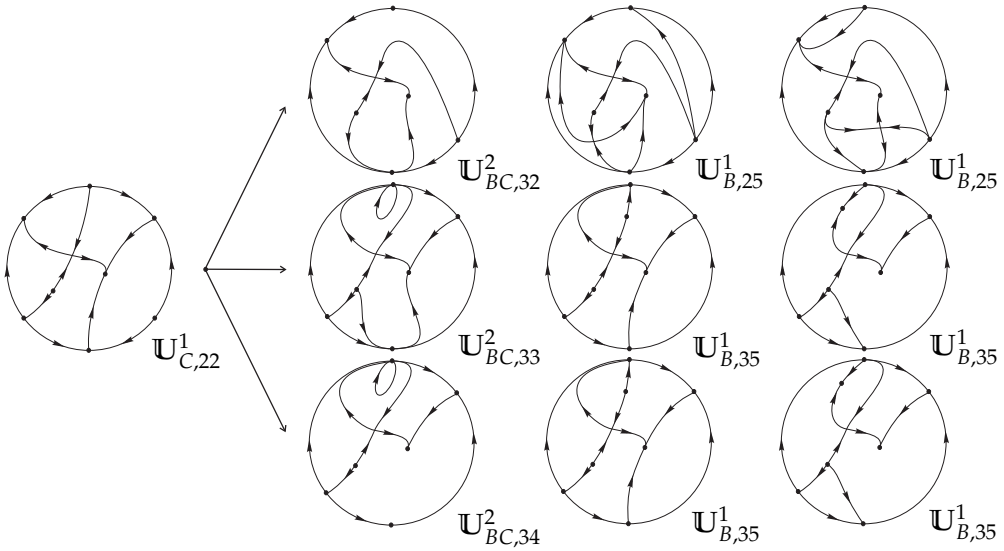


Figure 4.40: Unstable systems $\mathbb{U}^2_{BC,32}$, $\mathbb{U}^2_{BC,33}$, $\mathbb{U}^2_{BC,34}$.

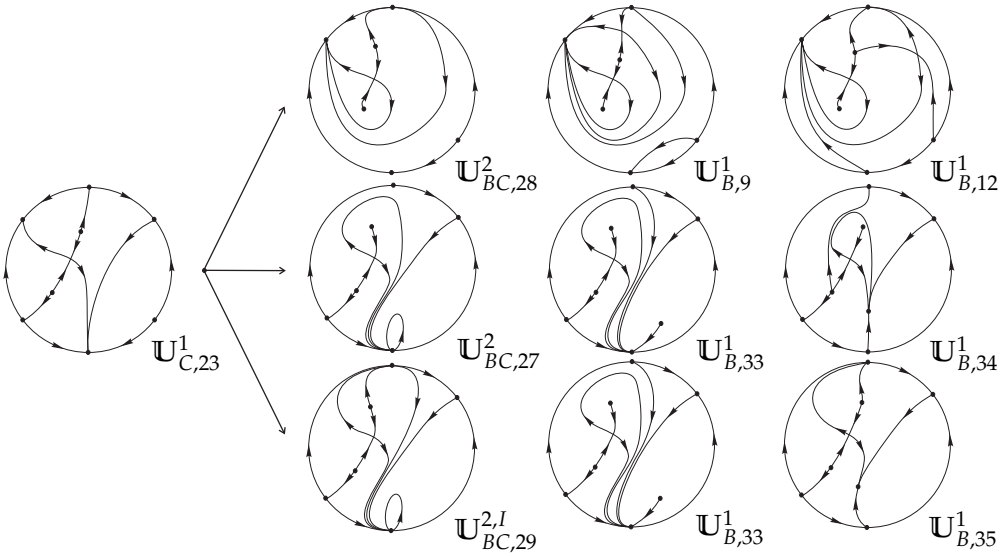


Figure 4.41: Unstable systems $\mathbb{U}^2_{BC,28}$, $\mathbb{U}^2_{BC,27}$ and impossible unstable phase portrait $\mathbb{U}^{2,I}_{BC,29}$.

Phase portrait $\mathbb{U}^1_{C,24}$ possesses an infinite saddle-node $\overline{\binom{1}{1}}\,SN$, an infinite node, and an infinite saddle. Applying Corollary 3.2 yields the three evolutions depicted in Figure 4.42. Specifically, evolution $\mathbb{U}^2_{BC,29}$ results from the coalescence of the infinite saddle with the infinite saddle-node $\overline{\binom{1}{1}}\,SN$, while evolutions $\mathbb{U}^2_{BC,30}$ and $\mathbb{U}^2_{BC,31}$ result from the coalescence of the infinite node with the infinite saddle-node $\overline{\binom{1}{1}}\,SN$.

- Regarding $\mathbb{U}^2_{BC,29}$, proceeding according to item 3 of Lemma 3.3, where the infinite elliptic-saddle releases a saddle into the finite plane, yields phase portraits $\mathbb{U}^1_{B,16}$ and $\mathbb{U}^1_{B,20}$.
- Regarding both $\mathbb{U}^2_{BC,30}$ and $\mathbb{U}^2_{BC,31}$, proceeding according to item 4 of Lemma 3.3, where the infinite elliptic-saddle releases a node into the finite plane, yields phase portraits

$\mathbb{U}^1_{B,34}$ and $\mathbb{U}^1_{B,36}$.

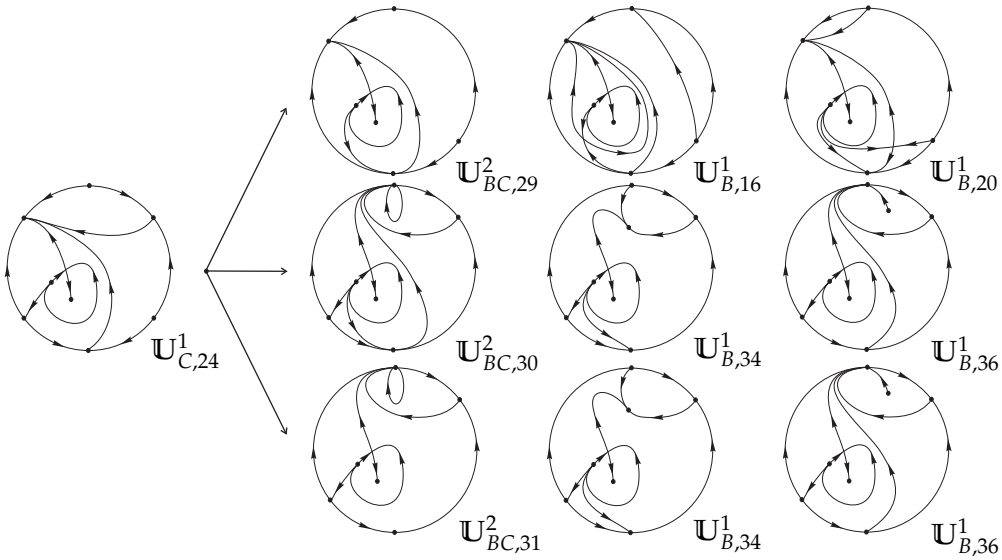


Figure 4.42: Unstable systems $\mathbb{U}^2_{BC,29}$, $\mathbb{U}^2_{BC,30}$, $\mathbb{U}^2_{BC,31}$.

Phase portrait $\mathbb{U}^1_{C,25}$ possesses an infinite saddle-node $\overline{\binom{1}{1}}\,SN$, an infinite node, and an infinite saddle. Applying Corollary 3.2 yields the three evolution depicted in Figure 4.43. Specifically, we obtain the impossible phase portraits $\mathbb{U}^{2,I}_{BC,30}$, $\mathbb{U}^{2,I}_{BC,31}$, and $\mathbb{U}^{2,I}_{BC,32}$.

- Regarding $\mathbb{U}^{2,I}_{BC,30}$, proceeding according to item 3 of Lemma 3.3 yields phase portrait $\mathbb{U}^{1,I}_{B,c}$. Since $\mathbb{U}^{1,I}_{B,c}$ is proven impossible in Lemma 3.11, it follows from Theorem 3.12 that $\mathbb{U}^{2,I}_{BC,30}$ is also impossible.

- Phase portraits $\mathbb{U}^{2,I}_{BC,31}$ and $\mathbb{U}^{2,I}_{BC,32}$ are impossible due to the presence of graphics that violate Lemma 3.9.

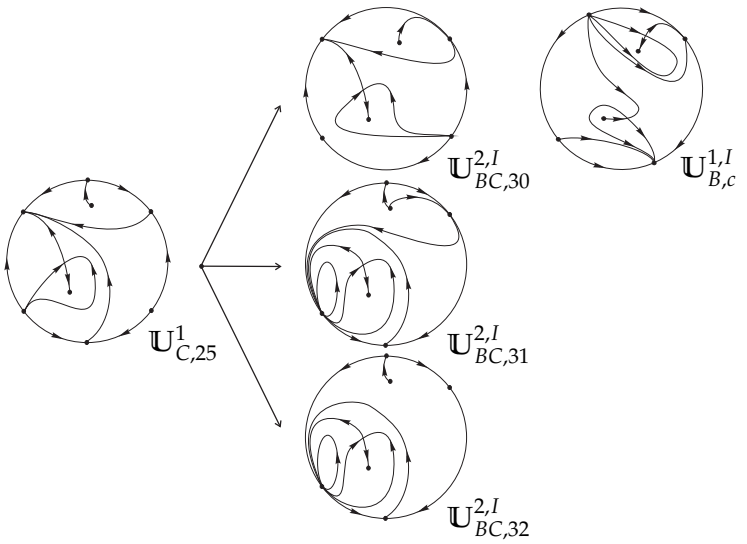


Figure 4.43: Impossible unstable phase portraits $\mathbb{U}^{2,I}_{BC,30}$, $\mathbb{U}^{2,I}_{BC,31}$, $\mathbb{U}^{2,I}_{BC,32}$.

Phase portrait $\mathbb{U}^1_{C,26}$ possesses an infinite saddle-node $\overline{\binom{1}{1}}\,SN$, an infinite node, and an infinite saddle. Applying Corollary 3.2 yields the five evolutions depicted in Figure 4.44. Specifically, we obtain the realizable phase portrait $\mathbb{U}^2_{BC,28}$ alongside the impossible phase portraits $\mathbb{U}^{2,I}_{BC,33}$, $\mathbb{U}^{2,I}_{BC,34}$, $\mathbb{U}^{2,I}_{BC,35}$, and $\mathbb{U}^{2,I}_{BC,36}$.

- Regarding $\mathbb{U}^2_{BC,28}$, proceeding according to item 3 of Lemma 3.3, where the infinite elliptic-saddle releases a saddle into the finite plane, yields phase portraits $\mathbb{U}^1_{B,9}$ and $\mathbb{U}^1_{B,12}$.
- The coalescence of the infinite node with the infinite saddle-node gives rise to evolutions $\mathbb{U}^{2,I}_{BC,33}$, $\mathbb{U}^{2,I}_{BC,34}$, $\mathbb{U}^{2,I}_{BC,35}$, and $\mathbb{U}^{2,I}_{BC,36}$, and it is necessary an analysis of the possible locations of the separatrix formed at the bifurcation moment.
  - Phase portraits $\mathbb{U}^{2,I}_{BC,33}$, $\mathbb{U}^{2,I}_{BC,34}$, and $\mathbb{U}^{2,I}_{BC,35}$ are impossible due to the presence of graphics that violate Lemma 3.9.
  - The impossibility of $\mathbb{U}^{2,I}_{BC,36}$ is established by Lemma 3.7.

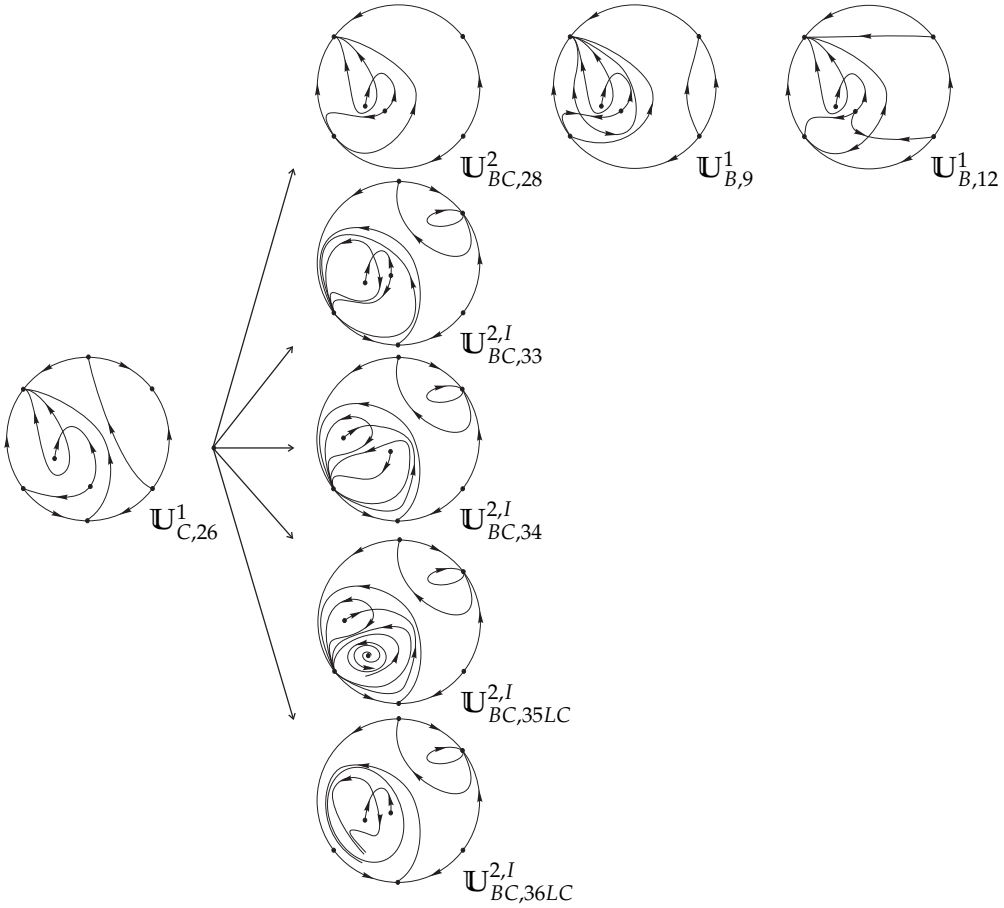


Figure 4.44: Unstable system $\mathbb{U}^2_{BC,28}$ and impossible unstable phase portraits $\mathbb{U}^{2,I}_{BC,33}$, $\mathbb{U}^{2,I}_{BC,34}$, $\mathbb{U}^{2,I}_{BC,35}$, $\mathbb{U}^{2,I}_{BC,36}$.

Phase portrait $\mathbb{U}^1_{C,27}$ possesses an infinite saddle-node $\overline{\binom{1}{1}}\,SN$, an infinite node, and an infinite saddle. Applying Corollary 3.2 yields the three evolutions depicted in Figure 4.45. Specifically, we obtain the impossible phase portraits $\mathbb{U}^{2,I}_{BC,30}$, $\mathbb{U}^{2,I}_{BC,37}$, and $\mathbb{U}^{2,I}_{BC,38}$.

- Phase portrait $\mathbb{U}^{2,I}_{BC,30}$ has previously been shown to be impossible.
- Phase portraits $\mathbb{U}^{2,I}_{BC,37}$ and $\mathbb{U}^{2,I}_{BC,38}$ are impossible due to the presence of graphics that violate Lemma 3.9.

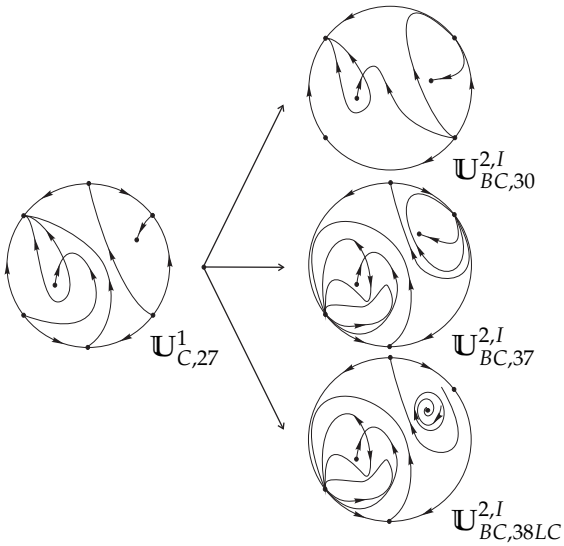


Figure 4.45: Impossible unstable phase portraits $\mathbb{U}^{2,I}_{BC,30}$, $\mathbb{U}^{2,I}_{BC,37}$, $\mathbb{U}^{2,I}_{BC,38}$.

Phase portrait $\mathbb{U}^{1}_{C,28}$ possesses an infinite saddle-node $\overline{\binom{1}{1}}\,SN$, an infinite node, and an infinite saddle. Applying Corollary 3.2 yields the four evolutions depicted in Figure 4.46. Specifically, evolution $\mathbb{U}^{2,I}_{BC,30}$ results from the coalescence of the infinite saddle with the infinite saddle-node $\overline{\binom{1}{1}}\,SN$, while evolutions $\mathbb{U}^{2,I}_{BC,39}$, $\mathbb{U}^{2}_{BC,33}$, and $\mathbb{U}^{2}_{BC,34}$ result from the coalescence of the infinite node with the infinite saddle-node $\overline{\binom{1}{1}}\,SN$.

- Phase portrait $\mathbb{U}^{2,I}_{BC,30}$ has previously been shown to be impossible.
- Phase portrait $\mathbb{U}^{2,I}_{BC,39}$ is proved to be impossible in Proposition 4.6.
- Regarding both $\mathbb{U}^{2}_{BC,33}$ and $\mathbb{U}^{2}_{BC,34}$, proceeding according to item 4 of Lemma 3.3, where the infinite elliptic-saddle releases a node into the finite plane, yields a phase portrait topologically equivalent to $\mathbb{U}^{1}_{B,35}$.

Proposition 4.6. *The phase portraits $\mathbb{U}^{2,I}_{BC,29}$ and $\mathbb{U}^{2,I}_{BC,39}$ are not realizable.*

Proof. We begin by drawing $\mathbb{U}^{2,I}_{BC,39}$ after applying both a vertical and a horizontal symmetry, together with a time reversal, so that the most relevant parts of the two phase portraits coincide; see Figure 4.47.

By the most relevant part of the phase portraits we mean the two repelling separatrices of the finite saddle that tend to the elliptic-saddle at infinity (one to the north pole and the other to the south pole). Both arrive tangent to the line at infinity and both are oriented from left to right. These two separatrices will play an important role in proving the impossibility of these phase portraits.

By means of a translation, we can place the finite saddle at the origin of the affine plane. Now consider the straight line given by the vertical axis. If the eigenvector of the saddle

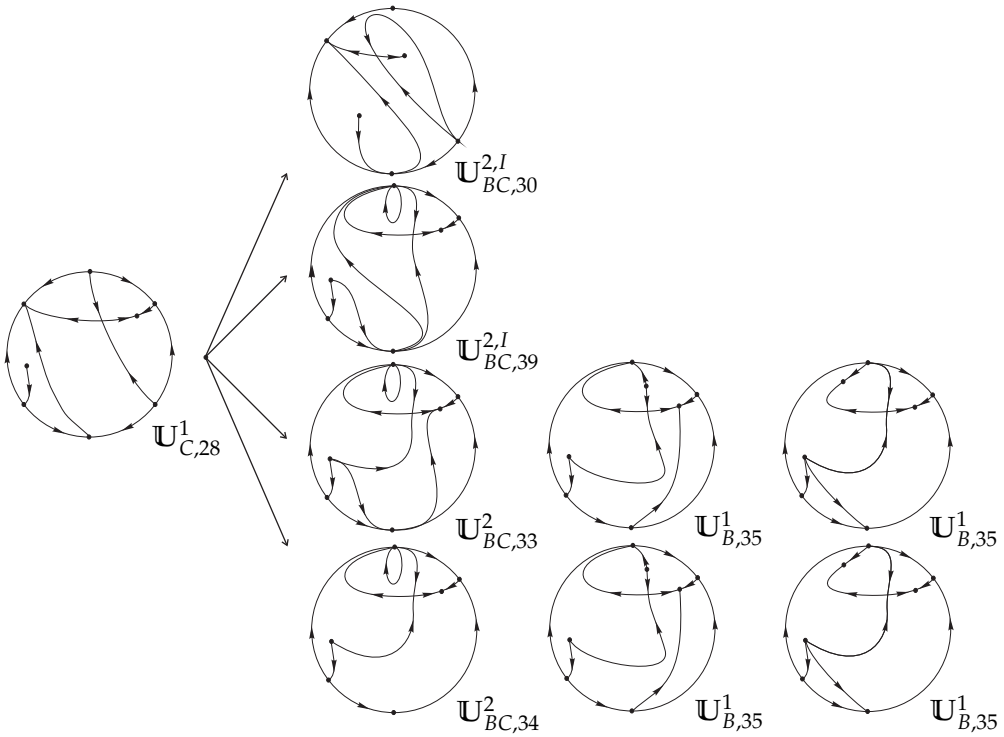


Figure 4.46: Impossible unstable phase portraits $\mathbb{U}^{2,I}_{BC,30}$, $\mathbb{U}^{2,I}_{BC,39}$ and unstable systems $\mathbb{U}^{2}_{BC,33}$, $\mathbb{U}^{2}_{BC,34}$.

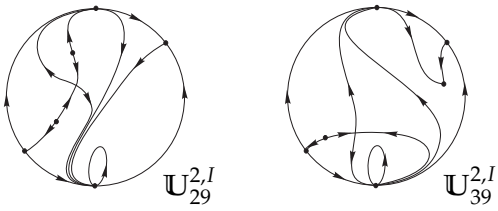


Figure 4.47: Impossible phase portraits $\mathbb{U}^{2,I}_{BC,29}$ and $\mathbb{U}^{2,I}_{BC,39}$.

tangent to these separatrices were aligned with the vertical axis, then the other eigenvector would be transversal to it, and the straight line $x = -\varepsilon < 0$ would have two contact points close to the saddle. Together with the singularity at infinity, this would lead to a contradiction (see Figure 4.48(a)).

Therefore, the set formed by the two separatrices (together with the saddle) must intersect the vertical axis at least twice, and the saddle must lie at one of these intersection points (see Figure 4.48(b)–(c)).

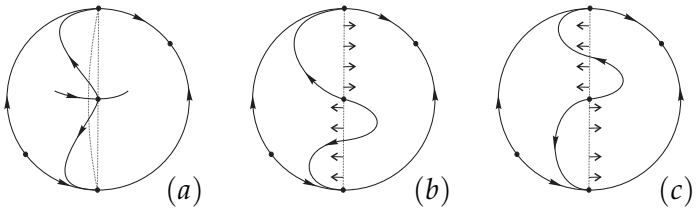


Figure 4.48: Schemes of the phase portraits.

Recall that we want to place an elliptic sector at the south pole. This implies that case (c)

is not realizable for either phase portrait. Hence, we must proceed with case (b). Observe also that if there were additional intersection points with the vertical axis, then the number of contact points between this axis and some orbits would increase.

Now we must consider the position of the other two separatrices of the finite saddle. They may be arranged as in Figure 4.49(ba) or (bb).

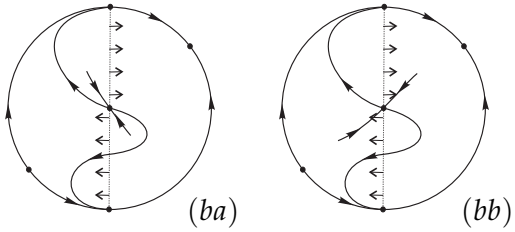


Figure 4.49: Schemes of the phase portraits.

However, Figure 4.49(bb), which would correspond to the phase portrait $\mathbb{U}^{2,I}_{BC,39}$, is not realizable because the flow on the vertical axis close to the finite saddle is incompatible with the separatrices. Thus, this phase portrait is already proved to be impossible.

We must therefore continue with scheme 4.49(ba) and try to produce $\mathbb{U}^{2,I}_{BC,29}$. In principle, it seems possible to add the two finite antisaddles and the separatrices from the infinite saddle on the left half-plane, together with the separatrix of the elliptic-saddle at the north pole that goes to the negative x–semiplane, without further contradiction.

We have drawn the antisaddles as nodes, but there is no contradiction if any of them is a focus. We draw the remaining separatrices in Figure 4.50(bab). We have also numbered the different canonical regions and the singularities so that we may refer to them easily. For the same reason, we have also named the infinite singularities, using different names for their opposite representations.

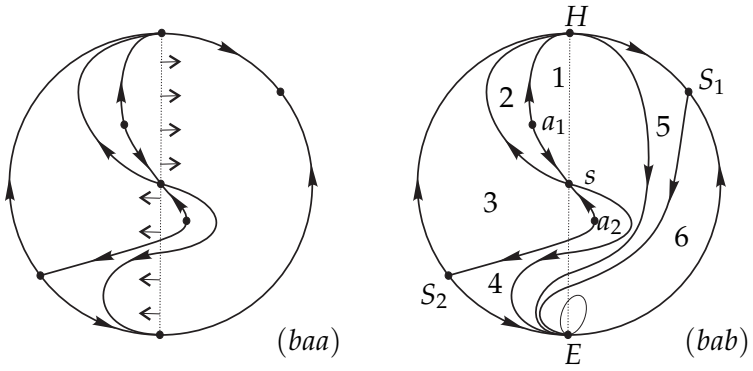


Figure 4.50: Scheme of the phase portrait $\mathbb{U}^{2,I}_{BC,29}$.

Now we must consider where the horizontal isocline, that is, the curve $y' = 0$, is located. Notice that this curve must be a conic and must pass through the three finite singularities and through the nilpotent infinite singularity, since it contains a finite singularity that has coalesced there. The isocline cannot be formed by complex components since we already have three finite real singularities. The possibilities for this isocline are therefore: an ellipse, a parabola, a hyperbola, two intersecting straight lines, two parallel straight lines, or a double straight line.

Among these possibilities we can immediately discard the ellipse (since it cannot contain

H and E), the parallel straight lines (since one would have to be the vertical axis, and a parallel to it cannot contain both a_1 and a_2), and the double straight line for obvious reasons.

Some of the orbits that leave a_1 and go to H through canonical region 1 must have a maximum in the y–variable, and this produces points of the isocline in region 1 joining H to a_1.

Some of the orbits that leave a_1 and go to s through canonical region 2 must have a minimum in the y–variable, producing points of the isocline in region 2 joining a_1 to s.

Yes, we know that we could have drawn the phase portrait so that a_1 would lie in the third quadrant, but this additional twisting of the separatrices would already produce extra contact points.

Some of the orbits that leave a_2 and go to E through canonical region 4 must have a maximum in y, producing further points of the isocline in region 4 joining s to a_2.

Now we consider the elliptic sector, which covers the whole canonical region 6. Every elliptic orbit must have a maximum in y, producing additional points of the isocline in region 6. These points clearly start at E but do not necessarily end at S_1. In fact, they may end at any point of the arc $\widehat{S_1E}$ or $\widehat{S_1H}$.

From all this we already conclude that the isocline cannot be a parabola and cannot consist of two intersecting straight lines. Hence, the only remaining possibility is a hyperbola. However, this "hyperbola" would have the vertical axis as one asymptote, and a hyperbola can never cross any of its asymptotes, as this one would do at s.

Therefore, we conclude that the phase portrait $\mathbb{U}^{2,I}_{BC,29}$ is not realizable. □

Phase portrait $\mathbb{U}^{1}_{C,29}$ possesses an infinite saddle-node $\overline{\binom{1}{1}}\,SN$, an infinite node, and an infinite saddle. By applying Corollary 3.2, and taking into account the orbital configurations resulting from the coalescence of infinite singularities, as well as the potential existence of two limit cycles in $\mathbb{U}^{1}_{C,29}$, we obtain the five evolutions depicted in Figure 4.51. Specifically, evolution $\mathbb{U}^{2,I}_{BC,28}$ results from the coalescence of the infinite saddle with the infinite saddle-node $\overline{\binom{1}{1}}\,SN$, while evolutions $\mathbb{U}^{2,I}_{BC,40}$, $\mathbb{U}^{2}_{BC,33}$, $\mathbb{U}^{2}_{BC,34}$, and $\mathbb{U}^{2,I}_{BC,41}$ result from the coalescence of the infinite node with the infinite saddle-node $\overline{\binom{1}{1}}\,SN$.

- Phase portrait $\mathbb{U}^{2,I}_{BC,28}$ has previously been shown to be impossible (see page 51).
- Phase portraits $\mathbb{U}^{2,I}_{BC,40}$ and $\mathbb{U}^{2,I}_{BC,41}$ are impossible due to their configuration of infinite singularities.
- Regarding both $\mathbb{U}^{2}_{BC,33}$ and $\mathbb{U}^{2}_{BC,34}$, proceeding according to item 4 of Lemma 3.3, where the infinite elliptic-saddle releases a node into the finite plane, yields a phase portrait topologically equivalent to $\mathbb{U}^{1}_{B,35}$.

Phase portrait $\mathbb{U}^{1}_{C,30}$ possesses an infinite saddle-node $\overline{\binom{1}{1}}\,SN$, an infinite node, and an infinite saddle. Applying Corollary 3.2, and taking into account the orbital configurations resulting from the coalescence of infinite singularities as well as the potential existence of two limit cycles in $\mathbb{U}^{1}_{C,30}$, we obtain the five evolutions depicted in Figure 4.52. Specifically, evolution $\mathbb{U}^{2}_{BC,32}$ results from the coalescence of the infinite saddle with the infinite saddle-node $\overline{\binom{1}{1}}\,SN$, while evolutions $\mathbb{U}^{2}_{BC,35}$, $\mathbb{U}^{2}_{BC,30}$, $\mathbb{U}^{2}_{BC,31}$, and $\mathbb{U}^{2,I}_{BC,42}$ result from the coalescence of the infinite node with the infinite saddle-node $\overline{\binom{1}{1}}\,SN$.

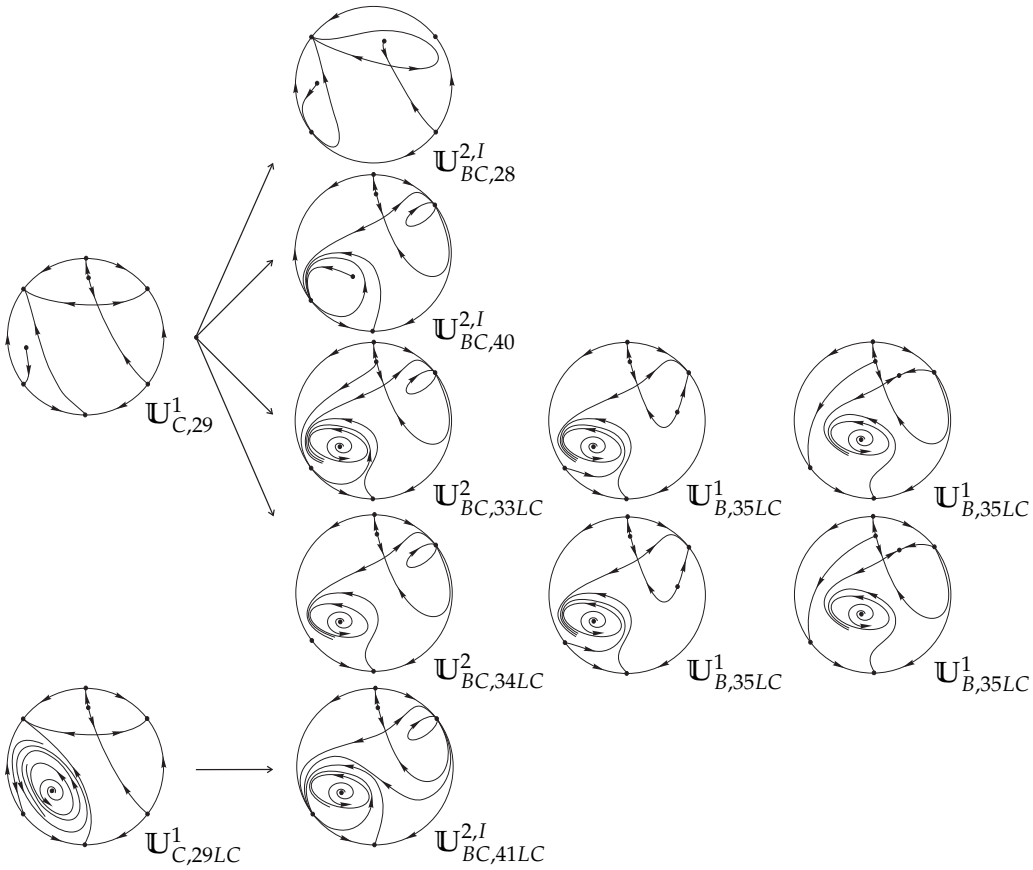


Figure 4.51: Impossible unstable phase portraits $\mathbb{U}^{2,I}_{BC,28}$, $\mathbb{U}^{2,I}_{BC,40}$, $\mathbb{U}^{2,I}_{BC,41}$ and unstable systems $\mathbb{U}^{2}_{BC,33}$, $\mathbb{U}^{2}_{BC,34}$.

- Regarding $\mathbb{U}^{2}_{BC,32}$, proceeding according to item 3 of Lemma 3.3, where the infinite elliptic-saddle releases a saddle into the finite plane, yields phase portrait $\mathbb{U}^{1}_{B,25}$.

- Regarding evolutions $\mathbb{U}^{2}_{BC,35}$, $\mathbb{U}^{2}_{BC,30}$, and $\mathbb{U}^{2}_{BC,31}$, proceeding according to item 4 of Lemma 3.3, where the infinite elliptic-saddle releases a node into the finite plane, yields phase portraits topologically equivalent to $\mathbb{U}^{1}_{B,34}$, $\mathbb{U}^{1}_{B,36}$, and $\mathbb{U}^{1}_{B,38}$.

- Phase portrait $\mathbb{U}^{2,I}_{BC,42}$ is impossible due to its configuration of infinite singularities.

Phase portrait $\mathbb{U}^{1}_{C,31}$ possesses an infinite saddle-node $\overline{\binom{1}{1}}\,SN$, an infinite node, and an infinite saddle. Applying Corollary 3.2 yields the three evolutions depicted in Figure 4.53. Specifically, we obtain the realizable phase portrait $\mathbb{U}^{2}_{BC,29}$ alongside the impossible phase portraits $\mathbb{U}^{2,I}_{BC,43}$ and $\mathbb{U}^{2,I}_{BC,44}$.

- Regarding $\mathbb{U}^{2}_{BC,29}$, proceeding according to item 3 of Lemma 3.3, where the infinite elliptic-saddle releases a saddle into the finite plane, yields phase portraits $\mathbb{U}^{1}_{B,16}$ and $\mathbb{U}^{1}_{B,20}$.

- Phase portraits $\mathbb{U}^{2,I}_{BC,43}$ and $\mathbb{U}^{2,I}_{BC,44}$ are impossible due to Lemma 3.8 and Lemma 3.7, respectively.

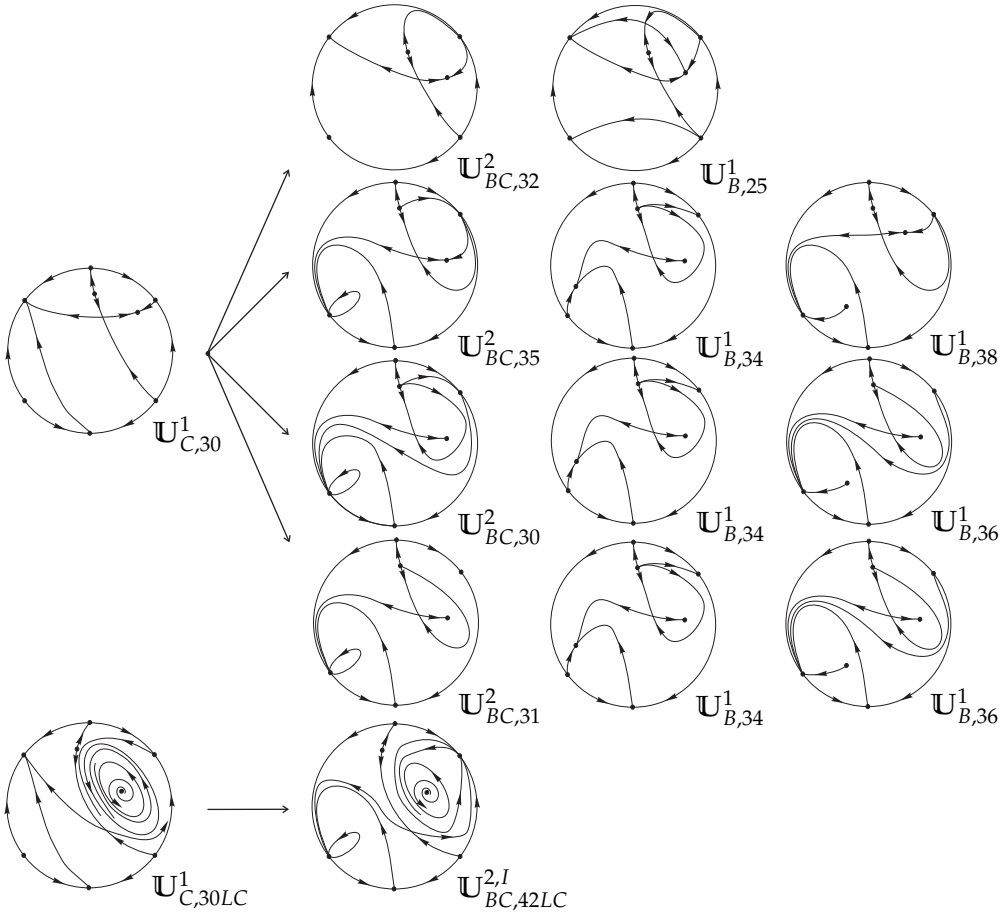


Figure 4.52: Impossible unstable phase portrait $\mathbb{U}^{2,I}_{BC,42}$ and unstable systems $\mathbb{U}^2_{BC,32}$, $\mathbb{U}^2_{BC,35}$, $\mathbb{U}^2_{BC,30}$, $\mathbb{U}^2_{BC,31}$.

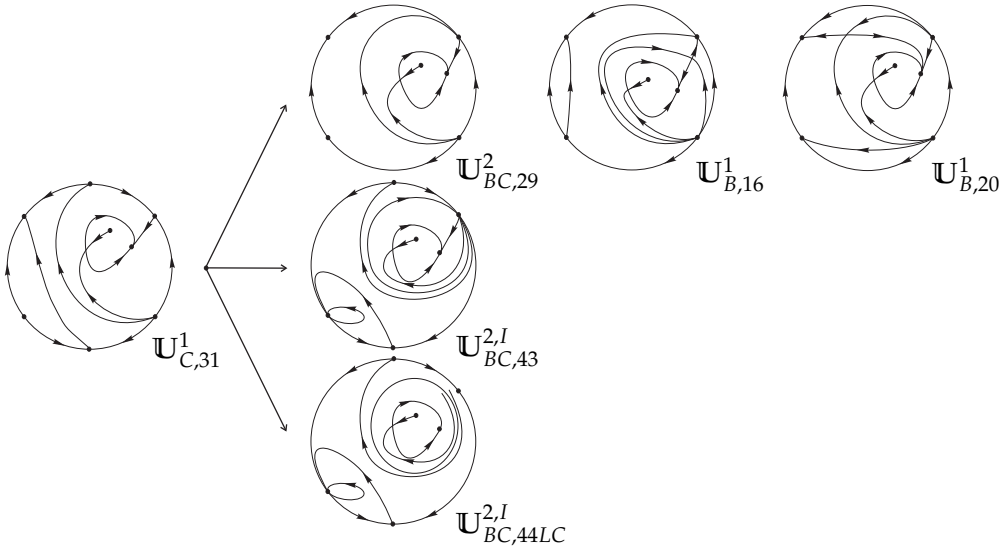


Figure 4.53: Unstable system $\mathbb{U}^2_{BC,29}$ and impossible unstable phase portraits $\mathbb{U}^{2,I}_{BC,43}$, $\mathbb{U}^{2,I}_{BC,44}$.

Phase portrait $\mathbb{U}^1_{C,32}$ possesses an infinite saddle-node $\overline{\binom{1}{1}}\,SN$, an infinite node, and an

infinite saddle. Applying Corollary 3.2 yields the three evolutions depicted in Figure 4.54. Specifically, we obtain the impossible phase portraits $\mathbb{U}^{2,I}_{BC,28}$, $\mathbb{U}^{2,I}_{BC,45}$, and $\mathbb{U}^{2,I}_{BC,46}$.

- Phase portrait $\mathbb{U}^{2,I}_{BC,28}$ has previously been shown to be impossible.
- Phase portraits $\mathbb{U}^{2,I}_{BC,45}$ and $\mathbb{U}^{2,I}_{BC,46}$ are impossible by virtue of Lemma 3.8.

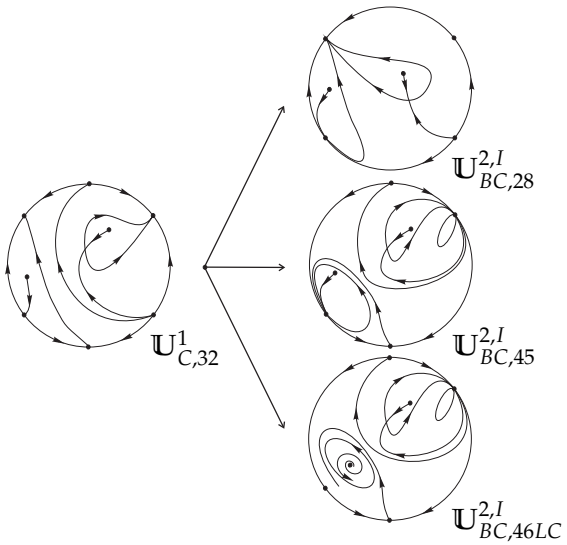


Figure 4.54: Impossible unstable phase portraits $\mathbb{U}^{2,I}_{BC,28}$, $\mathbb{U}^{2,I}_{BC,45}$, $\mathbb{U}^{2,I}_{BC,46}$.

4.3 The realization of the potential phase portraits

In the preceding two subsections, we identified all topologically potential phase portraits for structurally unstable quadratic systems of *codimension two** belonging to the set $\sum^2_2(BC)$. From this collection, 46 phase portraits were discarded as unrealizable based on the justifications previously detailed.

The goal of this subsection is to provide specific examples for the remaining 35 distinct topological classes of structurally unstable quadratic systems of *codimension two** within $\sum^2_2(BC)$, as presented in Figures 1.1 and 1.2.

We begin by considering the set (BC_{SNSN}), which comprises all quadratic systems possessing the infinite saddle-nodes $(\overline{\substack{0\\2}})SN$ and $(\overline{\substack{1\\1}})SN$. Subsection 4.1 yielded the topologically potential phase portraits $\mathbb{U}^2_{BC,1}$ through $\mathbb{U}^2_{BC,16}$ for this set. To establish the realization of these 16 phase portraits, we now present specific examples of quadratic systems exhibiting these dynamics.

In [11], the authors proved that every nondegenerate quadratic system possessing a finite semi-elemental saddle-node $\overline{sn}_{(2)}$ at the origin, a finite elemental singularity at $(1,0)$, and an infinite saddle-node of type $(\overline{\substack{1\\1}})SN$ can be brought, via affine transformation and time rescaling, to the previously mentioned normal form (3.8):

$$\begin{cases} \dot{x} = cx + cy - cx^2 + 2hxy, \\ \dot{y} = ex + ey - ex^2 + 2mxy, \end{cases}$$

where c, e, h, m are real parameters satisfying $eh \neq cm$. We note that the generic phase portraits obtained in that study were essential for the topological classification of the set (AC) (see [12]).

Furthermore, in the same study, it was shown that when $h = 1$ and $e = (c+2m)^2/8$, the corresponding phase portraits also possess an infinite saddle-node of type $(\overline{\begin{smallmatrix}0\\2\end{smallmatrix}})SN$. These phase portraits are denoted by $5S_j$ ($j \in \mathbb{N}$) in [11, Figures 3 and 4].

To establish the realization of the 16 phase portraits within the set (BC_{SNSN}), we use the configurations $5S_j$ from [11] and consider the perturbed system (3.9) from which, as previously explained, if $\varepsilon > 0$ the finite saddle-node splits into a saddle and a node, and if $\varepsilon < 0$ the finite saddle-node vanishes into the complex plane.

Table 4.4 presents the parameter values for system (3.9) that realize the 16 phase portraits of the set (BC_{SNSN}). We invite the reader to verify these phase portraits using the software P4 ([2]).

Codimension two* **from the set (BC_{SNSN})**	**Phase portrait from [11] to be perturbed**	ε	c	m
$\mathbb{U}^2_{BC,1}$	$5S_{17}$	-10^{-4}	$-1/2$	$-103/100$
$\mathbb{U}^2_{BC,2}$	$5S_1$	-10^{-3}	-30	4
$\mathbb{U}^2_{BC,3}$	$5S_4$	-10^{-3}	-10	4
$\mathbb{U}^2_{BC,4}$	$5S_{19}$	10^{-7}	$-3/80$	$-1/4$
$\mathbb{U}^2_{BC,5}$	$5S_5$	10^{-3}	-5	4
$\mathbb{U}^2_{BC,6}$	$5S_6$	10^{-3}	$-21/10$	4
$\mathbb{U}^2_{BC,7}$	$5S_4$	10^{-3}	-10	4
$\mathbb{U}^2_{BC,8}$	$5S_8$	10^{-3}	4	4
$\mathbb{U}^2_{BC,9}$	$5S_{18}$	10^{-4}	$-2/100$	$-1/4$
$\mathbb{U}^2_{BC,10}$	$5S_1$	10^{-3}	-30	4
$\mathbb{U}^2_{BC,11}$	$5S_{22}$	10^{-5}	$-47/100$	$-1/4$
$\mathbb{U}^2_{BC,12}$	$5S_{17}$	10^{-4}	$-1/2$	$-103/100$
$\mathbb{U}^2_{BC,13}$	$5S_{27}$	10^{-3}	$-3/2$	$-6/5$
$\mathbb{U}^2_{BC,14}$	$5S_3$	10^{-3}	-15	4
$\mathbb{U}^2_{BC,15}$	$5S_2$	10^{-3}	$-182/10$	4
$\mathbb{U}^2_{BC,16}$	$5S_{25}$	10^{-4}	$-135/100$	$-98/100$

Table 4.4: Correspondence between *codimension-two** phase portraits of the set (BC_{SNSN}) and perturbed phase portraits from [11, Figures 3 and 4]. In the first column we present the *codimension-two** phase portraits from the set (BC_{SNSN}) in the present paper, in the second column we show the corresponding phase portraits from [11, Figures 3 and 4] we shall perform a perturbation, and in the remaining columns we present the values of the parameters ε, c, and m of (3.9) which realizes such phase portrait.

We now examine the set (BC_{ESNS}), which comprises quadratic systems possessing either an infinite nilpotent elliptic-saddle (of type $(\widehat{\begin{smallmatrix}1\\2\end{smallmatrix}})PHP-E$, $(\widehat{\begin{smallmatrix}1\\2\end{smallmatrix}})H-E$, or $(\widehat{\begin{smallmatrix}1\\2\end{smallmatrix}})PEP-H$) or an infinite nilpotent saddle $(\widehat{\begin{smallmatrix}1\\2\end{smallmatrix}})\,HHH-H$. Subsection 4.2 identified the topologically potential phase

portraits $\mathbb{U}^2_{BC,17}$ through $\mathbb{U}^2_{BC,35}$ for this set. To establish the realization of these 19 phase portraits, we must identify specific quadratic systems exhibiting these dynamics.

In [13], we presented a geometric study of classes $\mathbf{Q\widehat{ES}(A)}$ and $\mathbf{Q\widehat{ES}(B)}$. Class $\mathbf{Q\widehat{ES}(A)}$ consists of quadratic systems with three real finite singular points, an elemental infinite singularity, and either an infinite nilpotent elliptic–saddle or an infinite nilpotent saddle. This class is described by the normal form (3.13). Class $\mathbf{Q\widehat{ES}(B)}$ consists of quadratic systems possessing one real and two complex finite singular points, alongside the same infinite configuration. This class is governed by the family (3.14).

To realize the 19 phase portraits $\mathbb{U}^2_{BC,17}$ through $\mathbb{U}^2_{BC,35}$ within set (BC_{ESNS}), we identify phase portraits corresponding to generic regions in the bifurcation diagrams of classes $\mathbf{Q\widehat{ES}(A)}$ (see [13, Figure 1]) and $\mathbf{Q\widehat{ES}(B)}$ (see [13, Figure 4]).

Tables 4.5 and 4.6 list the parameter values for systems (3.13) and (3.14), respectively, that realize the 19 phase portraits of set (BC_{ESNS}). We invite the reader to verify these results using the software P4 ([2]). This concludes the proof of our main result.

Codimension two* **from the set (BC_{ESNS})**	**Phase portrait from [13, Figure 1]**	c	e	f
$\mathbb{U}^2_{BC,18}$	V_{12}	3	-11	285/100
$\mathbb{U}^2_{BC,19}$	V_9	3	-4	28/10
$\mathbb{U}^2_{BC,20}$	V_1	3	12	5
$\mathbb{U}^2_{BC,26}$	V_{168}	$-125/100$	5	175/100
$\mathbb{U}^2_{BC,27}$	V_{89}	$-1/10$	1/2	1/2
$\mathbb{U}^2_{BC,28}$	V_{233}	-3	12	315/100
$\mathbb{U}^2_{BC,29}$	V_{238}	-3	85/10	3007/1000
$\mathbb{U}^2_{BC,30}$	V_{173}	$-125/100$	1	13/10
$\mathbb{U}^2_{BC,31}$	V_{94}	$-1/10$	25/10000	101/1000
$\mathbb{U}^2_{BC,32}$	V_{240}	-3	1001/100	17
$\mathbb{U}^2_{BC,33}$	V_{188}	$-125/100$	5/100	4/10
$\mathbb{U}^2_{BC,34}$	V_{101}	$-1/10$	1/1000	98/1000
$\mathbb{U}^2_{BC,35}$	V_{176}	$-125/100$	25/100	15/10

Table 4.5: Correspondence between phase portraits of the set (BC_{ESNS}) and phase portraits from class $\mathbf{Q\widehat{ES}(A)}$. In the first column we present the *codimension-two** phase portraits from the set (BC_{ESNS}) in the present paper, in the second column we show the corresponding phase portraits from [13, Figure 1], and in the remaining columns we present the values of the parameters c, e, and f of (3.13) which realize such phase portrait.

Codimension two* from the set (BC_{ESNS})	Phase portrait from [13, Figure 4]	g	u	ℓ
$\mathbb{U}^2_{BC,17}$	V_1	2	2	3
$\mathbb{U}^2_{BC,21}$	V_{20}	-3	2	1
$\mathbb{U}^2_{BC,22}$	V_{12}	$-3/2$	1	1
$\mathbb{U}^2_{BC,23}$	V_5	$-1/4$	3	1
$\mathbb{U}^2_{BC,24}$	V_{15}	$-3/2$	1	$-1/4$
$\mathbb{U}^2_{BC,25}$	V_{14}	$-3/2$	1	5/10000

Table 4.6: Correspondence between phase portraits of the set (BC_{ESNS}) and phase portraits from class $\mathbf{Q\widehat{ES}}(\mathbf{B})$. In the first column we present the *codimension-two** phase portraits from the set (BC_{ESNS}) in the present paper, in the second column we show the corresponding phase portraits from [13, Figure 4], and in the remaining columns we present the values of the parameters g, u, and ℓ of (3.14) which realize such phase portrait.

5 Some concluding remarks

The main goal of this paper was to provide a topological classification, modulo limit cycles, of the phase portraits within the set (BC), defined as the disjoint union of sets (BC_{SNSN}) and (BC_{ESNS}). The proof of Theorem 1.6 establishes the existence of exactly 35 topologically distinct phase portraits modulo limit cycles. Considering phase portraits primarily derived from [11,13], we realized all 35 unstable systems of *codimension two** within set (BC) presented in Figures 1.1 and 1.2, thereby providing concrete examples for every structurally unstable phase portrait in this classification.

All the 35 portraits from Figure 1.2 may have (or not) limit cycles, if at least one of the finite antisaddle is a focus. Even more, some of them may have a weak focus which induces to think that they may be perturbed so to obtain a limit cycle. However, there are two phase portraits, concretely $\mathbb{U}^2_{BC,23}$ and $\mathbb{U}^2_{BC,25}$ (see Figure 5.1) which have been proved here that indeed may appear with a limit cycle since some evolution of phase portrait $\mathbb{U}^1_{C,16}$ leads to these portraits without limit cycles, and others lead to these phase portraits with limit cycles.

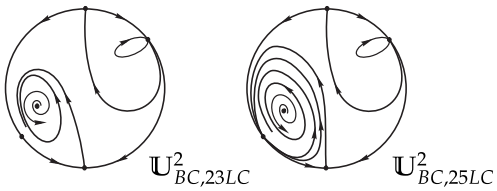


Figure 5.1: Phase portraits $\mathbb{U}^2_{BC,23}$ and $\mathbb{U}^2_{BC,25}$ with limit cycle.

In [13], the authors analyzed the bifurcation diagrams corresponding to classes $\mathbf{Q\widehat{ES}}(\mathbf{A})$ and $\mathbf{Q\widehat{ES}}(\mathbf{B})$, where the generic phase portraits correspond to elements of the set (BC_{ESNS}). In Sections 3.1.7 and 3.2.7 of that study, the bifurcation diagrams were described as coherent; that is, for any continuous path connecting two points in parameter space, the transitions in phase portraits across bifurcation surfaces could be fully accounted for. However, uncertainty re-

mained regarding the completeness of these diagrams for the considered families, specifically due to the potential existence of isolated regions or "islands" within the parameter space. The topological analysis presented herein partially addresses this issue by proving that all realizable phase portraits of set (BC_{ESNS}) indeed exist and that no other topological configurations are possible. Nevertheless, the potential existence of "islands" in the bifurcation diagrams remains an open question, as these may be associated with multiple limit cycles, as discussed in the aforementioned sections.

Regarding the set (BC_{SNSN}), the realization of phase portraits was established via perturbation of specific cases from [11]. The analysis of the corresponding complete bifurcation diagram remains a subject for future research. However, given the approach adopted in this paper, we anticipate that no additional phase portraits belonging to class (BC_{SNSN}), beyond those identified here, will emerge in future studies.

The current paper already conforms a proof that the codimension-two class (BC) modulo limit cycles contains exactly 35 phase portraits. For a further corroboration, the authors have developed a database from more than 100 articles dated from 1975 up to nowadays which have classified some families of quadratic systems. The database actually contains 6,816 phase portraits. The authors have assigned to all those phase portraits some topological invariants so to be able to detect with a simple filter (as in an Excel file) which phase portraits contain the same topological invariants or not, that is, if the phase portraits are topologically equivalent or not. Once we have confronted the 35 phase portraits presented here with the whole database, we have confirmed that none other phase portrait of codimension two containing a nilpotent infinite singularity has appeared ever in any other paper.

It is also worth to mention the existence of another paper [9] in which all the phase portraits of quadratic systems with a nilpotent or an intricate singularity (that is not topologically equivalent to an elemental or semi-elemental singularity) is studied. This paper uses techniques based on invariant polynomials which are powerful enough to detect the most degenerated cases, and provide a proof that the study is complete. However, for the most generic cases (codimension two), the paper relies on [13] and thus, the study is still subject to the "island" existence. However, the production of the current paper has been simultaneous with [9] so that all the potential phase portraits of our class had been already checked to exist, or proved not to exist, so the paper already incorporates the definitive notation that we will describe in Section 6.

In the present study, we observed a distinct phenomenon not previously encountered in earlier classifications. Specifically, when analyzing codimension-one phase portraits, we found that each typically unfolds into exactly two codimension-zero configurations. For instance, $\mathbb{U}^1_{A,1}$ bifurcates into $\mathbb{S}^2_{2,1}$ and $\mathbb{S}^2_{1,1}$, either via the separation of a saddle-node into a saddle and a node, or by their transition into complex conjugate points. This pattern holds for sets (B) and (C). Similarly, in set (D), $\mathbb{U}^1_{D,2}$ bifurcates into $\mathbb{S}^2_{3,1}$ and $\mathbb{S}^2_{3,2}$, depending on the mechanism of the connection breaking. Thus, while a codimension-zero phase portrait may possess multiple codimension-one boundaries, a codimension-one phase portrait consistently bifurcates into exactly two (invariant) codimension-zero phase portraits (or fewer, in cases of symmetry).

Furthermore, in our prior work on sets (AA), (AB), (AC), and (AD), we dealt with codimension-two scenarios representing the intersection of codimension-one bifurcations. Consequently, it is expected that each codimension-two phase portrait bifurcates into four codimension-one portraits (or fewer, allowing for symmetries). For example, $\mathbb{U}^2_{AB,1}$ bifurcates into $\mathbb{U}^1_{A,19}$ and $\mathbb{U}^1_{A,1}$, and also into $\mathbb{U}^1_{B,1}$ and $\mathbb{U}^1_{B,3}$.

However, the analysis of the set (BC) reveals a notable deviation from this norm. Certain

phase portraits, such as $\mathbb{U}^2_{BC,19}$, can bifurcate into four phase portraits from set (C) and two from set (B). One can verify that $\mathbb{U}^2_{BC,19}$ is adjacent to $\mathbb{U}^1_{C,6}$, $\mathbb{U}^1_{C,9}$, $\mathbb{U}^1_{C,11}$, and $\mathbb{U}^1_{C,13}$. This behavior arises because the coalescence of an infinite node (or saddle) with a $\overline{\binom{1}{1}}\,SN$ may result in the appearance or disappearance of separatrices, as detailed in Section 3. Depending on whether these separatrices exist, new topological possibilities emerge that were not previously present.

Finally, although this paper places limited emphasis on graphics and limit cycles, these remain two of the most critical elements in the qualitative theory of ordinary differential equations. The limited discussion of limit cycles is intentional; our goal is to provide a classification modulo limit cycles, establishing a robust foundation upon which we or others may subsequently incorporate limit cycle analysis. Similarly, the discussion of graphics is minimal because, at the codimension level considered here, very few of the 121 graphics described in [21] appear. Specifically, in this study, we identified the following graphics from [21] related to infinite singularities: (I^2_{19}), (I^2_{21}), (I^2_{24}), (I^1_{8a}), (I^1_{8b}), (I^2_{23}), (I^1_{7a}), and (I^1_{7b}).

6 Notation for phase portraits

Over the last five decades mathematicians have topologically classified quadratic phase portraits and assigned various labels or names to them. All these names followed the logic and the methodology of the classification carried out in each paper, and most of them were independent of one another. As a consequence, a given phase portrait often appears with different names in different papers. It is perhaps an appropriate moment to establish a systematic way to name all of them. We propose to do this as follows.

We have 207 different topological configurations of singularities. This implies that two phase portraits with different configurations of singularities cannot be topologically equivalent. Thus, the 207 configurations of singularities provide a convenient skeleton on which to classify the phase portraits. Many of these topological configurations lead to a single phase portrait, some lead to several phase portraits, and a few configurations may lead to dozens of phase portraits. For instance, we already have configuration (39): $s, a, sn; \binom{0}{2} SN, N$ with 99 confirmed topologically distinct phase portraits.

Notation 6.1. We propose to denote each phase portrait by $QSr^{(b)}_a$, where QS stands for "quadratic differential system", r is the number of the configuration of singularities from [7], b is the topological codimension of the phase portrait, and a is simply an index enumerating the different phase portraits with the same configuration and codimension. If the phase portrait has limit cycles, we add (i, j, k) to the subindex, obtaining $QS3^{(0)}_{a(i,j,k)LC}$, where $i + j + k > 0$ denote the total number of limit cycles around antisaddles present in the phase portrait.

Remark 6.2. We are aware that a quadratic system may have at most two nests of limit cycles, and thus using a notation that may suggest the existence of up to three nests may seem somewhat unusual. However, there exist skeletons of phase portraits that may contain up to three antisaddles, and any of them may be a focus. Therefore, a notation that may describe the limit cycles around each of the three antisaddles is needed.

In [9] the authors also assigned a topological codimension to each of the 207 global topological configurations of singularities from [7]. Thus, the topological codimension of the phase portraits that arise from each topological configuration of singularities will be either the same

or greater if the phase portrait exhibits one or more separatrix connections that are not already forced by the configuration of singularities.

To clarify why we use the codimension in this notation, recall that we start with a fixed global topological configuration of singularities. For this configuration there may exist a large number of phase portraits. The codimension splits this set into several subsets, each containing a much smaller number of phase portraits.

The codimension of a phase portrait comes from two sources: one is the codimension of the configuration of singularities, and the other is the codimension induced by separatrix connections. However, the codimension of the phase portrait is not simply the sum of both codimensions, since some configurations of singularities may already force the existence of certain separatrix connections. In the same way, the codimension of the configuration of singularities is not always a simple sum of the codimensions of its singularities, since sometimes the degeneracy of one singularity may also force the degeneracy of another.

Another important effect of the codimension is that it helps us locate the "neighbors" of phase portraits.

This notation was first introduced in [9], but only a few examples of its use were given there. Later it was also used in [16].

There are two types of papers dealing with classifications of phase portraits (mainly for quadratic systems). Most of them search for a certain geometrical property, obtain a normal form for it, and then produce a bifurcation diagram together with its phase portraits. Although most authors of papers of this kind claim that the obtained phase portraits are all the realizable ones for that family, this claim is not always proved. The reason is that many bifurcation diagrams may contain "islands" in the parameter space related to non-algebraic bifurcations which may be undetectable with the techniques used to obtain the bifurcation diagram.

The most obvious possible island is one whose boundary produces a double limit cycle and which contains two limit cycles in its interior. Since such islands may be arbitrarily small, they escape any possible numerical analysis. Other possible islands could also produce a non-algebraic separatrix connection on their boundary and a different phase portrait inside (without producing a limit cycle). In any case, no island of this kind has ever been reported in a classification, and all bifurcations producing double limit cycles located so far can be detected by continuity and coherence arguments from the surrounding regions in the bifurcation diagram.

The second type of papers is like the present one, where we exhibit all the potential phase portraits with a certain prescribed property. Among these potential phase portraits, we prove which ones are realizable by providing explicit examples and which ones are impossible by means of rigorous proofs. In some cases, a few situations may still remain undecided, that is, their existence is still uncertain (perhaps these are candidates to lie in one of the islands mentioned above, although we do not believe this to be the case).

From what we have explained about these two methods of studying phase portraits, it should be clear that it is preferable to assign definitive names to phase portraits arising from the second type of papers rather than from the first. The reason is that, if names are assigned to phase portraits from papers of the first type, which may not completely cover a given configuration of singularities and may still miss some phase portraits, newly discovered portraits might later need to be inserted in an unnatural order. In contrast, when one obtains all the potential and realizable phase portraits of a given class, one may be sure that no additional portraits will appear later. One may then assign definitive names to the realizable ones, and

even to the impossible ones and to those whose existence is still unconfirmed.

The five papers preceding the present one, [3], [5], [14], [12] and [1], were published before this notation was available. Thus, we take this opportunity to assign the notation to all the phase portraits of codimensions zero and one, and to many of the already studied phase portraits of codimension two, including those obtained in this paper.

All realizable phase portraits normally appear in each paper in the same relevant place in the introduction or in the presentation of results, together with a definitive name within that paper. However, most of the time the non-realizable phase portraits do not appear in such statements and are scattered throughout the paper. In the following list we indicate in which figure of each paper the realizable and non-realizable portraits appear, since this also provides information about their neighboring portraits. If they appear in more than one figure, we indicate the first occurrence.

All this information is being collected in a database and an electronic encyclopedia which will be available within time at https://www.gsd.uab.cat/Quadripedia/.

6.1 Codimension-zero phase portraits

In the paper [3] all structurally stable phase portraits of quadratic systems without limit cycles were studied, that is, what we now call the codimension-zero phase portraits. From that study it was established that there were exactly 72 potential phase portraits, but only 44 were realizable, while the remaining 28 were proved to be impossible. The 44 realizable phase portraits received names already related to their configurations of singularities, although the notation was not yet the definitive one. The 28 impossible portraits did not receive names at that time beyond the provisional codes they had while their realizability was being checked.

However, when studying the structurally unstable phase portraits of codimension one modulo limit cycles in [5], it became clear that it was necessary to refer to the codimension-zero phase portraits, both the realizable ones and the impossible ones, in order to prove other impossibility results in codimension one. For this reason, names were assigned there to the impossible codimension-zero phase portraits, although these were still not the definitive names that we introduce here. Moreover, in that second paper (in fact a book), other phase portraits of codimension zero with limit cycles appeared which were clearly impossible, since the limit cycle surrounded more than one finite singularity. We will not assign names to such phase portraits.

In these papers, the method of study requires that phase portraits receive a provisional name when they are first detected as potential phase portraits, and a final name once the realizable ones have been separated from the non-realizable ones. We will present a table with the most descriptive list of names in order to facilitate their identification.

The phase portraits of codimension zero are associated with 12 configurations of singularities, namely:

- (1) $s, s, s, a; N, N, N$;
- (3) $s, a, a, a; S$;
- (5) $s, a, a, a; S, S, N$;
- (8) $s, s, a, a; N$;
- (10) $s, s, a, a; S, N, N$;

- (12) $\emptyset; N;$
- (13) $\emptyset; S, N, N;$
- (15) $s, s; N, N, N;$
- (16) $a, a; S;$
- (19) $a, a; S, S, N;$
- (23) $s, a; N;$
- (25) $s, a; S, N, N.$

These 12 configurations correspond directly to subclasses 7, 5, 12, 3, 10, 1, 8, 6, 4, 11, 2, and 9, respectively, in [3]. Therefore, the definitive names of the phase portraits are given in Table 6.1.

Temp. name	Name in [3]	Definitive name	Temp. name	Name in [3]	Definitive name
$\mathbb{S}^2_{1,1}$	$\mathbb{S}^2_{1,1}$	$QS12^{(0)}_1$	$\mathbb{S}^2_{2,1}$	$\mathbb{S}^2_{2,1}$	$QS23^{(0)}_1$
$\mathbb{S}^2_{3,1}$	$\mathbb{S}^2_{3,1}$	$QS8^{(0)}_1$	$\mathbb{S}^2_{3,1}$	$\mathbb{S}^2_{3,2}$	$QS8^{(0)}_2$
$\mathbb{S}^2_{3,3}$	$\mathbb{S}^2_{3,3}$	$QS8^{(0)}_3$	$\mathbb{S}^2_{3,4}$	$\mathbb{S}^2_{3,4}$	$QS8^{(0)}_4$
$\mathbb{S}^2_{3,5}$	$\mathbb{S}^2_{3,5}$	$QS8^{(0)}_5$	$\mathbb{S}^2_{4,1}$	$\mathbb{S}^2_{4,1}$	$QS16^{(0)}_1$
$\mathbb{S}^2_{5,1}$	$\mathbb{S}^2_{5,1}$	$QS3^{(0)}_1$	$\mathbb{S}^2_{6,1}$	$\mathbb{S}^2_{6,1}$	$QS15^{(0)}_1$
7.1 Fig. 5.3	$\mathbb{S}^2_{7,1}$	$QS1^{(0)}_1$	7.2 Fig. 5.4	$\mathbb{S}^2_{7,2}$	$QS1^{(0)}_2$
7.3 Fig. 5.6	$\mathbb{S}^2_{7,3}$	$QS1^{(0)}_3$	7.4 Fig. 5.6	$\mathbb{S}^2_{7,4}$	$QS1^{(0)}_4$
$\mathbb{S}^2_{8,1}$	$\mathbb{S}^2_{8,1}$	$QS13^{(0)}_1$	9.1 Fig. 5.7	$\mathbb{S}^2_{9,1}$	$QS25^{(0)}_1$
9.2 Fig. 5.8	$\mathbb{S}^2_{9,2}$	$QS25^{(0)}_2$	9.3 Fig. 5.9	$\mathbb{S}^2_{9,3}$	$QS25^{(0)}_3$
4 Fig. 5.13	$\mathbb{S}^2_{10,1}$	$QS10^{(0)}_1$	8 Fig. 5.18	$\mathbb{S}^2_{10,2}$	$QS10^{(0)}_2$
10 Fig. 5.18	$\mathbb{S}^2_{10,3}$	$QS10^{(0)}_3$	12 Fig. 5.20	$\mathbb{S}^2_{10,4}$	$QS10^{(0)}_4$
13 Fig. 5.21	$\mathbb{S}^2_{10,5}$	$QS10^{(0)}_5$	14 Fig. 5.23	$\mathbb{S}^2_{10,6}$	$QS10^{(0)}_6$
23 Fig. 5.28	$\mathbb{S}^2_{10,7}$	$QS10^{(0)}_7$	25 Fig. 5.32	$\mathbb{S}^2_{10,8}$	$QS10^{(0)}_8$
26 Fig. 5.34	$\mathbb{S}^2_{10,9}$	$QS10^{(0)}_9$	28 Fig. 5.34	$\mathbb{S}^2_{10,10}$	$QS10^{(0)}_{10}$
29 Fig. 5.37	$\mathbb{S}^2_{10,11}$	$QS10^{(0)}_{11}$	30 Fig. 5.37	$\mathbb{S}^2_{10,12}$	$QS10^{(0)}_{12}$
32 Fig. 5.40	$\mathbb{S}^2_{10,13}$	$QS10^{(0)}_{13}$	34 Fig. 5.42	$\mathbb{S}^2_{10,14}$	$QS10^{(0)}_{14}$
35 Fig. 5.42	$\mathbb{S}^2_{10,15}$	$QS10^{(0)}_{15}$	36 Fig. 5.48	$\mathbb{S}^2_{10,16}$	$QS10^{(0)}_{16}$
$\mathbb{S}^2_{11,1}$	$\mathbb{S}^2_{11,1}$	$QS19^{(0)}_1$	$\mathbb{S}^2_{11,2}$	$\mathbb{S}^2_{11,2}$	$QS19^{(0)}_2$
$\mathbb{S}^2_{11,3}$	$\mathbb{S}^2_{11,3}$	$QS19^{(0)}_2$	2 Fig. 5.53	$\mathbb{S}^2_{12,1}$	$QS5^{(0)}_1$
3 Fig. 5.54	$\mathbb{S}^2_{12,2}$	$QS5^{(0)}_2$	4 Fig. 5.56	$\mathbb{S}^2_{12,3}$	$QS5^{(0)}_3$
6 Fig. 5.56	$\mathbb{S}^2_{12,4}$	$QS5^{(0)}_4$	9 Fig. 5.60	$\mathbb{S}^2_{12,5}$	$QS5^{(0)}_5$
10 Fig. 5.61	$\mathbb{S}^2_{12,6}$	$QS5^{(0)}_6$	12 Fig. 5.61	$\mathbb{S}^2_{12,7}$	$QS5^{(0)}_7$

Table 6.1: Definitive names assigned for codimension-zero phase portraits.

In Table 6.2 we assign definitive names to the potential codimension-zero phase portraits that were proved to be impossible in [3] and that are needed in other papers to establish further impossibility results. The names follow the same structure as those assigned to the

realizable phase portraits, but with the addition of the letter "I" to the codimension. Since these phase portraits did not receive a name in [3], we indicate the name assigned to them in [5].

Temp name	Name in [5]	Definitive name	Temp name	Name in [5]	Definitive name
7.5 Fig. 5.6	$\mathbb{I}_{7,1}$	$QS1_1^{(0,I)}$	7.6 Fig. 5.6	$\mathbb{I}_{7,2}$	$QS1_2^{(0,I)}$
9.4 Fig. 5.9	$\mathbb{I}_{9,1}$	$QS25_1^{(0,I)}$	1 Fig. 5.56	$\mathbb{I}_{10,1}$	$QS10_1^{(0,I)}$
2 Fig. 5.56	$\mathbb{I}_{10,2}$	$QS10_2^{(0,I)}$	3 Fig. 5.56	$\mathbb{I}_{10,3}$	$QS10_3^{(0,I)}$
5 Fig. 5.56	$\mathbb{I}_{10,4}$	$QS10_4^{(0,I)}$	6 Fig. 5.56	$\mathbb{I}_{10,5}$	$QS10_5^{(0,I)}$
7 Fig. 5.56	$\mathbb{I}_{10,6}$	$QS10_6^{(0,I)}$	9 Fig. 5.56	$\mathbb{I}_{10,7}$	$QS10_7^{(0,I)}$
11 Fig. 5.56	$\mathbb{I}_{10,8}$	$QS10_8^{(0,I)}$	15 Fig. 5.56	$\mathbb{I}_{10,9}$	$QS10_9^{(0,I)}$
16 Fig. 5.56	$\mathbb{I}_{10,10}$	$QS10_{10}^{(0,I)}$	17 Fig. 5.56	$\mathbb{I}_{10,11}$	$QS10_{11}^{(0,I)}$
18 Fig. 5.56	$\mathbb{I}_{10,12}$	$QS10_{12}^{(0,I)}$	19 Fig. 5.56	$\mathbb{I}_{10,13}$	$QS10_{13}^{(0,I)}$
20 Fig. 5.56	$\mathbb{I}_{10,14}$	$QS10_{14}^{(0,I)}$	21 Fig. 5.56	$\mathbb{I}_{10,15}$	$QS10_{15}^{(0,I)}$
22 Fig. 5.56	$\mathbb{I}_{10,16}$	$QS10_{16}^{(0,I)}$	24 Fig. 5.56	$\mathbb{I}_{10,17}$	$QS10_{17}^{(0,I)}$
27 Fig. 5.56	$\mathbb{I}_{10,18}$	$QS10_{18}^{(0,I)}$	31 Fig. 5.56	$\mathbb{I}_{10,19}$	$QS10_{19}^{(0,I)}$
33 Fig. 5.56	$\mathbb{I}_{10,20}$	$QS10_{20}^{(0,I)}$	1 Fig. 5.56	$\mathbb{I}_{12,1}$	$QS5_1^{(0,I)}$
5 Fig. 5.56	$\mathbb{I}_{12,2}$	$QS5_2^{(0,I)}$	7 Fig. 5.56	$\mathbb{I}_{12,3}$	$QS5_3^{(0,I)}$
8 Fig. 5.56	$\mathbb{I}_{12,4}$	$QS5_4^{(0,I)}$	11 Fig. 5.56	$\mathbb{I}_{12,5}$	$QS5_5^{(0,I)}$

Table 6.2: Definitive names assigned for the impossible codimension-zero phase portraits.

6.2 Codimension-one phase portraits

In the book [5] all structurally unstable phase portraits of quadratic systems without limit cycles of codimension one were considered. That study produced more than 500 potential phase portraits, and it took a long time to separate those that were realizable from those that were impossible. Even after this separation, seven phase portraits remained for which no example was provided, but neither was there a proof of their impossibility. Some arguments concerning the non-existence of related phase portraits with limit cycles seemed to suggest that they could be impossible, but up to now no proof has been obtained.

These seven phase portraits share a common property: all of them have a graphic with a focus inside, and the reduced configuration of separatrices with the focus having the opposite stability is realizable. This same phenomenon also appears in codimension two and higher.

Moreover, in [5]it was claimed that there were 204 phase portraits of codimension one. This claim, however, contains two errors, and two phase portraits that were claimed to be realizable were subsequently proved to be impossible.

Most of the impossible phase portraits of codimension one are not realizable because a perturbation of them leads to one of the 28 impossible phase portraits of codimension zero. Therefore, there is no need to name them, since a proof of the non-existence of a phase portrait of higher codimension that could require any of them may also be based on the impossible codimension-zero phase portraits.

Thus, we will assign names only to the 202 realizable phase portraits, the seven still uncertain ones, and those impossible phase portraits whose impossibility was proved in [5] and cannot be derived from the codimension-zero impossible phase portraits.

The codimension-one phase portraits were divided into four main sets according to the type of instability exhibited by the portraits, as already explained in the introduction, namely: (A) possessing a finite semi-elemental saddle-node $\overline{sn}_{(2)}$ formed by the coalescence of a finite saddle and a finite node; (B) possessing an infinite semi-elemental saddle-node $\overline{\binom{0}{2}}SN$ formed by the coalescence of an infinite saddle and an infinite node; (C) possessing an infinite semi-elemental saddle-node $\overline{\binom{1}{1}}SN$, obtained by the coalescence of a finite saddle (respectively, finite node) with an infinite node (respectively, infinite saddle); and (D) possessing a separatrix connection.

We cannot claim that all potential but impossible phase portraits of codimension one and higher have been drawn, since most studies are based on bifurcations that produce some realizable phase portraits of lower codimension. This is the reason why only a few impossible phase portraits appear in sets (A), (B), or (C), but many appear in set (D), since the technique used to produce the potential phase portraits was different in these two blocks. The same phenomenon occurs in higher codimensions.

The phase portraits of sets (A), (B), and (C) have configurations of singularities of codimension one from the following list:

- (7) s, a, a, a; $\binom{0}{2}SN$, S;
- (11) s, s, a, a; $\binom{0}{2}SN$, N;
- (14) $\emptyset$; $\binom{0}{2}SN$, N;
- (22) a, a; $\binom{0}{2}SN$, S;
- (27) s, a; $\binom{0}{2}SN$, N;
- (28) s, s, sn; N, N, N;
- (30) a, a, sn; S;
- (31) a, a, sn; S, S, N;
- (37) s, a, sn; N;
- (38) s, a, sn; S, N, N;
- (44) sn; N;
- (45) sn; S, N, N;
- (73) s, a, a; $\binom{1}{1}SN$;
- (74) s, a, a; $\binom{1}{1}SN$, S, N;
- (76) s, s, a; $\binom{1}{1}SN$, N, N;
- (84) a; $\binom{1}{1}SN$;
- (85) a; $\binom{1}{1}SN$, S, N;

- (87) s; $\binom{1}{1}SN$, N, N.

The phase portraits of set (D) have a configuration of singularities of codimension zero, already described in Subsection 6.1, together with a separatrix connection.

In Table 6.3 we describe the realizable phase portraits of set (A).

We show in Table 6.4 the impossible phase portraits of set (A). Some of them were immediately detected as impossible since they could bifurcate into an impossible phase portrait of codimension zero. Others required a proof not based on impossible codimension zero phase portraits, and one case was detected as impossible later in [14].

The four cases that were proved to be impossible in this book by means of proofs not based on impossible codimension zero phase portraits did not receive a name denoting them as impossible. The phase portrait that was proved to be impossible in [14] had the provisional name A_{51} and the definitive name $\mathbb{U}^1_{A,49}$. A reshuffling of names from 49 to 70 would have been necessary, but we decided not to do it in order to avoid further confusion and instead rely on a future definitive naming, as we are doing now.

We present in Table 6.5 the realizable phase portraits of set (B).

We show in Table 6.6 the impossible phase portraits of set (B). Some of them were immediately detected as impossible since they could bifurcate into an impossible phase portrait of codimension zero. Others required a proof not based on impossible codimension-zero phase portraits.

We present in Table 6.7 the realizable phase portraits of set (C).

We show in Table 6.8 the impossible phase portraits of set (C). Only two such phase portraits were found in [5], and both were immediately detected as impossible since they could bifurcate into an impossible phase portrait of codimension zero.

The study of set (D) was the most complicated in [5]. Sets (A), (B), and (C) were obtained by producing coalescences of singularities from the codimension-zero phase portraits, but set (D) required a complete check of all configurations of singularities of codimension zero together with all possible combinations of separatrices.

Moreover, in this class appeared the first graphics having a Poincaré return map, and thus the stability of the focus inside the graphic with respect to the other singularities could lead to different phase portraits unless some symmetry existed. This led the authors to introduce the concept of the *reduced separatrix configuration* in contrast with the *complete separatrix configuration*. In the latter, apart from the set of separatrices, an orbit inside each canonical region is also required, while in the former this latter condition is not imposed.

Thus, a given reduced separatrix configuration can correspond to two different phase portraits depending on the stability of the focus inside the graphic. The authors drew a single potential portrait for each of these reduced separatrix configurations and assigned the same provisional name to both possibilities, simply adding a subindex a or b to denote the relation between them, and later looked for the realizability of both portraits.

In some cases examples of both possibilities were obtained, but in seven cases only one of the possibilities was realized. The examples were obtained from the previous literature. However, for seven of them this was not possible. If any of these examples occurred, the breaking of the graphic would imply that a certain codimension-zero phase portrait with a specific configuration should exist. However, these seven phase portraits with limit cycles have never appeared in the previous literature, nor have they appeared in recent papers.

The existence of such codimension-zero phase portraits with a limit cycle would not yet constitute a proof of the existence of the respective codimension-one portrait still missing, but it could serve as a starting point to try a rotated vector field which might possibly prove

Temp name	Name in book	Definitive name	Temp name	Name in book	Definitive name
A_1 Fig. 5.1	$\mathbb{U}^1_{A,1}$	$QS44^{(1)}_1$	A_2 Fig. 5.2	$\mathbb{U}^1_{A,2}$	$QS37^{(1)}_1$
A_3 Fig. 5.2	$\mathbb{U}^1_{A,3}$	$QS37^{(1)}_2$	A_4 Fig. 5.2	$\mathbb{U}^1_{A,4}$	$QS37^{(1)}_3$
A_5 Fig. 5.3	$\mathbb{U}^1_{A,5}$	$QS37^{(1)}_4$	A_6 Fig. 5.4	$\mathbb{U}^1_{A,6}$	$QS37^{(1)}_5$
A_7 Fig. 5.5	$\mathbb{U}^1_{A,7}$	$QS37^{(1)}_6$	A_8 Fig. 5.6	$\mathbb{U}^1_{A,8}$	$QS37^{(1)}_7$
A_9 Fig. 5.6	$\mathbb{U}^1_{A,9}$	$QS37^{(1)}_8$	A_{10} Fig. 5.6	$\mathbb{U}^1_{A,10}$	$QS37^{(1)}_9$
A_{11} Fig. 5.7	$\mathbb{U}^1_{A,11}$	$QS30^{(1)}_1$	A_{12} Fig. 5.7	$\mathbb{U}^1_{A,12}$	$QS30^{(1)}_2$
A_{13} Fig. 5.7	$\mathbb{U}^1_{A,13}$	$QS30^{(1)}_3$	A_{14} Fig. 5.8	$\mathbb{U}^1_{A,14}$	$QS28^{(1)}_1$
A_{15} Fig. 5.9	$\mathbb{U}^1_{A,15}$	$QS28^{(1)}_2$	A_{16} Fig. 5.9	$\mathbb{U}^1_{A,16}$	$QS28^{(1)}_3$
A_{17} Fig. 5.10	$\mathbb{U}^1_{A,17}$	$QS28^{(1)}_4$	A_{18} Fig. 5.11	$\mathbb{U}^1_{A,18}$	$QS28^{(1)}_5$
A_{19} Fig. 5.12	$\mathbb{U}^1_{A,19}$	$QS45^{(1)}_1$	A_{20} Fig. 5.13	$\mathbb{U}^1_{A,20}$	$QS45^{(1)}_2$
A_{21} Fig. 5.14	$\mathbb{U}^1_{A,21}$	$QS45^{(1)}_3$	A_{22} Fig. 5.15	$\mathbb{U}^1_{A,22}$	$QS38^{(1)}_1$
A_{23} Fig. 5.15	$\mathbb{U}^1_{A,23}$	$QS38^{(1)}_2$	A_{24} Fig. 5.15	$\mathbb{U}^1_{A,24}$	$QS38^{(1)}_3$
A_{25} Fig. 5.16	$\mathbb{U}^1_{A,25}$	$QS38^{(1)}_4$	A_{26} Fig. 5.16	$\mathbb{U}^1_{A,26}$	$QS38^{(1)}_5$
A_{27} Fig. 5.17	$\mathbb{U}^1_{A,27}$	$QS38^{(1)}_6$	A_{28} Fig. 5.17	$\mathbb{U}^1_{A,28}$	$QS38^{(1)}_7$
A_{29} Fig. 5.18	$\mathbb{U}^1_{A,29}$	$QS38^{(1)}_8$	A_{30} Fig. 5.18	$\mathbb{U}^1_{A,30}$	$QS38^{(1)}_9$
A_{31} Fig. 5.19	$\mathbb{U}^1_{A,31}$	$QS38^{(1)}_{10}$	A_{32} Fig. 5.19	$\mathbb{U}^1_{A,32}$	$QS38^{(1)}_{11}$
A_{33} Fig. 5.19	$\mathbb{U}^1_{A,33}$	$QS38^{(1)}_{12}$	A_{34} Fig. 5.20	$\mathbb{U}^1_{A,34}$	$QS38^{(1)}_{13}$
A_{35} Fig. 5.20	$\mathbb{U}^1_{A,35}$	$QS38^{(1)}_{14}$	A_{36} Fig. 5.21	$\mathbb{U}^1_{A,36}$	$QS38^{(1)}_{15}$
A_{37} Fig. 5.21	$\mathbb{U}^1_{A,37}$	$QS38^{(1)}_{16}$	A_{39} Fig. 5.21	$\mathbb{U}^1_{A,38}$	$QS38^{(1)}_{17}$
A_{40} Fig. 5.22	$\mathbb{U}^1_{A,39}$	$QS38^{(1)}_{18}$	A_{41} Fig. 5.23	$\mathbb{U}^1_{A,40}$	$QS38^{(1)}_{19}$
A_{42} Fig. 5.23	$\mathbb{U}^1_{A,41}$	$QS38^{(1)}_{20}$	A_{43} Fig. 5.24	$\mathbb{U}^1_{A,42}$	$QS38^{(1)}_{21}$
A_{44} Fig. 5.24	$\mathbb{U}^1_{A,43}$	$QS38^{(1)}_{22}$	A_{46} Fig. 5.25	$\mathbb{U}^1_{A,44}$	$QS38^{(1)}_{23}$
A_{47} Fig. 5.26	$\mathbb{U}^1_{A,45}$	$QS38^{(1)}_{24}$	A_{48} Fig. 5.26	$\mathbb{U}^1_{A,46}$	$QS38^{(1)}_{25}$
A_{49} Fig. 5.27	$\mathbb{U}^1_{A,47}$	$QS38^{(1)}_{26}$	A_{50} Fig. 5.27	$\mathbb{U}^1_{A,48}$	$QS38^{(1)}_{27}$
A_{52} Fig. 5.27	$\mathbb{U}^1_{A,50}$	$QS38^{(1)}_{28}$	A_{53} Fig. 5.28	$\mathbb{U}^1_{A,51}$	$QS38^{(1)}_{29}$
A_{54} Fig. 5.28	$\mathbb{U}^1_{A,52}$	$QS38^{(1)}_{30}$	A_{55} Fig. 5.28	$\mathbb{U}^1_{A,53}$	$QS38^{(1)}_{31}$
A_{56} Fig. 5.29	$\mathbb{U}^1_{A,54}$	$QS38^{(1)}_{32}$	A_{57} Fig. 5.30	$\mathbb{U}^1_{A,55}$	$QS38^{(1)}_{33}$
A_{58} Fig. 5.31	$\mathbb{U}^1_{A,56}$	$QS31^{(1)}_1$	A_{59} Fig. 5.31	$\mathbb{U}^1_{A,57}$	$QS31^{(1)}_2$
A_{60} Fig. 5.32	$\mathbb{U}^1_{A,58}$	$QS31^{(1)}_3$	A_{61} Fig. 5.32	$\mathbb{U}^1_{A,59}$	$QS31^{(1)}_4$
A_{62} Fig. 5.32	$\mathbb{U}^1_{A,60}$	$QS31^{(1)}_5$	A_{63} Fig. 5.33	$\mathbb{U}^1_{A,61}$	$QS31^{(1)}_6$
A_{64} Fig. 5.33	$\mathbb{U}^1_{A,62}$	$QS31^{(1)}_7$	A_{65} Fig. 5.34	$\mathbb{U}^1_{A,63}$	$QS31^{(1)}_8$
A_{66} Fig. 5.34	$\mathbb{U}^1_{A,64}$	$QS31^{(1)}_9$	A_{68} Fig. 5.35	$\mathbb{U}^1_{A,65}$	$QS31^{(1)}_{10}$
A_{69} Fig. 5.35	$\mathbb{U}^1_{A,66}$	$QS31^{(1)}_{11}$	A_{70} Fig. 5.36	$\mathbb{U}^1_{A,67}$	$QS31^{(1)}_{12}$
A_{71} Fig. 5.36	$\mathbb{U}^1_{A,68}$	$QS31^{(1)}_{13}$	A_{72} Fig. 5.37	$\mathbb{U}^1_{A,69}$	$QS31^{(1)}_{14}$
A_{73} Fig. 5.37	$\mathbb{U}^1_{A,70}$	$QS31^{(1)}_{15}$			

Table 6.3: Definitive names assigned for codimension-one phase portraits of set (A).

Temp name	Name in [14]	Definitive name	Temp name	Name in [14]	Definitive name
$\mathbb{U}^1_{I,1}$ Fig. 5.17	$\mathbb{U}^1_{I,1}$	$QS38_1^{(1,I)}$	$\mathbb{U}^1_{I,2}$ Fig. 5.24	$\mathbb{U}^1_{I,2}$	$QS38_2^{(1,I)}$
$\mathbb{U}^1_{I,3}$ Fig. 5.28	$\mathbb{U}^1_{I,3}$	$QS38_3^{(1,I)}$	A_{38} Fig. 5.21	A_{38}	$QS38_4^{(1,I)}$
A_{45} Fig. 5.24	A_{45}	$QS38_5^{(1,I)}$	A_{51} Fig. 5.27	$\mathbb{U}^1_{A,49}$	$QS38_6^{(1,I)}$
A_{67} Fig. 5.34	A_{67}	$QS31_1^{(1,I)}$	A_{74} Fig. 5.37	A_{74}	$QS31_2^{(1,I)}$

Table 6.4: Definitive names assigned for impossible codimension-one phase portraits of set (A).

Temp name	Name in [14]	Definitive name	Temp name	Name in [14]	Definitive name
B_1 Fig. 5.38	$\mathbb{U}^1_{B,1}$	$QS14_1^{(1)}$	B_2 Fig. 5.38	$\mathbb{U}^1_{B,2}$	$QS14_2^{(1)}$
B_3 Fig. 5.39	$\mathbb{U}^1_{B,3}$	$QS27_1^{(1)}$	B_4 Fig. 5.39	$\mathbb{U}^1_{B,4}$	$QS27_2^{(1)}$
B_5 Fig. 5.40	$\mathbb{U}^1_{B,5}$	$QS27_3^{(1)}$	B_6 Fig. 5.40	$\mathbb{U}^1_{B,6}$	$QS27_4^{(1)}$
B_7 Fig. 5.41	$\mathbb{U}^1_{B,7}$	$QS27_5^{(1)}$	B_8 Fig. 5.41	$\mathbb{U}^1_{B,8}$	$QS27_6^{(1)}$
B_9 Fig. 5.42	$\mathbb{U}^1_{B,9}$	$QS11_1^{(1)}$	B_{10} Fig. 5.42	$\mathbb{U}^1_{B,10}$	$QS11_2^{(1)}$
B_{12} Fig. 5.43	$\mathbb{U}^1_{B,11}$	$QS11_3^{(1)}$	B_{13} Fig. 5.44	$\mathbb{U}^1_{B,12}$	$QS11_4^{(1)}$
B_{16} Fig. 5.45	$\mathbb{U}^1_{B,13}$	$QS11_5^{(1)}$	B_{17} Fig. 5.46	$\mathbb{U}^1_{B,14}$	$QS11_6^{(1)}$
B_{20} Fig. 5.47	$\mathbb{U}^1_{B,15}$	$QS11_7^{(1)}$	B_{21} Fig. 5.48	$\mathbb{U}^1_{B,16}$	$QS11_8^{(1)}$
B_{22} Fig. 5.48	$\mathbb{U}^1_{B,17}$	$QS11_9^{(1)}$	B_{24} Fig. 5.49	$\mathbb{U}^1_{B,18}$	$QS11_{10}^{(1)}$
B_{26} Fig. 5.50	$\mathbb{U}^1_{B,19}$	$QS11_{11}^{(1)}$	B_{27} Fig. 5.51	$\mathbb{U}^1_{B,20}$	$QS11_{12}^{(1)}$
B_{29} Fig. 5.52	$\mathbb{U}^1_{B,21}$	$QS11_{13}^{(1)}$	B_{32} Fig. 5.53	$\mathbb{U}^1_{B,22}$	$QS11_{14}^{(1)}$
B_{33} Fig. 5.54	$\mathbb{U}^1_{B,23}$	$QS11_{15}^{(1)}$	B_{34} Fig. 5.54	$\mathbb{U}^1_{B,24}$	$QS11_{16}^{(1)}$
B_{35} Fig. 5.55	$\mathbb{U}^1_{B,25}$	$QS11_{17}^{(1)}$	B_{36} Fig. 5.55	$\mathbb{U}^1_{B,26}$	$QS11_{18}^{(1)}$
B_{38} Fig. 5.56	$\mathbb{U}^1_{B,27}$	$QS11_{19}^{(1)}$	B_{39} Fig. 5.57	$\mathbb{U}^1_{B,28}$	$QS11_{20}^{(1)}$
B_{40} Fig. 5.58	$\mathbb{U}^1_{B,29}$	$QS22_1^{(1)}$	B_{41} Fig. 5.59	$\mathbb{U}^1_{B,30}$	$QS22_2^{(1)}$
B_{42} Fig. 5.59	$\mathbb{U}^1_{B,31}$	$QS22_3^{(1)}$	B_{43} Fig. 5.60	$\mathbb{U}^1_{B,32}$	$QS22_4^{(1)}$
B_{44} Fig. 5.61	$\mathbb{U}^1_{B,33}$	$QS7_1^{(1)}$	B_{45} Fig. 5.62	$\mathbb{U}^1_{B,34}$	$QS7_2^{(1)}$
B_{46} Fig. 5.63	$\mathbb{U}^1_{B,35}$	$QS7_3^{(1)}$	B_{47} Fig. 5.64	$\mathbb{U}^1_{B,36}$	$QS7_4^{(1)}$
B_{48} Fig. 5.65	$\mathbb{U}^1_{B,37}$	$QS7_5^{(1)}$	B_{49} Fig. 5.66	$\mathbb{U}^1_{B,38}$	$QS7_6^{(1)}$
B_{50} Fig. 5.66	$\mathbb{U}^1_{B,39}$	$QS7_7^{(1)}$	B_{51} Fig. 5.67	$\mathbb{U}^1_{B,40}$	$QS7_8^{(1)}$

Table 6.5: Definitive names assigned for codimension-one phase portraits of set (B).

its existence. On the contrary, if such codimension-zero phase portraits with a limit cycle could be proved to be impossible, then the respective codimension-one portraits would also be impossible.

All this evidence led to the conjecture that these seven phase portraits are not realizable.

In this set (D), the list of impossible phase portraits already proved is even longer than the list of realizable ones. Moreover, one of the phase portraits claimed to be realizable in [5] was based on an example from [33], which was not checked. This was phase portrait $\mathbb{U}^1_{D,62}$, which

Temp name	Name in [5]	Definitive name	Temp name	Name in [5]	Definitive name
$\mathbb{U}^1_{I,4}$ Fig. 5.61	$\mathbb{U}^1_{I,4}$	$QS7_1^{(1,I)}$	$\mathbb{U}^1_{I,5}$ Fig. 5.64	$\mathbb{U}^1_{I,5}$	$QS7_2^{(1,I)}$
$\mathbb{U}^1_{I,6}$ Fig. 5.65	$\mathbb{U}^1_{I,6}$	$QS7_3^{(1,I)}$	$\mathbb{U}^1_{I,7}$ Fig. 5.67	$\mathbb{U}^1_{I,7}$	$QS7_4^{(1,I)}$
B_{11} Fig. 5.43	B_{11}	$QS11_1^{(1,I)}$	B_{14} Fig. 5.44	B_{14}	$QS11_2^{(1,I)}$
B_{15} Fig. 5.45	B_{15}	$QS11_3^{(1,I)}$	B_{18} Fig. 5.46	B_{18}	$QS11_4^{(1,I)}$
B_{19} Fig. 5.47	B_{19}	$QS11_5^{(1,I)}$	B_{23} Fig. 5.49	B_{23}	$QS11_6^{(1,I)}$
B_{25} Fig. 5.50	B_{25}	$QS11_7^{(1,I)}$	B_{28} Fig. 5.51	B_{28}	$QS11_8^{(1,I)}$
B_{30} Fig. 5.52	B_{30}	$QS11_9^{(1,I)}$	B_{31} Fig. 5.53	B_{31}	$QS11_{10}^{(1,I)}$
B_{37} Fig. 5.56	B_{37}	$QS11_{11}^{(1,I)}$			

Table 6.6: Definitive names assigned for impossible codimension-one phase portraits of set (B).

Temp name	Name in [5]	Definitive name	Temp name	Name in [5]	Definitive name
C_1 Fig. 5.68	$\mathbb{U}^1_{C,1}$	$QS84_1^{(1)}$	C_2 Fig. 5.69	$\mathbb{U}^1_{C,2}$	$QS73_1^{(1)}$
C_3 Fig. 5.69	$\mathbb{U}^1_{C,3}$	$QS73_2^{(1)}$	C_4 Fig. 5.70	$\mathbb{U}^1_{C,4}$	$QS87_1^{(1)}$
C_5 Fig. 5.71	$\mathbb{U}^1_{C,5}$	$QS76_1^{(1)}$	C_6 Fig. 5.73	$\mathbb{U}^1_{C,6}$	$QS76_2^{(1)}$
C_7 Fig. 5.74	$\mathbb{U}^1_{C,7}$	$QS76_3^{(1)}$	C_8 Fig. 5.75	$\mathbb{U}^1_{C,8}$	$QS76_4^{(1)}$
C_9 Fig. 5.76	$\mathbb{U}^1_{C,9}$	$QS76_5^{(1)}$	C_{10} Fig. 5.78	$\mathbb{U}^1_{C,10}$	$QS76_6^{(1)}$
C_{11} Fig. 5.79	$\mathbb{U}^1_{C,11}$	$QS76_7^{(1)}$	C_{12} Fig. 5.80	$\mathbb{U}^1_{C,12}$	$QS76_8^{(1)}$
C_{13} Fig. 5.81	$\mathbb{U}^1_{C,13}$	$QS76_9^{(1)}$	C_{14} Fig. 5.82	$\mathbb{U}^1_{C,14}$	$QS76_{10}^{(1)}$
C_{15} Fig. 5.83	$\mathbb{U}^1_{C,15}$	$QS85_1^{(1)}$	C_{16} Fig. 5.84	$\mathbb{U}^1_{C,16}$	$QS85_2^{(1)}$
C_{17} Fig. 5.85	$\mathbb{U}^1_{C,17}$	$QS85_3^{(1)}$	C_{18} Fig. 5.86	$\mathbb{U}^1_{C,18}$	$QS74_1^{(1)}$
C_{19} Fig. 5.86	$\mathbb{U}^1_{C,19}$	$QS74_2^{(1)}$	C_{20} Fig. 5.87	$\mathbb{U}^1_{C,20}$	$QS74_3^{(1)}$
C_{21} Fig. 5.87	$\mathbb{U}^1_{C,21}$	$QS74_4^{(1)}$	C_{22} Fig. 5.88	$\mathbb{U}^1_{C,22}$	$QS74_5^{(1)}$
C_{23} Fig. 5.88	$\mathbb{U}^1_{C,23}$	$QS74_6^{(1)}$	C_{24} Fig. 5.89	$\mathbb{U}^1_{C,24}$	$QS74_7^{(1)}$
C_{25} Fig. 5.89	$\mathbb{U}^1_{C,25}$	$QS74_8^{(1)}$	C_{26} Fig. 5.90	$\mathbb{U}^1_{C,26}$	$QS74_9^{(1)}$
C_{27} Fig. 5.90	$\mathbb{U}^1_{C,27}$	$QS74_{10}^{(1)}$	C_{28} Fig. 5.91	$\mathbb{U}^1_{C,28}$	$QS74_{11}^{(1)}$
C_{29} Fig. 5.91	$\mathbb{U}^1_{C,29}$	$QS74_{12}^{(1)}$	C_{30} Fig. 5.91	$\mathbb{U}^1_{C,30}$	$QS74_{13}^{(1)}$
C_{31} Fig. 5.92	$\mathbb{U}^1_{C,31}$	$QS74_{14}^{(1)}$	C_{32} Fig. 5.92	$\mathbb{U}^1_{C,32}$	$QS74_{15}^{(1)}$

Table 6.7: Definitive names assigned for codimension-one phase portraits of set (C).

Temp name	Name in [5]	Definitive name	Temp name	Name in [5]	Definitive name
$\mathbb{U}^1_{I,8}$ Fig. 5.72	$\mathbb{U}^1_{I,8}$	$QS74_1^{(1,I)}$	$\mathbb{U}^1_{I,9}$ Fig. 5.77	$\mathbb{U}^1_{I,9}$	$QS74_2^{(1,I)}$

Table 6.8: Definitive names assigned for impossible codimension-one phase portraits of set (C).

was later proved to be impossible in [1]. Fortunately, this was the last portrait in the list, and its removal leaves no gap in the middle.

Thus, in this case we will give three lists: one for the realizable phase portraits, one for the impossible ones, and one for the conjectured impossible ones, which will be assigned a name including a "?" in the exponent.

We describe in Table 6.9 the realizable phase portraits of set (D).

Temp name	Name in [5]	Definitive name	Temp name	Name in [5]	Definitive name
D_1 Fig. 5.93	$\mathbb{U}^1_{D,1}$	$QS23^{(1)}_1$	D_2 Fig. 5.95	$\mathbb{U}^1_{D,2}$	$QS8^{(1)}_1$
D_3 Fig. 5.96	$\mathbb{U}^1_{D,3}$	$QS8^{(1)}_2$	D_4 Fig. 5.97	$\mathbb{U}^1_{D,4}$	$QS8^{(1)}_3$
D_7 Fig. 5.101	$\mathbb{U}^1_{D,5}$	$QS8^{(1)}_4$	D_{8a} Fig. 5.102	$\mathbb{U}^1_{D,6}$	$QS8^{(1)}_5$
D_{8b} Fig. 5.102	$\mathbb{U}^1_{D,7}$	$QS8^{(1)}_6$	D_{9a} Fig. 5.103	$\mathbb{U}^1_{D,8}$	$QS8^{(1)}_7$
D_{9b} Fig. 5.103	$\mathbb{U}^1_{D,9}$	$QS8^{(1)}_8$	D_{10a} Fig. 5.104	$\mathbb{U}^1_{D,10}$	$QS16^{(1)}_1$
D_{10b} Fig. 5.104	$\mathbb{U}^1_{D,11}$	$QS16^{(1)}_2$	D_{11} Fig. 5.105	$\mathbb{U}^1_{D,12}$	$QS3^{(1)}_1$
D_{12} Fig. 5.106	$\mathbb{U}^1_{D,13}$	$QS3^{(1)}_2$	D_{14} Fig. 5.108	$\mathbb{U}^1_{D,14}$	$QS15^{(1)}_1$
D_{15} Fig. 5.110	$\mathbb{U}^1_{D,15}$	$QS1^{(1)}_1$	D_{16} Fig. 5.114	$\mathbb{U}^1_{D,16}$	$QS1^{(1)}_2$
D_{17} Fig. 5.116	$\mathbb{U}^1_{D,17}$	$QS1^{(1)}_3$	D_{18} Fig. 5.117	$\mathbb{U}^1_{D,18}$	$QS1^{(1)}_4$
D_{19a} Fig. 5.120	$\mathbb{U}^1_{D,19}$	$QS1^{(1)}_5$	D_{19b} Fig. 5.120	$\mathbb{U}^1_{D,20}$	$QS1^{(1)}_6$
D_{20} Fig. 5.128	$\mathbb{U}^1_{D,21}$	$QS13^{(1)}_1$	D_{21a} Fig. 5.129	$\mathbb{U}^1_{D,22}$	$QS25^{(1)}_1$
D_{21b} Fig. 5.129	$\mathbb{U}^1_{D,23}$	$QS25^{(1)}_2$	D_{22} Fig. 5.130	$\mathbb{U}^1_{D,24}$	$QS25^{(1)}_3$
D_{23} Fig. 5.132	$\mathbb{U}^1_{D,25}$	$QS25^{(1)}_4$	D_{24} Fig. 5.134	$\mathbb{U}^1_{D,26}$	$QS25^{(1)}_5$
D_{25} Fig. 5.135	$\mathbb{U}^1_{D,27}$	$QS19^{(1)}_1$	D_{26a} Fig. 5.136	$\mathbb{U}^1_{D,28}$	$QS19^{(1)}_2$
D_{26b} Fig. 5.136	$\mathbb{U}^1_{D,29}$	$QS19^{(1)}_3$	D_{27b} Fig. 5.138	$\mathbb{U}^1_{D,30}$	$QS5^{(1)}_1$
D_{28} Fig. 5.139	$\mathbb{U}^1_{D,31}$	$QS5^{(1)}_2$	D_{29b} Fig. 5.142	$\mathbb{U}^1_{D,32}$	$QS5^{(1)}_3$
D_{31} Fig. 5.150	$\mathbb{U}^1_{D,33}$	$QS5^{(1)}_4$	D_{32} Fig. 5.152	$\mathbb{U}^1_{D,34}$	$QS5^{(1)}_5$
D_{33} Fig. 5.153	$\mathbb{U}^1_{D,35}$	$QS5^{(1)}_6$	D_{34} Fig. 5.155	$\mathbb{U}^1_{D,36}$	$QS5^{(1)}_7$
D_{38a} Fig. 5.159	$\mathbb{U}^1_{D,37}$	$QS5^{(1)}_8$	D_{39b} Fig. 5.160	$\mathbb{U}^1_{D,38}$	$QS5^{(1)}_9$
D_{40} Fig. 5.162	$\mathbb{U}^1_{D,39}$	$QS5^{(1)}_{10}$	D_{41} Fig. 5.168	$\mathbb{U}^1_{D,40}$	$QS10^{(1)}_1$
D_{42} Fig. 5.174	$\mathbb{U}^1_{D,41}$	$QS10^{(1)}_2$	D_{43} Fig. 5.177	$\mathbb{U}^1_{D,42}$	$QS10^{(1)}_3$
D_{45} Fig. 5.182	$\mathbb{U}^1_{D,43}$	$QS10^{(1)}_4$	D_{46} Fig. 5.183	$\mathbb{U}^1_{D,44}$	$QS10^{(1)}_5$
D_{47} Fig. 5.185	$\mathbb{U}^1_{D,45}$	$QS10^{(1)}_6$	D_{49b} Fig. 5.202	$\mathbb{U}^1_{D,46}$	$QS10^{(1)}_7$
D_{50a} Fig. 5.203	$\mathbb{U}^1_{D,47}$	$QS10^{(1)}_8$	D_{50b} Fig. 5.203	$\mathbb{U}^1_{D,48}$	$QS10^{(1)}_9$
D_{51a} Fig. 5.204	$\mathbb{U}^1_{D,49}$	$QS10^{(1)}_{10}$	D_{51b} Fig. 5.204	$\mathbb{U}^1_{D,50}$	$QS10^{(1)}_{11}$
D_{52a} Fig. 5.205	$\mathbb{U}^1_{D,51}$	$QS10^{(1)}_{12}$	D_{53b} Fig. 5.207	$\mathbb{U}^1_{D,52}$	$QS10^{(1)}_{13}$
D_{54a} Fig. 5.209	$\mathbb{U}^1_{D,53}$	$QS10^{(1)}_{14}$	D_{54b} Fig. 5.209	$\mathbb{U}^1_{D,54}$	$QS10^{(1)}_{15}$
D_{55} Fig. 5.211	$\mathbb{U}^1_{D,55}$	$QS10^{(1)}_{16}$	D_{57} Fig. 5.217	$\mathbb{U}^1_{D,56}$	$QS10^{(1)}_{17}$
D_{58} Fig. 5.220	$\mathbb{U}^1_{D,57}$	$QS10^{(1)}_{18}$	D_{59} Fig. 5.221	$\mathbb{U}^1_{D,58}$	$QS10^{(1)}_{19}$
D_{60} Fig. 5.225	$\mathbb{U}^1_{D,59}$	$QS10^{(1)}_{20}$	D_{61} Fig. 5.228	$\mathbb{U}^1_{D,60}$	$QS10^{(1)}_{21}$
D_{62} Fig. 5.235	$\mathbb{U}^1_{D,61}$	$QS10^{(1)}_{22}$	D_{63} Fig. 5.228	impossible	

Table 6.9: Definitive names assigned for codimension-one phase portraits of set (D).

We show in Table 6.10 the impossible phase portraits of set (D). Among them, 93 were immediately detected as impossible since they could bifurcate into an impossible phase portrait of codimension zero, 10 had a proof of impossibility given in [5], and one had a proof of impossibility found later in [1].

Some impossible portraits appeared in several bifurcations, so they may have received different names in [5]. Since they were not realizable, the authors did not worry to check whether there were equivalences among them. Now, with the help of the topological invariants, it becomes easier to detect such equivalences.

Finally, Table 6.12 shows the conjectured impossible phase portraits of set (D). All these conjectured impossible portraits appear grouped in Fig. 1.16 of [5].

6.3 Codimension-two phase portraits

When the study of codimension-two phase portraits was started, it was already realized that the complete study would be even longer than that of codimension one, which had already required a full book to present and prove the results. Thus, it was decided from the beginning to divide the work into a series of different articles, each covering one or two sets.

At present, three papers have already been written and four classes have been studied. In fact, the current paper is the fourth one and studies the fifth family.

Thus, we describe the five sets in independent tables.

Set (AA) covers the cases where there are either two finite saddle-nodes or one cusp. Hence, the configurations of singularities come from the following list:

- (29) s, s, cp; N, N, N;
- (34) a, a, cp; S;
- (35) a, a, cp; S, S, N;
- (40) s, a, cp; N;
- (42) s, a, cp; S, N, N;
- (47) cp; N;
- (48) cp; S, N, N;
- (50) sn, sn; N;
- (51) sn, sn; S, N, N.

Table 6.13 presents the assigned names for the set (AA).

In this set there also appear some impossible phase portraits of codimension two. Three of them were immediately proved to be impossible since they bifurcate into an impossible phase portrait of codimension one, but one required a detailed proof. We name them in Table 6.14.

The set (AB) covers the cases where there is one finite saddle-node and one infinite saddle-node produced by the coalescence of two infinite singularities. Thus, the configurations of singularities come from the following list:

- (32) a, a, sn; $\binom{0}{2}SN$, S;
- (39) s, a, sn; $\binom{0}{2}SN$, N;

- (46) sn; $\binom{0}{2}SN$, N.

In this paper, as our understanding of which nomenclature was most useful increased, we improved the names of some impossible portraits of codimension one. However, since we had already assigned them definitive names, we do not include them here.

All the potential but impossible phase portraits for this class were proved to be non-realizable because they bifurcated into some impossible portraits of codimension one. Therefore, all the names assigned to the portraits of this set were already appropriate for the paper. Thus, we may use a three-column format in this table to save space. The assigned names are presented in Table 6.15.

The impossible phase portraits of this class are given in Table 6.16.

The set (AC) covers the cases where there is one finite saddle-node and one infinite saddle-node produced by the coalescence of one infinite singularity with a finite one. Thus, the configurations of singularities come from the following list:

- (98) a, sn; $\binom{1}{1}SN$;
- (99) a, sn; $\binom{1}{1}SN$, S, N;
- (104) s, sn; $\binom{1}{1}SN$, N, N.

As for the set (AC), all the impossible phase portraits were detected while the potential phase portraits were being drawn, and there was no need to use temporary names. The assigned names are presented in Table 6.17.

The impossible phase portraits of this class are listed in Table 6.18.

The set (AD) covers the cases where there is one finite saddle-node together with a separatrix connection. Therefore, the configurations of singularities arise from those of codimension one with a finite saddle-node:

- (28) s, s, sn; N, N, N;
- (30) a, a, sn; S;
- (31) a, a, sn; S, S, N;
- (37) s, a, sn; N;
- (38) s, a, sn; S, N, N;
- (44) sn; N;
- (45) sn; S, N, N.

The potential phase portraits for this set were obtained in [1] and arise from phase portraits of codimension one of set (D) by the coalescence of two finite singularities. Consequently, the seven pending portraits of codimension one in set (D), whose realizability has not yet been established, generate additional portraits in set (AD) with the same uncertainty. Moreover, a few other portraits also join the list of cases whose existence has not yet been confirmed.

In that paper the authors denoted them with the exponent "I", intended to mean "conjectured impossible". However, the exponent "?" would have been more accurate, as we now adopt for the definitive nomenclature.

The assigned names are shown in Table 6.19.

The impossible phase portraits of the set (AD) are given in Table 6.20.

The conjectured impossible phase portraits of the set (AD) are given in Table 6.21.

The set (BB) corresponds to the codimension-two cases where exactly three infinite singularities have coalesced. In those cases one obtains either a semi-elemental infinite triple saddle or node, and this singularity is topologically equivalent to an elemental saddle or node, respectively. Therefore, the set (BB) does not bring any new topologically different phase portraits.

Finally, we arrive at the phase portraits that have been classified in this paper. As already explained, the set (BC) has been divided into two subsets: (BC$_{ESNS}$) and (BC$_{SNSN}$).

The set (BC_{SNSN}) covers the cases where there are two infinite nilpotent points of multiplicity 3. Thus, the configurations of singularities come from the following list:

- (75) s, a, a; $\binom{1}{1}SN$, $\binom{0}{2}SN$;
- (86) a; $\binom{1}{1}SN$, $\binom{0}{2}SN$;
- (132) s, a; $\binom{1}{1}SN$, $\binom{1}{1}SN$, N;
- (134) s, a; $\binom{1}{1}SN$, $\binom{1}{1}NS$, N;
- (140) $\emptyset$; $\binom{1}{1}SN$, $\binom{1}{1}SN$, N;
- (141) $\emptyset$; $\binom{1}{1}SN$, $\binom{1}{1}NS$, N.

When discussing this subset, we must mention that the study of this subclass by means of a complete bifurcation diagram based on polynomial invariants has not yet been carried out. Thus, when producing its potential phase portraits, we were not sure whether we would be able to find the corresponding examples in the existing literature. However, there exists the paper [33], where this topological configuration was studied, and therefore we trusted that we could rely on it and, moreover, confirm their results.

We have been very fortunate, since all their codimension-two phase portraits appear among our potential phase portraits. In addition, we proved that they missed two cases, whose examples we obtained from other sources. Therefore, it is still worthwhile to carry out the study of this subclass by means of a complete bifurcation diagram based on polynomial invariants in order to obtain the full diagram, including the regions missed by Reyn and Huang. Moreover, this study may reveal additional codimension-three examples that could also be missing in [33] and which will be needed in the future to complete the classification.

In Table 6.22 we present the assigned names.

The impossible phase portraits in this class are given in Table 6.23.

The class (BC$_{ESNS}$) covers the cases where there is one infinite nilpotent point of multiplicity 3. Thus, the configurations of singularities come from the following list:

- (77) s, s, a; $\binom{1}{2}$ $E-H$, N;
- (79) s, a, a; $\binom{1}{2}$ $E-H$, S;
- (80) s, a, a; $\binom{1}{2}$ $PHP-E$, S;
- (81) s, a, a; $\binom{1}{2}$ $HHH-H$, N;

- (88) s; $\binom{1}{2}$ $E-H$, N;
- (89) a; $\binom{1}{2}$ $E-H$, S;
- (91) a; $\binom{1}{2}$ $PHP-E$, S;
- (93) a; $\binom{1}{2}$ $HHH-H$, N.

Normally, this would be the type of paper in which the definitive names are assigned. However, the names were already given in [10], and there is nothing to criticize in that classification: no case was missed and none was repeated. Therefore, even though the paper has not yet been published, we will respect the names already given there, even if the order of the subindices does not follow the order obtained here.

In Table 6.24 we assign the definitive names to the realizable phase portraits.

In this subset there appear some phase portraits that are not realizable because the corresponding configuration of singularities is not realizable. They arise as potential phase portraits when we generate them, but the proof of their impossibility relies on the impossibility of the configuration itself.

In this case, we do not have a code corresponding to a configuration of singularities to assign to them, and we consider it unreasonable to assign a code to something that does not exist. Therefore, we substitute the code by the letters "NE" (not existing). Moreover, we do not distinguish between different impossible configurations of singularities.

In addition, we have not included topological invariants for the non-realizable phase portraits, so it is possible that some impossible phase portraits appearing with different names actually correspond to the same one.

The impossible phase portraits of this class are listed in Table 6.25.

Temp name	Name in [5]	Definitive name	Temp name	Name in [5]	Definitive name
$\mathbb{U}^1_{I,10}$ Fig. 5.103	$\mathbb{U}^1_{I,10}$	$QS8^{(1,I)}_1$	$\mathbb{U}^1_{I,11}$ Fig. 5.111	$\mathbb{U}^1_{I,11}$	$QS1^{(1,I)}_1$
$\mathbb{U}^1_{I,12}$ Fig. 5.113	$\mathbb{U}^1_{I,12}$	$QS1^{(1,I)}_2$	$\mathbb{U}^1_{I,13}$ Fig. 5.115	$\mathbb{U}^1_{I,13}$	$QS1^{(1,I)}_3$
$\mathbb{U}^1_{I,14}$ Fig. 5.118	$\mathbb{U}^1_{I,14}$	$QS1^{(1,I)}_4$	$\mathbb{U}^1_{I,15}$ Fig. 5.121	$\mathbb{U}^1_{I,15}$	$QS1^{(1,I)}_5$
$\mathbb{U}^1_{I,16}$ Fig. 5.122	$\mathbb{U}^1_{I,16}$	$QS1^{(1,I)}_6$	$\mathbb{U}^1_{I,17}$ Fig. 5.127	$\mathbb{U}^1_{I,17}$	$QS1^{(1,I)}_7$
$\mathbb{U}^1_{I,18}$ Fig. 5.131	$\mathbb{U}^1_{I,18}$	$QS25^{(1,I)}_1$	$\mathbb{U}^1_{I,19}$ Fig. 5.133	$\mathbb{U}^1_{I,19}$	$QS25^{(1,I)}_2$
$\mathbb{U}^1_{I,20}$ Fig. 5.140	$\mathbb{U}^1_{I,20}$	$QS5^{(1,I)}_1$	$\mathbb{U}^1_{I,21}$ Fig. 5.145	$\mathbb{U}^1_{I,21}$	$QS5^{(1,I)}_2$
$\mathbb{U}^1_{I,22}$ Fig. 5.147	$\mathbb{U}^1_{I,22}$	$QS5^{(1,I)}_3$	$\mathbb{U}^1_{I,23}$ Fig. 5.148	$\mathbb{U}^1_{I,23}$	$QS5^{(1,I)}_4$
$\mathbb{U}^1_{I,24}$ Fig. 5.151	$\mathbb{U}^1_{I,24}$	$QS5^{(1,I)}_5$	$\mathbb{U}^1_{I,25}$ Fig. 5.152	$\mathbb{U}^1_{I,25}$	$QS5^{(1,I)}_6$
$\mathbb{U}^1_{I,26}$ Fig. 5.154	$\mathbb{U}^1_{I,26}$	$QS5^{(1,I)}_7$	$\mathbb{U}^1_{I,27}$ Fig. 5.157	$\mathbb{U}^1_{I,27}$	$QS5^{(1,I)}_8$
$\mathbb{U}^1_{I,28}$ Fig. 5.159	$\mathbb{U}^1_{I,28}$	$QS5^{(1,I)}_9$	$\mathbb{U}^1_{I,29}$ Fig. 5.163	$\mathbb{U}^1_{I,29}$	$QS5^{(1,I)}_{10}$
$\mathbb{U}^1_{I,30}$ Fig. 5.167	$\mathbb{U}^1_{I,30}$	$QS10^{(1,I)}_2$	$\mathbb{U}^1_{I,31}$ Fig. 5.167	$\mathbb{U}^1_{I,31}$	$QS10^{(1,I)}_3$
$\mathbb{U}^1_{I,32}$ Fig. 5.167	$\mathbb{U}^1_{I,32}$	$QS10^{(1,I)}_4$	$\mathbb{U}^1_{I,33}$ Fig. 5.167	$\mathbb{U}^1_{I,33}$	$QS10^{(1,I)}_5$
$\mathbb{U}^1_{I,34}$ Fig. 5.169	$\mathbb{U}^1_{I,34}$	$QS10^{(1,I)}_6$	$\mathbb{U}^1_{I,35}$ Fig. 5.170	$\mathbb{U}^1_{I,35}$	$QS10^{(1,I)}_7$
$\mathbb{U}^1_{I,36}$ Fig. 5.171	$\mathbb{U}^1_{I,36}$	$QS10^{(1,I)}_8$	$\mathbb{U}^1_{I,37}$ Fig. 5.171	$\mathbb{U}^1_{I,37}$	$QS10^{(1,I)}_9$
$\mathbb{U}^1_{I,38}$ Fig. 5.172	$\mathbb{U}^1_{I,38}$	$QS10^{(1,I)}_{10}$	$\mathbb{U}^1_{I,39}$ Fig. 5.173	$\mathbb{U}^1_{I,39}$	$QS10^{(1,I)}_{11}$
$\mathbb{U}^1_{I,40}$ Fig. 5.177	$\mathbb{U}^1_{I,40}$	$QS10^{(1,I)}_{12}$	$\mathbb{U}^1_{I,41}$ Fig. 5.178	$\mathbb{U}^1_{I,41}$	$QS10^{(1,I)}_{13}$
$\mathbb{U}^1_{I,42}$ Fig. 5.184	$\mathbb{U}^1_{I,42}$	$QS10^{(1,I)}_{14}$	$\mathbb{U}^1_{I,43}$ Fig. 5.185	$\mathbb{U}^1_{I,43}$	$QS10^{(1,I)}_{15}$
$\mathbb{U}^1_{I,44}$ Fig. 5.186	$\mathbb{U}^1_{I,44}$	$QS10^{(1,I)}_{16}$	$\mathbb{U}^1_{I,45}$ Fig. 5.187	$\mathbb{U}^1_{I,45}$	$QS10^{(1,I)}_{17}$
$\mathbb{U}^1_{I,46}$ Fig. 5.187	$\mathbb{U}^1_{I,46}$	$QS10^{(1,I)}_{13}$	$\mathbb{U}^1_{I,47}$ Fig. 5.189	$\mathbb{U}^1_{I,47}$	$QS10^{(1,I)}_{18}$
$\mathbb{U}^1_{I,48}$ Fig. 5.189	$\mathbb{U}^1_{I,48}$	$QS10^{(1,I)}_{19}$	$\mathbb{U}^1_{I,49}$ Fig. 5.189	$\mathbb{U}^1_{I,49}$	$QS10^{(1,I)}_{20}$
$\mathbb{U}^1_{I,50}$ Fig. 5.189	$\mathbb{U}^1_{I,50}$	$QS10^{(1,I)}_{21}$	$\mathbb{U}^1_{I,51}$ Fig. 5.191	$\mathbb{U}^1_{I,51}$	$QS10^{(1,I)}_{22}$
$\mathbb{U}^1_{I,52}$ Fig. 5.193	$\mathbb{U}^1_{I,52}$	$QS10^{(1,I)}_{23}$	$\mathbb{U}^1_{I,53}$ Fig. 5.193	$\mathbb{U}^1_{I,53}$	$QS10^{(1,I)}_{24}$
$\mathbb{U}^1_{I,54}$ Fig. 5.194	$\mathbb{U}^1_{I,54}$	$QS10^{(1,I)}_{25}$	$\mathbb{U}^1_{I,55}$ Fig. 5.194	$\mathbb{U}^1_{I,55}$	$QS10^{(1,I)}_{26}$
$\mathbb{U}^1_{I,56}$ Fig. 5.194	$\mathbb{U}^1_{I,56}$	$QS10^{(1,I)}_{27}$	$\mathbb{U}^1_{I,57}$ Fig. 5.194	$\mathbb{U}^1_{I,57}$	$QS10^{(1,I)}_{28}$
$\mathbb{U}^1_{I,58}$ Fig. 5.195	$\mathbb{U}^1_{I,58}$	$QS10^{(1,I)}_{29}$	$\mathbb{U}^1_{I,59}$ Fig. 5.195	$\mathbb{U}^1_{I,59}$	$QS10^{(1,I)}_{30}$
$\mathbb{U}^1_{I,60}$ Fig. 5.197	$\mathbb{U}^1_{I,60}$	$QS10^{(1,I)}_{31}$	$\mathbb{U}^1_{I,61}$ Fig. 5.197	$\mathbb{U}^1_{I,61}$	$QS10^{(1,I)}_{32}$
$\mathbb{U}^1_{I,62}$ Fig. 5.198	$\mathbb{U}^1_{I,62}$	$QS10^{(1,I)}_{33}$	$\mathbb{U}^1_{I,63}$ Fig. 5.198	$\mathbb{U}^1_{I,63}$	$QS10^{(1,I)}_{34}$
$\mathbb{U}^1_{I,64}$ Fig. 5.198	$\mathbb{U}^1_{I,64}$	$QS10^{(1,I)}_{35}$	$\mathbb{U}^1_{I,65}$ Fig. 5.198	$\mathbb{U}^1_{I,65}$	$QS10^{(1,I)}_{36}$
$\mathbb{U}^1_{I,66}$ Fig. 5.199	$\mathbb{U}^1_{I,66}$	$QS10^{(1,I)}_{16}$	$\mathbb{U}^1_{I,67}$ Fig. 5.200	$\mathbb{U}^1_{I,67}$	$QS10^{(1,I)}_{17}$
$\mathbb{U}^1_{I,68}$ Fig. 5.202	$\mathbb{U}^1_{I,68}$	$QS10^{(1,I)}_{37}$	$\mathbb{U}^1_{I,69}$ Fig. 5.202	$\mathbb{U}^1_{I,69}$	$QS10^{(1,I)}_{38}$
$\mathbb{U}^1_{I,70}$ Fig. 5.204	$\mathbb{U}^1_{I,70}$	$QS10^{(1,I)}_{39}$	$\mathbb{U}^1_{I,71}$ Fig. 5.206	$\mathbb{U}^1_{I,71}$	$QS10^{(1,I)}_{40}$
$\mathbb{U}^1_{I,72}$ Fig. 5.206	$\mathbb{U}^1_{I,72}$	$QS10^{(1,I)}_{41}$	$\mathbb{U}^1_{I,73}$ Fig. 5.209	$\mathbb{U}^1_{I,73}$	$QS10^{(1,I)}_{42}$
$\mathbb{U}^1_{I,74}$ Fig. 5.210	$\mathbb{U}^1_{I,74}$	$QS10^{(1,I)}_{43}$	$\mathbb{U}^1_{I,75}$ Fig. 5.210	$\mathbb{U}^1_{I,75}$	$QS10^{(1,I)}_{44}$
$\mathbb{U}^1_{I,76}$ Fig. 5.210	$\mathbb{U}^1_{I,76}$	$QS10^{(1,I)}_{45}$	$\mathbb{U}^1_{I,77}$ Fig. 5.211	$\mathbb{U}^1_{I,77}$	$QS10^{(1,I)}_{46}$
$\mathbb{U}^1_{I,78}$ Fig. 5.212	$\mathbb{U}^1_{I,78}$	$QS10^{(1,I)}_{47}$	$\mathbb{U}^1_{I,79}$ Fig. 5.213	$\mathbb{U}^1_{I,79}$	$QS10^{(1,I)}_{48}$
$\mathbb{U}^1_{I,80}$ Fig. 5.214	$\mathbb{U}^1_{I,80}$	$QS10^{(1,I)}_{49}$	$\mathbb{U}^1_{I,81}$ Fig. 5.214	$\mathbb{U}^1_{I,81}$	$QS10^{(1,I)}_{50}$

Table 6.10: Definitive names assigned for impossible codimension-one phase portraits of set (D).

Temp name	Name in [5]	Definitive name	Temp name	Name in [5]	Definitive name
$\mathbb{U}^1_{I,82}$ Fig. 5.215	$\mathbb{U}^1_{I,82}$	$QS10^{(1,I)}_{51}$	$\mathbb{U}^1_{I,83}$ Fig. 5.215	$\mathbb{U}^1_{I,83}$	$QS10^{(1,I)}_{52}$
$\mathbb{U}^1_{I,84}$ Fig. 5.216	$\mathbb{U}^1_{I,84}$	$QS10^{(1,I)}_{53}$	$\mathbb{U}^1_{I,85}$ Fig. 5.216	$\mathbb{U}^1_{I,85}$	$QS10^{(1,I)}_{54}$
$\mathbb{U}^1_{I,86}$ Fig. 5.216	$\mathbb{U}^1_{I,86}$	$QS10^{(1,I)}_{55}$	$\mathbb{U}^1_{I,87}$ Fig. 5.218	$\mathbb{U}^1_{I,87}$	$QS10^{(1,I)}_{56}$
$\mathbb{U}^1_{I,88}$ Fig. 5.219	$\mathbb{U}^1_{I,88}$	$QS10^{(1,I)}_{57}$	$\mathbb{U}^1_{I,89}$ Fig. 5.220	$\mathbb{U}^1_{I,89}$	$QS10^{(1,I)}_{58}$
$\mathbb{U}^1_{I,90}$ Fig. 5.222	$\mathbb{U}^1_{I,90}$	$QS10^{(1,I)}_{59}$	$\mathbb{U}^1_{I,91}$ Fig. 5.224	$\mathbb{U}^1_{I,91}$	$QS10^{(1,I)}_{60}$
$\mathbb{U}^1_{I,92}$ Fig. 5.230	$\mathbb{U}^1_{I,92}$	$QS10^{(1,I)}_{61}$	$\mathbb{U}^1_{I,93}$ Fig. 5.231	$\mathbb{U}^1_{I,93}$	$QS10^{(1,I)}_{62}$
$\mathbb{U}^1_{I,94}$ Fig. 5.232	$\mathbb{U}^1_{I,94}$	$QS10^{(1,I)}_{63}$	$\mathbb{U}^1_{I,95}$ Fig. 5.234	$\mathbb{U}^1_{I,95}$	$QS10^{(1,I)}_{64}$
$\mathbb{U}^1_{I,96}$ Fig. 5.234	$\mathbb{U}^1_{I,96}$	$QS10^{(1,I)}_{65}$	$\mathbb{U}^1_{I,97}$ Fig. 5.234	$\mathbb{U}^1_{I,97}$	$QS10^{(1,I)}_{66}$
$\mathbb{U}^1_{I,98}$ Fig. 5.235	$\mathbb{U}^1_{I,98}$	$QS10^{(1,I)}_{67}$	$\mathbb{U}^1_{I,99}$ Fig. 5.237	$\mathbb{U}^1_{I,99}$	$QS10^{(1,I)}_{68}$
$\mathbb{U}^1_{I,100}$ Fig. 5.237	$\mathbb{U}^1_{I,100}$	$QS10^{(1,I)}_{69}$	$\mathbb{U}^1_{I,101}$ Fig. 5.238	$\mathbb{U}^1_{I,101}$	$QS10^{(1,I)}_{70}$
$\mathbb{U}^1_{I,102}$ Fig. 5.239	$\mathbb{U}^1_{I,102}$	$QS10^{(1,I)}_{71}$	D_5 Fig. 5.98	D_5	$QS8^{(1,I)}_{2}$
D_6 Fig. 5.99	D_6	$QS8^{(1,I)}_{3}$	D_{44} Fig. 5.180	D_{44}	$QS10^{(1,I)}_{72}$
D_{48} Fig. 5.193	D_{48}	$QS10^{(1,I)}_{73}$	D_{13} Fig. 5.107	D_{13}	$QS3^{(1,I)}_{1}$
D_{30} Fig. 5.149	D_{30}	$QS5^{(1,I)}_{11}$	D_{35} Fig. 5.156	D_{35}	$QS5^{(1,I)}_{12}$
D_{56} Fig. 5.213	D_{56}	$QS10^{(1,I)}_{74}$	D_{36} Fig. 5.157	D_{36}	$QS5^{(1,I)}_{13}$
D_{37} Fig. 5.158	D_{37}	$QS5^{(1,I)}_{14}$	D_{63} Fig. 5.236	D_{63}	$QS10^{(1,I)}_{1}$

Table 6.11: *(Cont. Table 6.10)* Definitive names assigned for impossible codimension-one phase portraits of set (D).

Temp. name	Name in [5]	Definitive name	Temp. name	Name in [5]	Definitive name
D_{27a} Fig. 5.138	$\mathbb{U}^1_{D,30a}$	$QS5^{(1,?)}_{1}$	D_{29a} Fig. 5.142	$\mathbb{U}^1_{D,32a}$	$QS5^{(1,?)}_{2}$
D_{38b} Fig. 5.159	$\mathbb{U}^1_{D,37b}$	$QS5^{(1,?)}_{3}$	D_{39a} Fig. 5.160	$\mathbb{U}^1_{D,38a}$	$QS5^{(1,?)}_{4}$
D_{49a} Fig. 5.202	$\mathbb{U}^1_{D,46a}$	$QS10^{(1,?)}_{1}$	D_{52b} Fig. 5.205	$\mathbb{U}^1_{D,51b}$	$QS10^{(1,?)}_{2}$
D_{53a} Fig. 5.207	$\mathbb{U}^1_{D,52a}$	$QS10^{(1,?)}_{3}$			

Table 6.12: Definitive names assigned for conjectured impossible codimension-one phase portraits of set (D).

Temp. name	Name in paper	Definitive name	Temp. name	Name in paper	Definitive name
AA_1^{cp} Fig. 5	$\mathbb{U}^2_{AA,1}$	$QS47_1^{(2)}$	AA_2^{cp} Fig. 6	$\mathbb{U}^2_{AA,2}$	$QS40_1^{(2)}$
AA_3^{cp} Fig. 7	$\mathbb{U}^2_{AA,3}$	$QS40_2^{(2)}$	AA_4^{cp} Fig. 8	$\mathbb{U}^2_{AA,4}$	$QS34_1^{(2)}$
AA_5^{cp} Fig. 9	$\mathbb{U}^2_{AA,5}$	$QS29_1^{(2)}$	AA_6^{cp} Fig. 10	$\mathbb{U}^2_{AA,6}$	$QS48_1^{(2)}$
AA_7^{cp} Fig. 11	$\mathbb{U}^2_{AA,7}$	$QS42_1^{(2)}$	AA_8^{cp} Fig. 12	$\mathbb{U}^2_{AA,8}$	$QS42_2^{(2)}$
AA_9^{cp} Fig. 13	$\mathbb{U}^2_{AA,9}$	$QS42_3^{(2)}$	AA_{10}^{cp} Fig. 14	$\mathbb{U}^2_{AA,10}$	$QS42_4^{(2)}$
AA_{11}^{cp} Fig. 15	$\mathbb{U}^2_{AA,11}$	$QS42_5^{(2)}$	AA_{12}^{cp} Fig. 16	$\mathbb{U}^2_{AA,12}$	$QS42_6^{(2)}$
AA_{13}^{cp} Fig. 17	$\mathbb{U}^2_{AA,13}$	$QS35_1^{(2)}$	AA_{14}^{cp} Fig. 18	$\mathbb{U}^2_{AA,14}$	$QS35_2^{(2)}$
AA_{15}^{cp} Fig. 19	$\mathbb{U}^2_{AA,15}$	$QS35_3^{(2)}$	AA_1^{snsn} Fig. 20	$\mathbb{U}^2_{AA,16}$	$QS50_1^{(2)}$
AA_2^{snsn} Fig. 21	$\mathbb{U}^2_{AA,17}$	$QS50_2^{(2)}$	AA_3^{snsn} Fig. 22	$\mathbb{U}^2_{AA,18}$	$QS50_3^{(2)}$
AA_4^{snsn} Fig. 23	$\mathbb{U}^2_{AA,19}$	$QS50_4^{(2)}$	AA_5^{snsn} Fig. 24	$\mathbb{U}^2_{AA,20}$	$QS50_5^{(2)}$
AA_6^{snsn} Fig. 25	$\mathbb{U}^2_{AA,21}$	$QS51_1^{(2)}$	AA_7^{snsn} Fig. 26	$\mathbb{U}^2_{AA,22}$	$QS51_2^{(2)}$
AA_8^{snsn} Fig. 29	$\mathbb{U}^2_{AA,23}$	$QS51_3^{(2)}$	AA_9^{snsn} Fig. 30	$\mathbb{U}^2_{AA,24}$	$QS51_4^{(2)}$
AA_{10}^{snsn} Fig. 31	$\mathbb{U}^2_{AA,25}$	$QS51_5^{(2)}$	AA_{11}^{snsn} Fig. 32	$\mathbb{U}^2_{AA,26}$	$QS51_6^{(2)}$
AA_{12}^{snsn} Fig. 33	$\mathbb{U}^2_{AA,27}$	$QS51_7^{(2)}$	AA_{13}^{snsn} Fig. 34	$\mathbb{U}^2_{AA,28}$	$QS51_8^{(2)}$
AA_{14}^{snsn} Fig. 36	$\mathbb{U}^2_{AA,29}$	$QS51_9^{(2)}$	AA_{15}^{snsn} Fig. 37	$\mathbb{U}^2_{AA,30}$	$QS51_{10}^{(2)}$
AA_{16}^{snsn} Fig. 38	$\mathbb{U}^2_{AA,31}$	$QS51_{11}^{(2)}$	AA_{18}^{snsn} Fig. 40	$\mathbb{U}^2_{AA,32}$	$QS51_{12}^{(2)}$
AA_{19}^{snsn} Fig. 42	$\mathbb{U}^2_{AA,33}$	$QS51_{13}^{(2)}$	AA_{20}^{snsn} Fig. 43	$\mathbb{U}^2_{AA,34}$	$QS51_{14}^{(2)}$

Table 6.13: Definitive names assigned for codimension-two phase portraits of set (AA).

Temp name	Name in paper	Def. name	Temp name	Name in paper	Def. name
$\mathbb{U}^2_{I,1}$ Fig. 28	$\mathbb{U}^2_{I,1}$	$QS51_1^{(2,I)}$	$\mathbb{U}^2_{I,2}$ Fig. 35	$\mathbb{U}^2_{I,2}$	$QS51_2^{(2,I)}$
$\mathbb{U}^2_{I,3}$ Fig. 41	$\mathbb{U}^2_{I,3}$	$QS51_3^{(2,I)}$	AA_{17}^{snsn} Fig. 39	no final name	$QS51_4^{(2,I)}$

Table 6.14: Definitive names assigned for impossible codimension-two phase portraits of set (AA).

Name in paper	Def. name	Name in paper	Def. name	Name in paper	Def. name
$\mathbb{U}^2_{AB,1}$ Fig. 16	$QS46^{(2)}_1$	$\mathbb{U}^2_{AB,2}$ Fig. 16	$QS46^{(2)}_2$	$\mathbb{U}^2_{AB,3}$ Fig. 17	$QS46^{(2)}_3$
$\mathbb{U}^2_{AB,4}$ Fig. 17	$QS46^{(2)}_4$	$\mathbb{U}^2_{AB,5}$ Fig. 18	$QS46^{(2)}_5$	$\mathbb{U}^2_{AB,6}$ Fig. 18	$QS46^{(2)}_6$
$\mathbb{U}^2_{AB,7}$ Fig. 19	$QS39^{(2)}_1$	$\mathbb{U}^2_{AB,8}$ Fig. 19	$QS39^{(2)}_2$	$\mathbb{U}^2_{AB,9}$ Fig. 20	$QS39^{(2)}_3$
$\mathbb{U}^2_{AB,10}$ Fig. 20	$QS39^{(2)}_4$	$\mathbb{U}^2_{AB,11}$ Fig. 21	$QS39^{(2)}_5$	$\mathbb{U}^2_{AB,12}$ Fig. 21	$QS39^{(2)}_6$
$\mathbb{U}^2_{AB,13}$ Fig. 22	$QS39^{(2)}_7$	$\mathbb{U}^2_{AB,14}$ Fig. 24	$QS39^{(2)}_8$	$\mathbb{U}^2_{AB,15}$ Fig. 26	$QS39^{(2)}_9$
$\mathbb{U}^2_{AB,16}$ Fig. 28	$QS39^{(2)}_{10}$	$\mathbb{U}^2_{AB,17}$ Fig. 30	$QS39^{(2)}_{11}$	$\mathbb{U}^2_{AB,18}$ Fig. 32	$QS39^{(2)}_{12}$
$\mathbb{U}^2_{AB,19}$ Fig. 34	$QS39^{(2)}_{13}$	$\mathbb{U}^2_{AB,20}$ Fig. 36	$QS39^{(2)}_{14}$	$\mathbb{U}^2_{AB,21}$ Fig. 38	$QS39^{(2)}_{15}$
$\mathbb{U}^2_{AB,22}$ Fig. 40	$QS39^{(2)}_{16}$	$\mathbb{U}^2_{AB,23}$ Fig. 42	$QS39^{(2)}_{17}$	$\mathbb{U}^2_{AB,24}$ Fig. 44	$QS39^{(2)}_{18}$
$\mathbb{U}^2_{AB,25}$ Fig. 44	$QS39^{(2)}_{19}$	$\mathbb{U}^2_{AB,26}$ Fig. 45	$QS39^{(2)}_{20}$	$\mathbb{U}^2_{AB,27}$ Fig. 45	$QS39^{(2)}_{21}$
$\mathbb{U}^2_{AB,28}$ Fig. 46	$QS39^{(2)}_{22}$	$\mathbb{U}^2_{AB,29}$ Fig. 46	$QS39^{(2)}_{23}$	$\mathbb{U}^2_{AB,30}$ Fig. 47	$QS39^{(2)}_{24}$
$\mathbb{U}^2_{AB,31}$ Fig. 49	$QS39^{(2)}_{25}$	$\mathbb{U}^2_{AB,32}$ Fig. 51	$QS39^{(2)}_{26}$	$\mathbb{U}^2_{AB,33}$ Fig. 53	$QS39^{(2)}_{27}$
$\mathbb{U}^2_{AB,34}$ Fig. 55	$QS39^{(2)}_{28}$	$\mathbb{U}^2_{AB,35}$ Fig. 57	$QS39^{(2)}_{29}$	$\mathbb{U}^2_{AB,36}$ Fig. 59	$QS39^{(2)}_{30}$
$\mathbb{U}^2_{AB,37}$ Fig. 61	$QS39^{(2)}_{31}$	$\mathbb{U}^2_{AB,38}$ Fig. 63	$QS39^{(2)}_{32}$	$\mathbb{U}^2_{AB,39}$ Fig. 63	$QS39^{(2)}_{33}$
$\mathbb{U}^2_{AB,40}$ Fig. 64	$QS39^{(2)}_{34}$	$\mathbb{U}^2_{AB,41}$ Fig. 64	$QS39^{(2)}_{35}$	$\mathbb{U}^2_{AB,42}$ Fig. 65	$QS39^{(2)}_{36}$
$\mathbb{U}^2_{AB,43}$ Fig. 65	$QS39^{(2)}_{37}$	$\mathbb{U}^2_{AB,44}$ Fig. 66	$QS39^{(2)}_{38}$	$\mathbb{U}^2_{AB,45}$ Fig. 66	$QS39^{(2)}_{39}$
$\mathbb{U}^2_{AB,46}$ Fig. 67	$QS39^{(2)}_{40}$	$\mathbb{U}^2_{AB,47}$ Fig. 67	$QS39^{(2)}_{41}$	$\mathbb{U}^2_{AB,48}$ Fig. 68	$QS39^{(2)}_{42}$
$\mathbb{U}^2_{AB,49}$ Fig. 68	$QS39^{(2)}_{43}$	$\mathbb{U}^2_{AB,50}$ Fig. 69	$QS39^{(2)}_{44}$	$\mathbb{U}^2_{AB,51}$ Fig. 71	$QS39^{(2)}_{45}$
$\mathbb{U}^2_{AB,52}$ Fig. 71	$QS39^{(2)}_{46}$	$\mathbb{U}^2_{AB,53}$ Fig. 72	$QS32^{(2)}_1$	$\mathbb{U}^2_{AB,54}$ Fig. 74	$QS32^{(2)}_2$
$\mathbb{U}^2_{AB,55}$ Fig. 76	$QS32^{(2)}_3$	$\mathbb{U}^2_{AB,56}$ Fig. 77	$QS32^{(2)}_4$	$\mathbb{U}^2_{AB,57}$ Fig. 77	$QS32^{(2)}_5$
$\mathbb{U}^2_{AB,58}$ Fig. 78	$QS32^{(2)}_6$	$\mathbb{U}^2_{AB,59}$ Fig. 79	$QS32^{(2)}_7$	$\mathbb{U}^2_{AB,60}$ Fig. 79	$QS32^{(2)}_8$
$\mathbb{U}^2_{AB,61}$ Fig. 80	$QS32^{(2)}_9$	$\mathbb{U}^2_{AB,62}$ Fig. 81	$QS32^{(2)}_{10}$	$\mathbb{U}^2_{AB,63}$ Fig. 83	$QS32^{(2)}_{11}$
$\mathbb{U}^2_{AB,64}$ Fig. 85	$QS32^{(2)}_{12}$	$\mathbb{U}^2_{AB,65}$ Fig. 87	$QS32^{(2)}_{13}$	$\mathbb{U}^2_{AB,66}$ Fig. 89	$QS32^{(2)}_{14}$
$\mathbb{U}^2_{AB,67}$ Fig. 89	$QS32^{(2)}_{15}$	$\mathbb{U}^2_{AB,68}$ Fig. 90	$QS32^{(2)}_{16}$	$\mathbb{U}^2_{AB,69}$ Fig. 90	$QS32^{(2)}_{17}$
$\mathbb{U}^2_{AB,70}$ Fig. 91	$QS32^{(2)}_{18}$	$\mathbb{U}^2_{AB,71}$ Fig. 93	$QS32^{(2)}_{19}$		

Table 6.15: Definitive names assigned for codimension-two phase portraits of set (AB).

Name in paper	Def. name	Name in paper	Def. name	Name in paper	Def. name
$\mathbb{U}^{2,I}_{AB,1}$ Fig. 23	$QS39^{(2,I)}_{1}$	$\mathbb{U}^{2,I}_{AB,2}$ Fig. 25	$QS39^{(2,I)}_{2}$	$\mathbb{U}^{2,I}_{AB,3}$ Fig. 27	$QS39^{(2,I)}_{3}$
$\mathbb{U}^{2,I}_{AB,4}$ Fig. 29	$QS39^{(2,I)}_{4}$	$\mathbb{U}^{2,I}_{AB,5}$ Fig. 31	$QS39^{(2,I)}_{5}$	$\mathbb{U}^{2,I}_{AB,6}$ Fig. 33	$QS39^{(2,I)}_{6}$
$\mathbb{U}^{2,I}_{AB,7}$ Fig. 35	$QS39^{(2,I)}_{7}$	$\mathbb{U}^{2,I}_{AB,8}$ Fig. 37	$QS39^{(2,I)}_{8}$	$\mathbb{U}^{2,I}_{AB,9}$ Fig. 39	$QS39^{(2,I)}_{9}$
$\mathbb{U}^{2,I}_{AB,10}$ Fig. 41	$QS39^{(2,I)}_{10}$	$\mathbb{U}^{2,I}_{AB,11}$ Fig. 43	$QS39^{(2,I)}_{11}$	$\mathbb{U}^{2,I}_{AB,12}$ Fig. 48	$QS39^{(2,I)}_{12}$
$\mathbb{U}^{2,I}_{AB,13}$ Fig. 50	$QS39^{(2,I)}_{13}$	$\mathbb{U}^{2,I}_{AB,14}$ Fig. 52	$QS39^{(2,I)}_{14}$	$\mathbb{U}^{2,I}_{AB,15}$ Fig. 54	$QS39^{(2,I)}_{15}$
$\mathbb{U}^{2,I}_{AB,16}$ Fig. 56	$QS39^{(2,I)}_{16}$	$\mathbb{U}^{2,I}_{AB,17}$ Fig. 58	$QS39^{(2,I)}_{17}$	$\mathbb{U}^{2,I}_{AB,18}$ Fig. 60	$QS39^{(2,I)}_{18}$
$\mathbb{U}^{2,I}_{AB,19}$ Fig. 62	$QS39^{(2,I)}_{19}$	$\mathbb{U}^{2,I}_{AB,20}$ Fig. 70	$QS39^{(2,I)}_{20}$	$\mathbb{U}^{2,I}_{AB,21}$ Fig. 73	$QS32^{(2,I)}_{1}$
$\mathbb{U}^{2,I}_{AB,22}$ Fig. 75	$QS32^{(2,I)}_{2}$	$\mathbb{U}^{2,I}_{AB,23}$ Fig. 82	$QS32^{(2,I)}_{3}$	$\mathbb{U}^{2,I}_{AB,24}$ Fig. 84	$QS32^{(2,I)}_{4}$
$\mathbb{U}^{2,I}_{AB,25}$ Fig. 86	$QS32^{(2,I)}_{5}$	$\mathbb{U}^{2,I}_{AB,26}$ Fig. 88	$QS32^{(2,I)}_{6}$	$\mathbb{U}^{2,I}_{AB,27}$ Fig. 92	$QS32^{(2,I)}_{7}$
$\mathbb{U}^{2,I}_{AB,28}$ Fig. 94	$QS32^{(2,I)}_{8}$	$\mathbb{U}^{2,I}_{AB,29}$ Fig. 95	$QS32^{(2,I)}_{9}$	$\mathbb{U}^{2,I}_{AB,30}$ Fig. 96	$QS32^{(2,I)}_{10}$
$\mathbb{U}^{2,I}_{AB,31}$ Fig. 97	$QS32^{(2,I)}_{11}$	$\mathbb{U}^{2,I}_{AB,32}$ Fig. 98	$QS32^{(2,I)}_{12}$	$\mathbb{U}^{2,I}_{AB,33}$ Fig. 98	$QS32^{(2,I)}_{13}$
$\mathbb{U}^{2,I}_{AB,34}$ Fig. 99	$QS32^{(2,I)}_{14}$	$\mathbb{U}^{2,I}_{AB,35}$ Fig. 100	$QS32^{(2,I)}_{15}$	$\mathbb{U}^{2,I}_{AB,36}$ Fig. 101	$QS32^{(2,I)}_{16}$
$\mathbb{U}^{2,I}_{AB,37}$ Fig. 102	$QS32^{(2,I)}_{17}$	$\mathbb{U}^{2,I}_{AB,38}$ Fig. 103	$QS32^{(2,I)}_{18}$	$\mathbb{U}^{2,I}_{AB,39}$ Fig. 104	$QS32^{(2,I)}_{19}$

Table 6.16: Definitive names assigned for impossible codimension-two phase portraits of set (AB).

Name in paper	Def. name	Name in paper	Def. name	Name in paper	Def. name
$\mathbb{U}^{2}_{AC,1}$ Fig. 105	$QS98^{(2)}_{1}$	$\mathbb{U}^{2}_{AC,2}$ Fig. 106	$QS98^{(2)}_{2}$	$\mathbb{U}^{2}_{AC,3}$ Fig. 107	$QS98^{(2)}_{3}$
$\mathbb{U}^{2}_{AC,4}$ Fig. 108	$QS98^{(2)}_{4}$	$\mathbb{U}^{2}_{AC,5}$ Fig. 109	$QS104^{(2)}_{1}$	$\mathbb{U}^{2}_{AC,6}$ Fig. 110	$QS104^{(2)}_{2}$
$\mathbb{U}^{2}_{AC,7}$ Fig. 110	$QS104^{(2)}_{3}$	$\mathbb{U}^{2}_{AC,8}$ Fig. 111	$QS104^{(2)}_{4}$	$\mathbb{U}^{2}_{AC,9}$ Fig. 111	$QS104^{(2)}_{5}$
$\mathbb{U}^{2}_{AC,10}$ Fig. 111	$QS104^{(2)}_{6}$	$\mathbb{U}^{2}_{AC,11}$ Fig. 112	$QS104^{(2)}_{7}$	$\mathbb{U}^{2}_{AC,12}$ Fig. 112	$QS104^{(2)}_{8}$
$\mathbb{U}^{2}_{AC,13}$ Fig. 112	$QS104^{(2)}_{9}$	$\mathbb{U}^{2}_{AC,14}$ Fig. 113	$QS104^{(2)}_{10}$	$\mathbb{U}^{2}_{AC,15}$ Fig. 113	$QS104^{(2)}_{11}$
$\mathbb{U}^{2}_{AC,16}$ Fig. 113	$QS104^{(2)}_{12}$	$\mathbb{U}^{2}_{AC,17}$ Fig. 114	$QS99^{(2)}_{1}$	$\mathbb{U}^{2}_{AC,18}$ Fig. 115	$QS99^{(2)}_{2}$
$\mathbb{U}^{2}_{AC,19}$ Fig. 116	$QS99^{(2)}_{3}$	$\mathbb{U}^{2}_{AC,20}$ Fig. 118	$QS99^{(2)}_{4}$	$\mathbb{U}^{2}_{AC,21}$ Fig. 119	$QS99^{(2)}_{5}$
$\mathbb{U}^{2}_{AC,22}$ Fig. 119	$QS99^{(2)}_{6}$	$\mathbb{U}^{2}_{AC,23}$ Fig. 120	$QS99^{(2)}_{7}$	$\mathbb{U}^{2}_{AC,24}$ Fig. 120	$QS99^{(2)}_{8}$
$\mathbb{U}^{2}_{AC,25}$ Fig. 121	$QS99^{(2)}_{9}$	$\mathbb{U}^{2}_{AC,26}$ Fig. 122	$QS99^{(2)}_{10}$	$\mathbb{U}^{2}_{AC,27}$ Fig. 123	$QS99^{(2)}_{11}$
$\mathbb{U}^{2}_{AC,28}$ Fig. 124	$QS99^{(2)}_{12}$	$\mathbb{U}^{2}_{AC,29}$ Fig. 125	$QS99^{(2)}_{13}$	$\mathbb{U}^{2}_{AC,30}$ Fig. 126	$QS99^{(2)}_{14}$
$\mathbb{U}^{2}_{AC,31}$ Fig. 127	$QS99^{(2)}_{15}$	$\mathbb{U}^{2}_{AC,32}$ Fig. 129	$QS99^{(2)}_{16}$	$\mathbb{U}^{2}_{AC,33}$ Fig. 129	$QS99^{(2)}_{17}$
$\mathbb{U}^{2}_{AC,34}$ Fig. 130	$QS99^{(2)}_{18}$	$\mathbb{U}^{2}_{AC,35}$ Fig. 130	$QS99^{(2)}_{19}$	$\mathbb{U}^{2}_{AC,36}$ Fig. 131	$QS99^{(2)}_{20}$
$\mathbb{U}^{2}_{AC,37}$ Fig. 132	$QS99^{(2)}_{21}$	$\mathbb{U}^{2}_{AC,38}$ Fig. 133	$QS99^{(2)}_{22}$	$\mathbb{U}^{2}_{AC,39}$ Fig. 134	$QS99^{(2)}_{23}$
$\mathbb{U}^{2}_{AC,40}$ Fig. 134	$QS99^{(2)}_{24}$				

Table 6.17: Definitive names assigned for codimension-two phase portraits of set (AC).

Name in paper	Def. name	Name in paper	Def. name	Name in paper	Def. name
$\mathbb{U}^{2,I}_{AC,1}$ Fig. 23	$QS99^{(2,I)}_1$	$\mathbb{U}^{2,I}_{AC,2}$ Fig. 25	$QS99^{(2,I)}_2$	$\mathbb{U}^{2,I}_{AC,3}$ Fig. 27	$QS99^{(2,I)}_3$
$\mathbb{U}^{2,I}_{AC,4}$ Fig. 29	$QS99^{(2,I)}_4$	$\mathbb{U}^{2,I}_{AC,5}$ Fig. 31	$QS99^{(2,I)}_5$		

Table 6.18: Definitive names assigned for impossible codimension-two phase portraits of set (AC).

Name in [1]	Def. name	Name in [1]	Def. name	Name in [1]	Def. name
$\mathbb{U}^2_{AD,1}$ Fig. 13	$QS37^{(2)}_1$	$\mathbb{U}^2_{AD,2}$ Fig. 13	$QS37^{(2)}_2$	$\mathbb{U}^2_{AD,3}$ Fig. 14	$QS37^{(2)}_3$
$\mathbb{U}^2_{AD,4}$ Fig. 15	$QS37^{(2)}_4$	$\mathbb{U}^2_{AD,5}$ Fig. 16	$QS37^{(2)}_5$	$\mathbb{U}^2_{AD,6}$ Fig. 16	$QS37^{(2)}_6$
$\mathbb{U}^2_{AD,7}$ Fig. 16	$QS37^{(2)}_7$	$\mathbb{U}^2_{AD,8}$ Fig. 17	$QS37^{(2)}_8$	$\mathbb{U}^2_{AD,9}$ Fig. 17	$QS37^{(2)}_9$
$\mathbb{U}^2_{AD,10}$ Fig. 19	$QS37^{(2)}_{10}$	$\mathbb{U}^2_{AD,11}$ Fig. 20	$QS37^{(2)}_{11}$	$\mathbb{U}^2_{AD,12}$ Fig. 21	$QS30^{(2)}_1$
$\mathbb{U}^2_{AD,13}$ Fig. 22	$QS30^{(2)}_2$	$\mathbb{U}^2_{AD,14}$ Fig. 22	$QS30^{(2)}_3$	$\mathbb{U}^2_{AD,15}$ Fig. 23	$QS28^{(2)}_1$
$\mathbb{U}^2_{AD,16}$ Fig. 23	$QS28^{(2)}_2$	$\mathbb{U}^2_{AD,17}$ Fig. 24	$QS28^{(2)}_3$	$\mathbb{U}^2_{AD,18}$ Fig. 25	$QS28^{(2)}_4$
$\mathbb{U}^2_{AD,19}$ Fig. 26	$QS28^{(2)}_5$	$\mathbb{U}^2_{AD,20}$ Fig. 27	$QS45^{(2)}_1$	$\mathbb{U}^2_{AD,21}$ Fig. 28	$QS45^{(2)}_2$
$\mathbb{U}^2_{AD,22}$ Fig. 29	$QS45^{(2)}_3$	$\mathbb{U}^2_{AD,23}$ Fig. 30	$QS31^{(2)}_1$	$\mathbb{U}^2_{AD,24}$ Fig. 31	$QS31^{(2)}_2$
$\mathbb{U}^2_{AD,25}$ Fig. 32	$QS31^{(2)}_3$	$\mathbb{U}^2_{AD,26}$ Fig. 33	$QS31^{(2)}_4$	$\mathbb{U}^2_{AD,27}$ Fig. 33	$QS31^{(2)}_5$
$\mathbb{U}^2_{AD,28}$ Fig. 34	$QS31^{(2)}_6$	$\mathbb{U}^2_{AD,29}$ Fig. 34	$QS31^{(2)}_7$	$\mathbb{U}^2_{AD,30}$ Fig. 35	$QS31^{(2)}_8$
$\mathbb{U}^2_{AD,31}$ Fig. 35	$QS31^{(2)}_9$	$\mathbb{U}^2_{AD,32}$ Fig. 35	$QS31^{(2)}_{10}$	$\mathbb{U}^2_{AD,33}$ Fig. 36	$QS31^{(2)}_{11}$
$\mathbb{U}^2_{AD,34}$ Fig. 36	$QS31^{(2)}_{12}$	$\mathbb{U}^2_{AD,35}$ Fig. 37	$QS31^{(2)}_{13}$	$\mathbb{U}^2_{AD,36}$ Fig. 37	$QS31^{(2)}_{14}$
$\mathbb{U}^2_{AD,37}$ Fig. 38	$QS31^{(2)}_{15}$	$\mathbb{U}^2_{AD,38}$ Fig. 38	$QS31^{(2)}_{16}$	$\mathbb{U}^2_{AD,39}$ Fig. 39	$QS31^{(2)}_{17}$
$\mathbb{U}^2_{AD,40}$ Fig. 39	$QS31^{(2)}_{18}$	$\mathbb{U}^2_{AD,41}$ Fig. 40	$QS38^{(2)}_1$	$\mathbb{U}^2_{AD,42}$ Fig. 40	$QS38^{(2)}_2$
$\mathbb{U}^2_{AD,43}$ Fig. 41	$QS38^{(2)}_3$	$\mathbb{U}^2_{AD,44}$ Fig. 41	$QS38^{(2)}_4$	$\mathbb{U}^2_{AD,45}$ Fig. 42	$QS38^{(2)}_5$
$\mathbb{U}^2_{AD,46}$ Fig. 42	$QS38^{(2)}_6$	$\mathbb{U}^2_{AD,47}$ Fig. 43	$QS38^{(2)}_7$	$\mathbb{U}^2_{AD,48}$ Fig. 43	$QS38^{(2)}_8$
$\mathbb{U}^2_{AD,49}$ Fig. 43	$QS38^{(2)}_9$	$\mathbb{U}^2_{AD,50}$ Fig. 44	$QS38^{(2)}_{10}$	$\mathbb{U}^2_{AD,51}$ Fig. 45	$QS38^{(2)}_{11}$
$\mathbb{U}^2_{AD,52}$ Fig. 45	$QS38^{(2)}_{12}$	$\mathbb{U}^2_{AD,53}$ Fig. 46	$QS38^{(2)}_{13}$	$\mathbb{U}^2_{AD,54}$ Fig. 46	$QS38^{(2)}_{14}$
$\mathbb{U}^2_{AD,55}$ Fig. 48	$QS38^{(2)}_{15}$	$\mathbb{U}^2_{AD,56}$ Fig. 50	$QS38^{(2)}_{16}$	$\mathbb{U}^2_{AD,57}$ Fig. 51	$QS38^{(2)}_{17}$
$\mathbb{U}^2_{AD,58}$ Fig. 52	$QS38^{(2)}_{18}$	$\mathbb{U}^2_{AD,59}$ Fig. 53	$QS38^{(2)}_{19}$	$\mathbb{U}^2_{AD,60}$ Fig. 54	$QS38^{(2)}_{20}$
$\mathbb{U}^2_{AD,61}$ Fig. 55	$QS38^{(2)}_{21}$	$\mathbb{U}^2_{AD,62}$ Fig. 55	$QS38^{(2)}_{22}$	$\mathbb{U}^2_{AD,63}$ Fig. 56	$QS38^{(2)}_{23}$
$\mathbb{U}^2_{AD,64}$ Fig. 56	$QS38^{(2)}_{24}$	$\mathbb{U}^2_{AD,65}$ Fig. 57	$QS38^{(2)}_{25}$	$\mathbb{U}^2_{AD,66}$ Fig. 57	$QS38^{(2)}_{26}$
$\mathbb{U}^2_{AD,67}$ Fig. 58	$QS38^{(2)}_{27}$	$\mathbb{U}^2_{AD,68}$ Fig. 58	$QS38^{(2)}_{28}$	$\mathbb{U}^2_{AD,69}$ Fig. 59	$QS38^{(2)}_{29}$
$\mathbb{U}^2_{AD,70}$ Fig. 59	$QS38^{(2)}_{30}$	$\mathbb{U}^2_{AD,71}$ Fig. 59	$QS38^{(2)}_{31}$	$\mathbb{U}^2_{AD,72}$ Fig. 60	$QS38^{(2)}_{32}$
$\mathbb{U}^2_{AD,73}$ Fig. 60	$QS38^{(2)}_{33}$	$\mathbb{U}^2_{AD,74}$ Fig. 60	$QS38^{(2)}_{34}$	$\mathbb{U}^2_{AD,75}$ Fig. 61	$QS38^{(2)}_{35}$
$\mathbb{U}^2_{AD,76}$ Fig. 61	$QS38^{(2)}_{36}$	$\mathbb{U}^2_{AD,77}$ Fig. 18	$QS37^{(2)}_{12}$		

Table 6.19: Definitive names assigned for codimension-two phase portraits of set (AD).

Name in [1]	Def. name	Name in [1]	Def. name	Name in [1]	Def. name
$\mathbb{U}^{2,I}_{AD,38}$ Fig. 38	$QS31^{(2,I)}_1$	$\mathbb{U}^{2,I}_{AD,46}$ Fig. 42	$QS38^{(2,I)}_1$	$\mathbb{U}^{2,I}_{AD,56a}$ Fig. 49	$QS38^{(2,I)}_2$
$\mathbb{U}^{2,I}_{AD,56b}$ Fig. 50	$QS38^{(2,I)}_3$	$\mathbb{U}^{2,I}_{AD,69}$ Fig. 59	$QS38^{(2,I)}_4$	$\mathbb{U}^{2,I}_{AD,74}$ Fig. 49	$QS38^{(2,I)}_5$

Table 6.20: Definitive names assigned for impossible codimension-two phase portraits of set (AD).

Name in [1]	Def. name	Name in [1]	Def. name	Name in [1]	Def. name
$\mathbb{U}^{2,I}_{AD,9}$ Fig. 18	$QS37^{(2,?)}_1$	$\mathbb{U}^{2,I}_{AD,12}$ Fig. 21	$QS30^{(2,?)}_1$	$\mathbb{U}^{2,I}_{AD,24}$ Fig. 31	$QS31^{(2,?)}_1$
$\mathbb{U}^{2,I}_{AD,55}$ Fig. 47	$QS38^{(2,?)}_1$	$\mathbb{U}^{2,I}_{AD,56}$ Fig. 49	$QS38^{(2,?)}_2$		

Table 6.21: Definitive names assigned for conjectured impossible codimension-two phase portraits of set (AD).

Name in paper	Def. name	Name in paper	Def. name	Name in paper	Def. name
$\mathbb{U}^{2}_{BC,1}$ Fig. 19	$QS86^{(2)}_1$	$\mathbb{U}^{2}_{BC,2}$ Fig. 20	$QS86^{(2)}_2$	$\mathbb{U}^{2}_{BC,3}$ Fig. 21	$QS86^{(2)}_3$
$\mathbb{U}^{2}_{BC,4}$ Fig. 23	$QS75^{(2)}_1$	$\mathbb{U}^{2}_{BC,5}$ Fig. 24	$QS75^{(2)}_2$	$\mathbb{U}^{2}_{BC,6}$ Fig. 25	$QS75^{(2)}_3$
$\mathbb{U}^{2}_{BC,7}$ Fig. 26	$QS75^{(2)}_4$	$\mathbb{U}^{2}_{BC,8}$ Fig. 27	$QS75^{(2)}_5$	$\mathbb{U}^{2}_{BC,9}$ Fig. 29	$QS75^{(2)}_6$
$\mathbb{U}^{2}_{BC,10}$ Fig. 30	$QS75^{(2)}_7$	$\mathbb{U}^{2}_{BC,11}$ Fig. 31	$QS75^{(2)}_8$	$\mathbb{U}^{2}_{BC,12}$ Fig. 32	$QS75^{(2)}_9$
$\mathbb{U}^{2}_{BC,13}$ Fig. 33	$QS75^{(2)}_{10}$	$\mathbb{U}^{2}_{BC,14}$ Fig. 34	$QS75^{(2)}_{11}$	$\mathbb{U}^{2}_{BC,15}$ Fig. 35	$QS75^{(2)}_{12}$
$\mathbb{U}^{2}_{BC,16}$ Fig. 36	$QS75^{(2)}_{13}$				

Table 6.22: Definitive names assigned for codimension-two phase portraits of set (BC_{SNSN}).

Name in paper	Def. name	Name in paper	Def. name
$\mathbb{U}^{2,I}_{BC,1}$ Fig. 22	$QS75^{(2,I)}_1$	$\mathbb{U}^{2,I}_{BC,2}$ Fig. 28	$QS75^{(2,I)}_1$

Table 6.23: Definitive names assigned for impossible codimension-two phase portraits of set (BC_{SNSN}).

Name in [10]	Def. name	Name in [10]	Def. name	Name in [10]	Def. name
$\mathbb{U}^2_{BC,17}$ Fig. 39	$QS88^{(2)}_1$	$\mathbb{U}^2_{BC,18}$ Fig. 40	$QS77^{(2)}_3$	$\mathbb{U}^2_{BC,19}$ Fig. 41	$QS77^{(2)}_2$
$\mathbb{U}^2_{BC,20}$ Fig. 42	$QS77^{(2)}_1$	$\mathbb{U}^2_{BC,21}$ Fig. 50	$QS93^{(2)}_1$	$\mathbb{U}^2_{BC,22}$ Fig. 50	$QS91^{(2)}_1$
$\mathbb{U}^2_{BC,23}$ Fig. 50	$QS89^{(2)}_1$	$\mathbb{U}^2_{BC,23LC}$ Fig. 51	$QS89^{(2)}_{1(1)LC}$	$\mathbb{U}^2_{BC,24}$ Fig. 51	$QS91^{(2)}_3$
$\mathbb{U}^2_{BC,25LC}$ Fig. 51	$QS91^{(2)}_{2(1)LC}$	$\mathbb{U}^2_{BC,26}$ Fig. 54	$QS89^{(2)}_1$	$\mathbb{U}^2_{BC,27}$ Fig. 54	$QS81^{(2)}_1$
$\mathbb{U}^2_{BC,28}$ Fig. 54	$QS80^{(2)}_1$	$\mathbb{U}^2_{BC,29}$ Fig. 56	$QS81^{(2)}_2$	$\mathbb{U}^2_{BC,30}$ Fig. 56	$QS80^{(2)}_2$
$\mathbb{U}^2_{BC,31}$ Fig. 56	$QS79^{(2)}_2$	$\mathbb{U}^2_{BC,32}$ Fig. 58	$QS81^{(2)}_3$	$\mathbb{U}^2_{BC,33}$ Fig. 58	$QS80^{(2)}_4$
$\mathbb{U}^2_{BC,34}$ Fig. 58	$QS79^{(2)}_3$				

Table 6.24: Definitive names assigned for codimension-two phase portraits of set (BC_{ESNS}).

Name in paper	Def. name	Name in paper	Def. name	Name in paper	Def. name
$\mathbb{U}^{2,I}_{BC,3}$ Fig. 39	$QSNE^{(2,I)}_1$	$\mathbb{U}^{2,I}_{BC,4}$ Fig. 39	$QSNE^{(2,I)}_2$	$\mathbb{U}^{2,I}_{BC,5}$ Fig. 40	$QSNE^{(2,I)}_3$
$\mathbb{U}^{2,I}_{BC,6}$ Fig. 40	$QS77^{(2,I)}_1$	$\mathbb{U}^{2,I}_{BC,7}$ Fig. 40	$QSNE^{(2,I)}_4$	$\mathbb{U}^{2,I}_{BC,8}$ Fig. 41	$QSNE^{(2,I)}_5$
$\mathbb{U}^{2,I}_{BC,9}$ Fig. 41	$QSNE^{(2,I)}_6$	$\mathbb{U}^{2,I}_{BC,10}$ Fig. 41	$QS77^{(2,I)}_2$	$\mathbb{U}^{2,I}_{BC,11}$ Fig. 42	$QSNE^{(2,I)}_7$
$\mathbb{U}^{2,I}_{BC,12}$ Fig. 42	$QSNE^{(2,I)}_8$	$\mathbb{U}^{2,I}_{BC,13}$ Fig. 43	$QSNE^{(2,I)}_9$	$\mathbb{U}^{2,I}_{BC,14}$ Fig. 43	$QSNE^{(2,I)}_{10}$
$\mathbb{U}^{2,I}_{BC,15}$ Fig. 44	$QSNE^{(2,I)}_{11}$	$\mathbb{U}^{2,I}_{BC,16}$ Fig. 44	$QSNE^{(2,I)}_{12}$	$\mathbb{U}^{2,I}_{BC,17}$ Fig. 45	$QSNE^{(2,I)}_{13}$
$\mathbb{U}^{2,I}_{BC,18}$ Fig. 45	$QSNE^{(2,I)}_{14}$	$\mathbb{U}^{2,I}_{BC,19}$ Fig. 45	$QS77^{(2,I)}_3$	$\mathbb{U}^{2,I}_{BC,20}$ Fig. 46	$QSNE^{(2,I)}_{15}$
$\mathbb{U}^{2,I}_{BC,21}$ Fig. 46	$QSNE^{(2,I)}_{16}$	$\mathbb{U}^{2,I}_{BC,22}$ Fig. 47	$QSNE^{(2,I)}_{17}$	$\mathbb{U}^{2,I}_{BC,23}$ Fig. 48	$QSNE^{(2,I)}_{18}$
$\mathbb{U}^{2,I}_{BC,24}$ Fig. 48	$QSNE^{(2,I)}_{19}$	$\mathbb{U}^{2,I}_{BC,25}$ Fig. 49	$QSNE^{(2,I)}_{20}$	$\mathbb{U}^{2,I}_{BC,26}$ Fig. 55	$QS77^{(2,I)}_4$
$\mathbb{U}^{2,I}_{BC,27}$ Fig. 55	$QS79^{(2,I)}_1$	$\mathbb{U}^{2,I}_{BC,28}$ Fig. 55	$QS81^{(2,I)}_1$	$\mathbb{U}^{2,I}_{BC,29}$ Fig. 59	$QS80^{(2,I)}_1$
$\mathbb{U}^{2,I}_{BC,30}$ Fig. 62	$QS81^{(2,I)}_2$	$\mathbb{U}^{2,I}_{BC,31}$ Fig. 62	$QS80^{(2,I)}_2$	$\mathbb{U}^{2,I}_{BC,32}$ Fig. 62	$QS79^{(2,I)}_2$
$\mathbb{U}^{2,I}_{BC,33}$ Fig. 63	$QS79^{(2,I)}_3$	$\mathbb{U}^{2,I}_{BC,34}$ Fig. 63	$QS80^{(2,I)}_4$	$\mathbb{U}^{2,I}_{BC,35}$ Fig. 63	$QS80^{(2,I)}_{4(1)LC}$
$\mathbb{U}^{2,I}_{BC,36}$ Fig. 63	$QS79^{(2,I)}_4$	$\mathbb{U}^{2,I}_{BC,37}$ Fig. 64	$QS80^{(2,I)}_5$	$\mathbb{U}^{2,I}_{BC,38}$ Fig. 64	$QS79^{(2,I)}_{2(1)LC}$

Table 6.25: Definitive names assigned for impossible codimension-two phase portraits of set (BC_{ESNS}).

Acknowledgements

The first author is partially supported by Agencia Estatal de Investigación of Spain grant PID2022-136613NB-100. The second author was financed in part by CAPES. The third author is partially supported by CAPES, by FAPESP Processes no. 2018/21320-7, 2019/21181-0, and 2024/13454-4, and by CNPq - Process no. 401974/2025-1.

References

[1] J. C. Artés, Structurally unstable quadratic vector fields of codimension two: families possessing one finite saddle-node and a separatrix connection, *Qual. Theory Dyn. Syst.* **23**(2024), Art. 40, 88 pp. https://doi.org/10.1007/s12346-023-00882-0

[2] J. C. Artés, F. Dumortier, C. Herssens, J. Llibre, P. De Maesschalck, Computer program P4 to study phase portraits of planar polynomial differential equations, 2005. http://mat.uab.es/~artes/p4/p4.htm

[3] J. C. Artés, R. E. Kooij, J. Llibre, *Structurally stable quadratic vector fields*, Mem. Amer. Math. Soc. **134**(1998), No. 639, viii+108 pp. https://doi.org/10.1090/memo/0639

[4] J. C. Artés, J. Llibre, Quadratic vector fields with a weak focus of third order, *Publ. Mat.* **41**(1997), No. 1, 7–39. https://doi.org/10.5565/PUBLMAT_41197_02

[5] J. C. Artés, J. Llibre, A. C. Rezende, *Structurally unstable quadratic vector fields of codimension one*, Birkhäuser, Cham, 2018. https://doi.org/10.1007/978-3-319-92117-4

[6] J. C. Artés, J. Llibre, D. Schlomiuk, N. Vulpe, From topological to geometric equivalence in the classification of singularities at infinity for quadratic vector fields, *Rocky Mountain J. Math.* **45**(2015), No. 1, 29–113. https://doi.org/10.1216/RMJ-2015-45-1-29

[7] J. C. Artés, J. Llibre, D. Schlomiuk, N. Vulpe, Global topological configurations of singularities for the whole family of quadratic differential systems, *Qual. Theory Dyn. Syst.* **19**(2020), Art. 51, 32 pp. https://doi.org/10.1007/s12346-020-00372-7

[8] J. C. Artés, J. Llibre, D. Schlomiuk, N. Vulpe, *Geometric configurations of singularities of planar polynomial differential systems. A global classification in the quadratic case*, Birkhäuser, Cham, 2021. https://doi.org/10.1007/978-3-030-50570-7

[9] J. C. Artés, J. Llibre, D. Schlomiuk, N. I. Vulpe, Codimension in planar polynomial differential systems, *Electron. J. Differential Equations* **2026**, No. 28, 1–47. https://doi.org/10.58997/ejde.2026.28

[10] J. C. Artés, J. Llibre, D. Schlomiuk, N. I. Vulpe, Phase portraits of a family of real quadratic differential systems possessing a nilpotent or intricate singularity at infinity, preprint, 2026, 41 pp.

[11] J. C. Artés, M. C. Mota, A. C. Rezende, Quadratic differential systems with a finite saddle-node and an infinite saddle-node $(1,1)SN$-(B), *Internat. J. Bifur. Chaos Appl. Sci. Engrg.* **31**(2021), No. 9, Art. 2130026, 110 pp. https://doi.org/10.1142/S0218127421300263

[12] J. C. Artés, M. C. Mota, A. C. Rezende, Structurally unstable quadratic vector fields of codimension two: families possessing a finite saddle-node and an infinite saddle-node, *Electron. J. Qual. Theory Differ. Equ.* **2021**, No. 35, 1–89. https://doi.org/10.14232/ejqtde.2021.1.35

[13] J. C. Artés, M. C. Mota, A. C. Rezende, Quadratic systems possessing an infinite elliptic-saddle or an infinite nilpotent saddle, *Internat. J. Bifur. Chaos Appl. Sci. Engrg.* **34**(2024), No. 11, Art. 2430023. https://doi.org/10.1142/S0218127424300234

[14] J. C. Artés, R. D. S. Oliveira, A. C. Rezende, Structurally unstable quadratic vector fields of codimension two: families possessing either a cusp point or two finite saddle-nodes, *J. Dynam. Differential Equations* **33**(2021), No. 4, 1779–1821. https://doi.org/10.1007/s10884-020-09871-2

[15] J. C. Artés, A. C. Rezende, R. D. S. Oliveira, The geometry of quadratic polynomial differential systems with a finite and an infinite saddle-node (C), *Internat. J. Bifur. Chaos Appl. Sci. Engrg.* **25**(2015), No. 3, Art. 1530009, 111 pp. https://doi.org/10.1142/S0218127415300098

[16] J. C. Artés, N. I. Vulpe, The codimension of the phase portraits for degenerate quadratic differential systems, *Bul. Acad. Ştiinţe Repub. Mold. Mat.* **106**(2024), No. 3, 29–53. https://doi.org/10.56415/basm.y2024.i3.p29

[17] W. A. Coppel, A survey of quadratic systems, *J. Differential Equations* **2**(1966), 293–304. https://doi.org/10.1016/0022-0396(66)90070-2

[18] P. de Jager, Phase portraits for quadratic systems with a higher order singularity with two zero eigenvalues, *J. Differential Equations* **87**(1990), No. 1, 169–204. https://doi.org/10.1016/0022-0396(90)90021-G

[19] F. Dumortier, P. Fiddelaers, Quadratic models for generic local 3-parameter bifurcations on the plane, *Trans. Amer. Math. Soc.* **326**(1991), No. 1, 101–126. https://doi.org/10.1090/S0002-9947-1991-1049864-0

[20] F. Dumortier, J. Llibre, J. C. Artés, *Qualitative theory of planar differential systems*, Universitext, Springer, Berlin, 2006. https://doi.org/10.1007/978-3-540-32902-2

[21] F. Dumortier, R. Roussarie, C. Rousseau, Hilbert's 16th problem for quadratic vector fields, *J. Differential Equations* **110**(1994), No. 1, 86–133. https://doi.org/10.1006/jdeq.1994.1061

[22] A. Gasull, L.-R. Sheng, J. Llibre, Chordal quadratic systems, *Rocky Mountain J. Math.* **16**(1986), No. 4, 751–782. https://doi.org/10.1216/RMJ-1986-16-4-751

[23] D. Hilbert, Mathematical problems, *Bull. Amer. Math. Soc. (N.S.)* **37**(2000), No. 4, 407–436. https://doi.org/10.1090/S0273-0979-00-00881-8

[24] P.-S. Laplace, *Théorie analytique des probabilités Vol. I*, Éditions Jacques Gabay, Paris, 1995.

[25] J. Llibre, D. Schlomiuk, The geometry of quadratic differential systems with a weak focus of third order, *Canad. J. Math.* **56**(2004), No. 2, 310–343. https://doi.org/10.4153/CJM-2004-015-2

[26] J. Pal, D. Schlomiuk, Summing up the dynamics of quadratic Hamiltonian systems with a center, *Canad. J. Math.* **49**(1997), No. 3, 583–599. https://doi.org/10.4153/CJM-1997-027-0

[27] H. Poincaré, Mémoire sur les courbes définies par une équation différentielle, *J. Math. Pures Appl. (3)* **7**(1881), 375–422.

[28] J. W. Reyn, Phase portraits of a quadratic system of differential equations occurring frequently in applications, *Nieuw Arch. Wisk. (4)* **5**(1987), 107–155.

[29] J. W. Reyn, *A bibliography of the qualitative theory of quadratic systems of differential equations in the plane*, Delft University of Technology, 1992.

[30] J. W. Reyn, Phase portraits of quadratic systems without finite critical points, *Nonlinear Anal.* **27**(1996), No. 2, 207–222. https://doi.org/10.1016/0362-546X(95)00007-I

[31] J. W. Reyn, Phase portraits of quadratic systems with finite multiplicity one, *Nonlinear Anal.* **28**(1997), No. 4, 755–778. https://doi.org/10.1016/0362-546X(95)00177-W

[32] J. W. Reyn, *Phase portraits of planar quadratic systems*, Math. Appl., Vol. 583, Springer, New York, 2007. https://doi.org/10.1007/978-0-387-35215-2

[33] J. W. Reyn, X. Huang, Phase portraits of quadratic systems with finite multiplicity three and a degenerate critical point at infinity, *Rocky Mountain J. Math.* **27**(1997), No. 3, 929–978. https://doi.org/10.1216/rmjm/1181071903

[34] D. Schlomiuk, Algebraic particular integrals, integrability and the problem of the center, *Trans. Amer. Math. Soc.* **338**(1993), No. 2, 799–841. https://doi.org/10.2307/2154430

[35] N. I. Vulpe, Affine-invariant conditions for topological distinguishing of quadratic systems in the presence of a center, *Differ. Uravn.* **19**(1983), No. 3, 371–379.

[36] Y. Ye, S. Cai, L. Chen, K. Huang, D. Luo, Z. Ma, E. Wang, M. Wang, X. Yang, *Theory of limit cycles*, Transl. Math. Monogr., Vol. 66, American Mathematical Society, Providence, RI, 1986.

[37] H. Żołądek, Quadratic systems with center and their perturbations, *J. Differential Equations* **109**(1994), No. 2, 223–273. https://doi.org/10.1006/jdeq.1994.1049